LOCAL BUCKLING OF HIGH STRENGTH STEEL W-SHAPED SECTIONS

by

Bing Yuan, B.A.Sc.

A Thesis

Submitted to the School of Graduate Studies

in Partial Fulfilment of the Requirements

for the Degree

Master of Engineering

McMaster University

MASTER OF ENGINEERING (1997)
(Department of Civil Engineering)

McMaster University
Hamilton, Ontario

TITLE: Local Buckling of High Strength Steel W-shaped Sections

AUTHOR: Bing Yuan, B.A.Sc. (University of Waterloo)

SUPERVISOR: Dr. K.S. Sivakumaran

NUMBER OF PAGES: xi, 155

Abstract

W-shaped steel members are widely used in various structural applications, such as buildings, bridges, and industrial complexes. The recent trend is to produce W-shaped sections using higher and higher strength steel as a replacement for mild-carbon steel, such as 300W steel. However, the width-to-thickness ratios (b/t or w/t) specified in the current CSA steel design standard (1995) for local buckling strength and ductility are based on studies using 300W steel. An investigation was carried out to study the local buckling behavior, with an emphasis placed on flange buckling of compression members, of W-shaped sections made of high strength steel. First, stress-strain characteristics of high strength steel of 350W, 480W and 700Q steel, along with the mild-carbon 300W steel, were determined using standard tensile tests. Based on these experimental material properties, analysis material models were derived for the finite element analysis. Analysis material models used in the finite element modeling were the multi-linear, modified tri-linear, and modified bi-linear models. The next part of the investigation included tests on stub columns of these selected steel grades having flanges at Class 1 limit based on the current design standard (CSA 1995). Based on the experimental results from these stub column tests, the applicability of b/t Class 1 limits for high strength steel sections were assessed. The experimental results showed that the reserve capacity (f_u/f_y) of all the stub columns were close to the same, regardless of the steel grade. However, the ductility of the W-shaped sections corresponding to each grade differed substantially. The 300W and 350W steel displayed much more ductility than the 480W and 700Q steel. It was concluded that the b/t limits of a Class 1 section, which was based on studies on the 300W steel, is also applicable to the 350W steel, but are not transferrable to the higher strength steels.

The third part of this study used the analysis material models determined from the tensile tests into a finite element modeling, where a 9-node "assumed strain" shell element was employed. Due to the symmetric behavior of a stub column, a quarter of a stub column was used to simulate the W-shaped section subjected to uniform compression. Meanwhile, an idealized residual stress with parabolic distribution across the web and flange of the W-shaped section was assumed and incorporated in the finite element modeling. Comparing the finite element analysis results with the corresponding experimental results from the stub column tests, an appropriate material model was selected to be used for further finite element analysis. It was found that the results obtained from the tri-linear and multi-linear models were similar to each other, and the modified bi-linear material model best represented the experimental results. Using this bi-linear material model in the finite element analysis, strength and ductility of W-shaped sections with varying flange b/t ratios but constant w/t ratio were determined from the finite element analysis. Results showed that the 350W steel demonstrated characteristics similar to the 300W steel. However, the 700Q steel possessed very little ductility and reserve capacity. The 480W steel was excluded in this part of the study due to the uncertain results from its tensile test. In all of these steel grades, it was found that ductility and reserve capacity decreased as the b/t ratio increased. From both the experimental investigation and the finite element analysis, the b/t limits in the current design standards were found to be applicable to both 300W and 350W steel, but not to the 700Q steel.

Acknowledgments

The author would like to express his sincere and heartfelt appreciation to his supervisor, Dr. K.S. Sivakumaran, for his diligent, systematic and precious guidance, and financial support, during the course of this study.

Dave Perrett is also to be thanked for assisting the author with the experimental setup in the laboratory.

Financial assistance from the Department of Civil Engineering was greatly appreciated.

Thanks are extended to the author's friend Bill Fitzgerald, fiancée Kate Wong, sister and parents for their support and encouragement throughout the preparation of this thesis.

To Kate Wong, my sister and parents

Table of Contents

List of Tables

List of Figures

Chapter 1

Introduction

1.1 The Structural Steel

Structural steel is one of the most popular and useful metals known to mankind and has been widely used in various structures such as buildings, bridges, industrial complexes, etc. Steel is also used in other applications such as vehicles and aircraft. The wide variety of applications of steel is because it possesses more desirable material properties in comparison with other construction materials, such as concrete and timber. The desirable material properties of structural steel include high strength/weight ratio, and high ductility. The high strength of structural steel makes it possible to build lighter and stronger structures that could not be built otherwise. Meanwhile, ductility of steel relieves the overstressed portion of a structural member by permitting a steel element to yield and cause a redistribution of stresses in the structure, thus preventing a fracture type failure. Strength and ductility of a structural steel material are customarily determined by means of a standard tensile test, which consists of pulling a standard-size coupon until the coupon fractures (Kulak, Adam, and Gilmor 1995).

The relationship between the stress and strain of a steel material can be obtained from the standard tensile test of a steel coupon. For example, the stress-strain relationship of mild-carbon steel has been well documented in various sources of the literature (Haaijer 1958, Kulak, Adam, and Gilmor 1995). Schematically, typical stress-strain relationships for steel

are as shown in the Figure 1.1. Referring to the relationships shown in Figure 1.1, in general steel material obeys Hooke's Law ($\sigma = E\varepsilon$) during the initial loading stage, defined as the elastic range, with the strain being linearly proportional to the applied stress. In the elastic range, on an atomic level the applied force has partially overcome the attractive force between the atoms lying in different planes and a relative displacement between the atomic planes occurs. The attractive force between the plane of atoms is unaffected due to this relative displacement and, therefore, the planes will return to their original positions when the applied load is released. The numerous planes in the steel material account for this elastic behaviour. When the load exceeds the elastic range to the plastic range, gradual yielding of the cross-section begins and causes permanent or plastic deformation. Low and medium strength structural steel, such as mild-carbon steel, exhibits an obvious point of yielding. At this stress level the strain undergoes a relatively large increase called the yield plateau with very little increase in the applied stress. This yield plateau is caused by slippage of the material along oblique surfaces, usually the result of grain planes slipping over each other by the action of shear stress. As the specimen undergoes more plastic deformation, grains tend to line up in the same way, a preferred orientation, in relation to the applied stress. At this stage, the specimen is capable of resisting more load, resulting in the strain-hardening stage until the ultimate load is reached. Loading beyond the ultimate tensile strength causes unstable deformation, and necking begins until the specimen fractures.

The yield strength and the ultimate strength of steel material can be easily controlled. These strengths vary significantly with chemical constituents of the steel, the most important of

which are carbon and manganese. From an atomic perspective level, both of these two chemical constituents impede the movement of crystals and grains, and thus increase the yield stress. The yield strength also varies with heat treatment used during the steel production process. For example, high strength steel may be obtained by quenching rather high carbon steel with carbon content of 0.4~0.5% (Smith 1979). Quenching of high carbon steel results in a high degree of distortion of the slip planes; more movements of crystals and grains can be impeded and thus the yield and ultimate strengths tend to be higher. The material properties of steel from batch to batch, however, may vary due to the slight difference in chemical constituents in each batch from which the steel is produced.

High strength structural steel is produced by the addition of an alloy into the batch while producing the steel. The presence of an alloy causes distortion of the slip planes, making greater stresses necessary to promote the movement of slippage, and thus the steel is more resistant to deformation. Also, the distribution of fine particles of the alloy throughout the steel has the effect of resisting the change in shape of the grains of the base metal during deformation, making greater stress necessary for deformation, thus the steel becomes stronger. The standard tensile test performed on high strength steel (Stewart 1995) reveals that the basic behaviour of high strength steel differs from that of steel with lower strength. The stress-strain relationship of high strength steel is also schematically shown in Figure 1.1. Referring to the stress-strain relationship of high strength steel in Figure 1.1, indicates that high strength steel also exhibits a well-defined yield point. However, strain-hardening starts immediately after the yield point is reached. This is different from that, in the mild-carbon

streel, where there is a long, flat plateau before the occurrence of strain-hardening. In the strain-hardening range, the slope of the stress-strain curve tends to be smaller than that of mild-carbon steel. This smaller slope indicates that the amount of strain-hardening, or the reserve capacity, which may be measured by the ratio of ultimate strength, F_u, to yield strength F_y (Stewart 1995), is comparatively low for high strength steel. In addition, the stress-strain relationship in Figure 1.1 also shows that high strength steel tends to rupture at a much lower elongated strain. Therefore, based on the test performed on tensile coupons, high strength steel possesses much less ductility than does mild-carbon steel. Overall, the material properties of high strength steel are different from those of mild-carbon steel. Depending on the amount of chemical constituents (i.e. carbon, manganese) and the other alloys added to the steel, many steel products with different material properties can be produced. There are more than twenty different types of steel material available on the Canadian market.

Such a large variety of structural steels available in Canada has given the designer freedom in selecting the most suitable type of steel for a particular application. For example, the structures in a highly earthquake-prone zone must preferably have more ductility. In some cases, such as bridge construction, steel products are required to have good weldability and corrosion resistance in order to withstand severe outdoor weather conditions. The Canadian Institute of Steel Construction (1995) defines each grade of steel by a number and a letter. The number indicates the specified minimum yield strength of the thinnest plate and lightest section available in that grade of steel. The letter refers to the characteristics of the type of

steel (i.e. 300W means the steel product possesses a specified yield strength of 300 MPa and is weldable). The specified strength gives the minimum yield strength of a certain grade of steel, and is usually the measured yield strength from tensile tests. This value tends to be considerably higher than the specified yield strength.

1.2 The W-Shaped Steel Sections

Prefabricated steel shapes, such as, hot-rolled sections, welded steel sections, and cold-formed sections are widely used in structural systems. The hot-rolled sections and welded sections are usually associated with the heavy steel construction such as bridges and high-rise buildings. Cold-formed steel members are commonly employed in residential houses and low-rise commercial buildings. Hot-rolled or welded structural steel sections are usually fabricated into I-shaped members, referred to as W-shaped. W-shaped sections are cost effective and provide efficient resistance to bending moments and shear forces. The flanges and the webs of a W-shaped steel members are slender and the cross-sections are classified as open thin-walled sections.

Depending on the way by which the forces are transmitted into the structure and into the structural members, a W-shaped steel member may be considered as a beam, a column, or a beam-column. The failure modes of W-shaped sections under such loads may be primarily due to overall failure of the member or as a result of local buckling failure in the plates making up the cross-section. The current structural steel design standards specification (CISC 1995) attempts to achieve overall member failure modes, by preventing pre-matured

local buckling of the flange and/or web of the sections. The actual strength and the ductility associated with the overall member failure mode, however, depends on the load at which the flange and/or web element locally buckles. The width-to-thickness ratios of the plate elements of the cross-section determine the local buckling resistance of a section (CISC 1995). The width-to-thickness ratios for different target strength and ductility have been given in the current design codes. Table 1.1 shows such width-to-thickness ratios limits for flange and web in flexural compression, and web subjected to axial compression. Depending on the width-to-thickness ratio, a W-shaped section can be classified into one of the four classes of sections as indicated in Table 1.1 (CISC 1995).

The classification for steel sections as given in code are primarily based on the attainment and redistribution characteristics of moment capacity of a flexural member. A Class 1 section, or a plastic design cross-section, is one that can both reach its plastic moment capacity and has enough rotation capacity to permit redistribution of moments (CISC 1995). A Class 2 section, or a compact section, can just reach its plastic moment capacity but does not have enough rotation capacity to permit redistribution of moments beyond this point. A Class 3 section, or a non-compact section, is one that can only reach the yield moment. The Class 4 section is the one which fails prior to reaching the yield moment. Note that the limits of the width-to-thickness ratio are functions of the yield strength of steel. The limits as shown in Table 1.1 were derived from material properties associated with the mild-carbon steel which possesses good ductility and relatively low yield and ultimate strength (Kulak 1983). Also the slenderness limits for flange and web thickness are independent of each

other, and thus may not be associated with overall member ductility (Stewart 1995).

As indicated earlier, currently steel having many grades is available on the market. Recently, a variety of new steel products using high strength steel have been introduced to the market. For example, effective May 1997, all standard sections produced by Algoma Steel Inc. will be using CSA G40.21-M350W grade steel. Previously, all Algoma steel sections were using CSA G40.21-M300W, thus the change represents a 17% increase in specified yield strength over the old steel material. When the design is governed by the strength requirements, smaller beam and columns sizes may be allowed to be used, and thus one may benefit from material saving with the use of 350W steel. However, in situations where serviceability requirements or fatigue considerations govern the design, the use of 350W steel in structural design might not be suitable. Also, even though these new sections have higher strength, they may have less member ductility. Little research has been done on such high strength structural steel sections. Therefore it is necessary to have a better understanding of how the high strength steel sections behave and whether the current design specifications are applicable to structural members made of such material. This investigation intends to study the material behaviour of high strength steel. This investigation also intends to determine whether the current specifications related to local buckling of W-shaped sections are suitable to high strength structural steel members.

1.3 Objective and Scope

As briefly discussed earlier, high strength steel behaves differently from that of relatively lower strength mild carbon steel. The first objective of this investigation is to study the material behaviour of high strength steel based on standard tensile tests. Analysis models for material behaviour will then be derived from these experimentally based material properties. Even though it may be more theoretically sound to use the material properties obtained from compression tests on such steel specimens for finite element modelling purposes, the compression material properties of steel material are difficult to measure. Therefore, material models corresponding to the properties obtained from standard tensile tests will be used for finite element modelling.

The width-to-thickness ratios associated with the local buckling in the existing design standard were established from mild-carbon steel (Kulak 1984), and might not be suitable for high strength steel (Stewart 1995). The second objective of this study is to determine the applicability of the present local buckling rules to high strength steel sections. Stub columns made of different grades of steel having width-to-thickness (b/t) limits falling at the Class 1 limit will be tested. From the stub column tests, the local buckling load, ultimate load, and the ductility of each column will be determined. The b/t limits in the current CSA design code (CISC 1995) will be assessed as to their suitability for high strength steel W-shaped sections.

The third objective of this research is to establish a finite element model to determine the local buckling behaviour of stub columns of W-shaped steel sections. The material models for finite element analysis are primarily based on tensile test results. However, simplified material analysis models will also be considered. The analytical results calculated from finite element modelling, using different material models, will be compared with the results acquired from the stub column tests. The appropriate material model will then be selected in order to further use in finite element modelling of W-shaped stub columns. In addition, the results obtained from finite element modelling will be compared with the present design codes, and b/t limits for plastic sections of high strength steel will be established to improve the efficiency in plastic and ductile seismic designs.

In this thesis, Chapter 2 reviews the related research work done in the past few decades. In Chapter 3, experimental evaluation of material properties of different grades of steel will be discussed. Multi-linear material models accurately representing each grade of steel will be established for the use of finite element modelling. For the purpose of comparison in finite element modelling, simplified material analysis models, such as bi-linear and tri-linear models, will also be developed based on test results. In Chapter 4, details of the experimental investigation on Class 1 stub columns with different specified yield strengths associated with the tensile tests in Chapter 3 will be presented. The corresponding buckling load, overall behaviour, and ductility will then be established. In Chapter 5, based on the material models derived from tensile tests, the local buckling behaviour of high strength W-shaped sections including residual stress and initial imperfection will be investigated using

the finite element method. This analytical model will be constructed using large deformation elasto-plastic shell elements. Results obtained from the finite element modelling will be compared with the experimental results. The suitability of b/t limits defined from the current CSA standard (1995) to high strength steel will be assessed. In Chapter 6, this study will be summarized, conclusions drawn, and recommendations made regarding the current design standards.

Table 1.1 Slenderness Limits of W-shaped Sections

Plate Element	Class 1	Class 2	Class 3	Class 4
Flange in flexural compression	$b/t \le 145/\sqrt{F_y}$	$b/t \le 170/\sqrt{F_y}$	$b/t \le 200/\sqrt{F_y}$	$b/t > 200/\sqrt{F_y}$
Web in flexural compression	$h/w \le 1100/\sqrt{F_y}$	$h/w \le 1700/\sqrt{F_y}$	$h/w \le 1900/\sqrt{F_y}$	$h/w > 1900/\sqrt{F_y}$
Web in Axial Compression (C_f=C_y)	--------	--------	$h/w \le 670/\sqrt{F_y}$	$h/w > 670/\sqrt{F_y}$

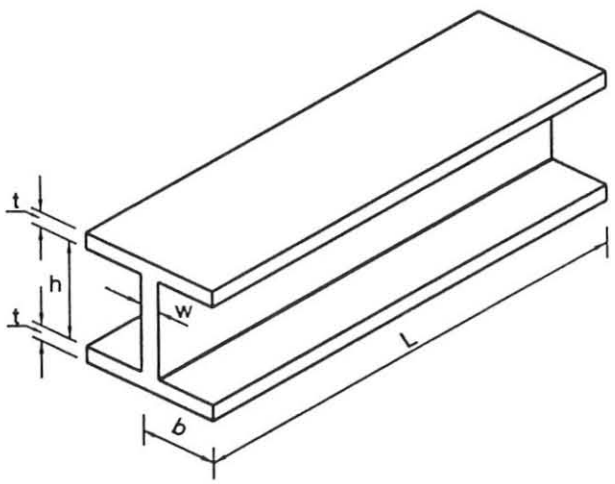

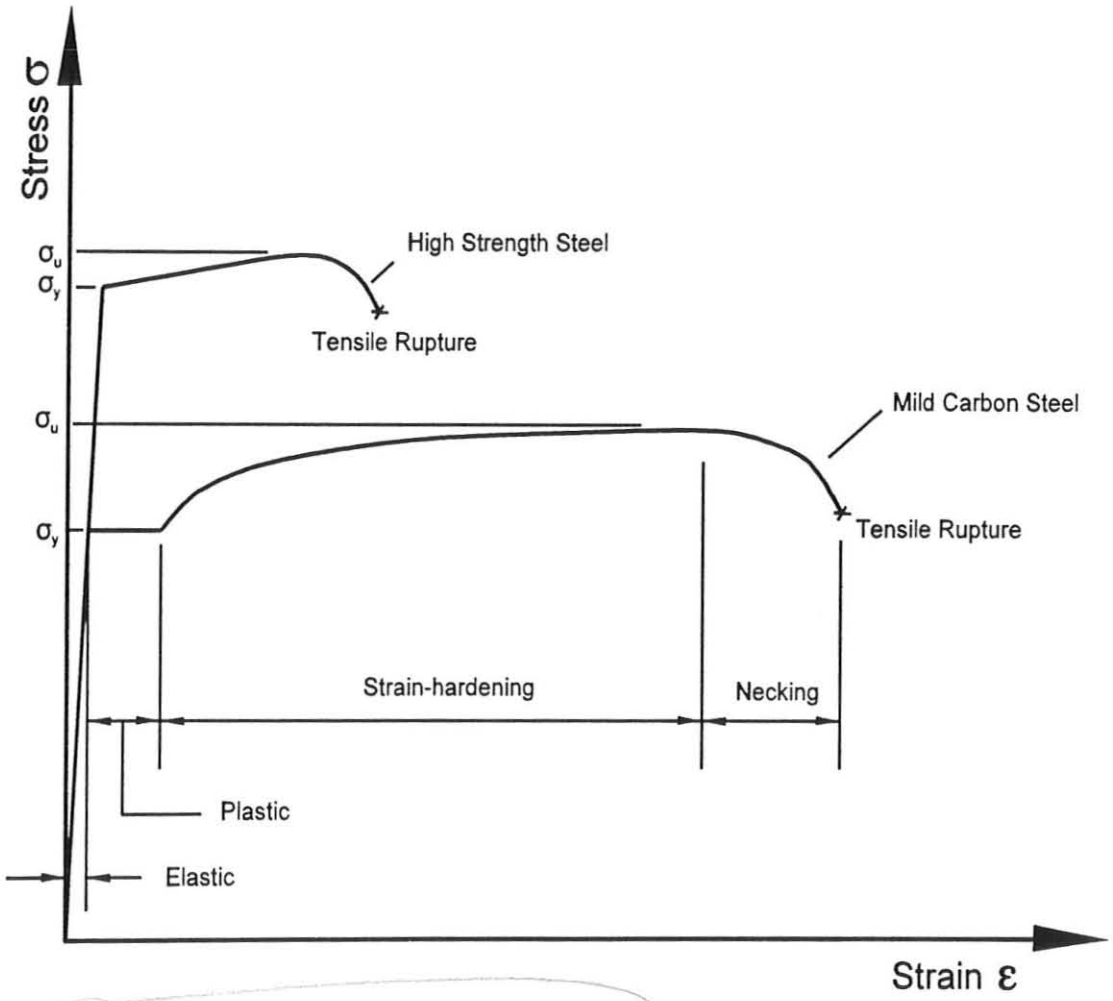

Figure 1.1 Stress-Strain Relationship of Steel

Chapter 2

Literature Review

2.1 Introduction

Historically, buckling of structural members have long been recognized as a potentially dangerous failure mode. Buckling of columns was first brought to attention by Euler (1744) more than two hundred years ago. Bryan (1891) first introduced the theoretical work on the elastic buckling of plates. He presented how the elastic buckling of plates could be applied to the sides of a ship. It was quickly realized that the buckling behaviour of a plate was quite different from that of a column. For a column, buckling terminates the ability of a member to resist axial load, and the buckling load is thus the failure load of the member. However, this might not be the behaviour for plate elements. Most of the structural plate elements can, subsequent to reaching the buckling load, continue to resist increasing axial loads. These structural plate elements do not fail until a load considerably in excess of the buckling load. In essence plate elements possess substantial post-buckling strength. The buckling load of a plate is therefore not the failure load. Also the failure load of a structural member made up with these plate elements may not correspond to the local buckling of its plate elements. Thus, one must determine the load-carrying capacity of a plate or a structural member made of plate elements by considering the post-buckling behaviour.

In the past half century, studies on local buckling of plates in both the elastic and inelastic ranges have been carried out, theoretically and experimentally, by several prominent

researchers (Lay 1956, Galambos 1958, Kulak 1984, and Kemp 1986). Their findings had been adopted to the structural design standards in different countries. For instance, in Canada most of the current design standards related to local buckling of the flange and web plates are based on the results and conclusions drawn from Kulak's findings (Dawe and Kulak 1981). However, only a few researchers have attempted to investigate the local buckling behaviour of high strength steel plates and structural members. In the present Canadian steel design standards (CISC 1995), there are no local buckling rules dealing with high strength steel.

2.2 Elastic and Inelastic Instability of Plates

As described previously, studies on instability of plates have been carried out experimentally and theoretically for more than a century. In the late 19th century, Bryan (1891) studied and successfully solved the buckling problem for an elastic, simply supported plate subjected to uniaxial compression. Later, Timoshenko and Gere (1961) studied the plate buckling problems with various boundary conditions, and various loading conditions. Based on elastic plate buckling theory, Timoshenko and Gere (1961) presented close-form and approximate solutions to various plate buckling problems. However, since these solutions were derived solely based on the elastic buckling theory, these solutions are not applicable to inelastic plate buckling. In the early 20th century, plate buckling beyond the proportional limit was recognized. Bleich (1933) sought solutions to such inelastic problems and he demonstrated that the buckling stresses for plate buckling between the proportional limit and yield stress could be approximated. He proposed, based on the linear elastic theory, that the

Young's modulus E may be replaced with $\sqrt{EE_t}$, where E_t is the tangent modulus, to determine the buckling stress. Subsequently, researchers working independently (Stowel 1948; Handelman and Prager 1948; Bijlaard 1949; Onat and Drucker 1953) attempted to develop plastic buckling theories based on different theories of plasticity. The effects of material properties idealization for steel, and the effects of initial imperfections on the buckling behaviour of plates were also considered by some other researchers (Haaijer and Thurlimann 1958; Lay 1965). More recent work was done by Dawe and Grondin (1985) on inelastic buckling of steel plates. It reveals that buckling of plates in the inelastic range is a much more complicated problem than that in the elastic range. They also showed that theoretical predictions based on various existing theories on inelastic plate buckling are not always accurate and not consistent when correlated with experimental results. According to the evaluation by Dawe and Grondin (1985), it seems that there were no universally accepted theories in studying the inelastic buckling behaviour of steel plates.

2.3 Local Buckling of W-shaped Sections

Local buckling of W-shaped sections refers to conditions under which the compression flange or web, or portion of the web in compression, buckles in a local region of the section. Such local buckling of plate elements inhibits development of the full resistance, and the ductility of the member. Prior to the 1950s, research studies paid less attention to local buckling problems, than that to the examination of the overall stability of the member. The early studies on the local buckling of W-shaped sections was carried out by Haaijer and Thaürlimann (1957). They published the results of an investigation of inelastic local

buckling of W-shaped steel sections. This investigation was intended to establish the maximum plate width-to-thickness ratios suitable for plastic design. They provided analytical solutions for buckling problems of single web or flange plates with assumed boundary conditions at the web-to-flange junctions. The experimental work in their investigation consisted of the tests on compression and flexural members. The results from their findings were later adopted to the standard for plastic design until more recent developments by Dawe and Kulak (1981). In the sixties, Galambos and Lay (1966) further studied the local buckling behaviour of W-shaped sections under moment gradient. They found that a beam, which could be loaded into the inelastic range, must be able to attain the fully yielded condition without prior local buckling. Their studies showed that flange local buckling predictions depended primarily on the knowledge of the inelastic shear modulus. Limiting flange b/t ratios were derived and they concluded that the occurrence of local buckling depended not only on the b/t ratios, but also on the moment gradient on the beam, the length of the yielded region, and the strain-hardening stiffness of the steel.

Subsequent to the studies performed by Galambos and Lay (1966), both experimental and analytical studies on the local buckling problems have increased in number, and more and more modifications have been made to the design specifications dealing with local buckling (Kemp 1996). Recent studies in this field were pursued analytically and experimentally by Dawe and Kulak (1981, 1984, and 1986). The main purpose of their study was to establish and suggest more appropriate flange and web slenderness limits for W-shaped sections to be incorporated in the steel design standards (CISC 1995). The method used to establish

suitable slenderness limits for a given class of a section is schematically shown in Figure 2.1. For demonstration purposes there are only three groups of flange slenderness shown in Figure 2.1. It is evident that the strength of W-shaped sections varies with different combinations of web and flange slenderness. For a given flange slenderness, the strength of a W-shaped section tends to decrease as the web slenderness increases. These relations between the flange and web slenderness were calculated using the finite strip method by Dawe and Kulak (1981). Holding the flange slenderness constant, the local buckling strengths associated with a wide range of varying web slenderness were calculated using the computer program. Based on the analytical results from the finite strip method and the confirmation from the comparison with experimental results, Dawe and Kulak (1981) were able to establish the slenderness limits for various classes of sections.

These slenderness limits are established in such a way that the necessitated stress level, P_y, M_y, or M_p, are satisfied. Based on this requirement, Dawe and Kulak (1981) proposed the suitable width-to-thickness limits so that the strength demand, for example, P_y for columns, M_y for Class 3 beams, and M_p for Class 2 beams, is achieved before local buckling occurs. A Class 1 section is expected to reach M_p and to undergo sufficient rotation to permit redistribution of stresses while sustaining the plastic moment value. The limits of a Class 1 section as provided by Dawe and Kulak (1981) were established by employing two conditions namely, that a section is Class 1 if its strength exceeds M_p, and that the strain in the compression flanges can reach the strain-hardening range before local buckling occurs. For mild-carbon steel, such as the 300W steel, the strain at the onset of strain-hardening is

approximately ten times of the yield strain. In other words, the Class 1 b/t limits ensure that the strain in the compression flange can reach at least ten times of the yield strain prior to local buckling. Therefore the strain in the compression flange also indicates the ductility of a Class 1 section. These slenderness limits proposed by Dawe and Kulak (1981) have been adopted by the Canadian Standard Association (CISC 1995) to form the local buckling rules for structural steel design.

However, it should be noted that the strength graphs shown correspond to the moment resistance associated with the local buckling state, for a given flange slenderness and varying the web slenderness. The results from this numerical analysis provided only the local buckling load of a section corresponding to the combination of flange and web slenderness. In other words, the flange and web slenderness limits were independent of each other and the overall post-buckling behaviour was, to some degree, ambiguous. Also, it must be noted that the analytical material model used by Dawe and Kulak (1981) was limited to local buckling behaviour of mild-carbon steel, and more specifically, it was the steel grade with a minimum specified yield strength of 300 MPa. The material model they used was a tri-linear model, which consists of an elastic range, a perfectly plastic range and a strain-hardening range. This tri-linear model well represents the material characteristics of mild-carbon steel, but does not satisfy those of high strength steel, which possesses higher strength, no yield plateau, and less ductility. Therefore it must be recognized that there is a need to modify the material model to deal with high strength steel. In addition, the applicability of the current design standards to high strength steel is questionable.

2.4 Local Buckling of High Strength Steel W-shaped Sections

As mentioned earlier, the local buckling rules as given in the Canadian steel design standards (CISC 1995) were established based on the investigations on 300W grade steel sections by Dawe and Kulak (1981, 1984). The current CSA standard (CISC 1995) does not provide any rules or information about high strength steel, even though some researchers have studied its local buckling behaviour previously. McDermott (1969) investigated the local buckling behaviour on high strength steel (A514) beams and stated that such members developed sufficient rotation capacity and could be used in plastic design provided the width-to-thickness ratio did not exceed 5. Hancock (1992) studied the local buckling behaviour of steel with nominal yield stress of 690 MPa by performing a compression test on W-shaped and cruciform stub columns, and carrying out analysis using the finite strip method. He concluded that the same slenderness limits apply to both ordinary and high strength steel plates. However, his results were limited to Class 3 sections and provided no information on buckling strength and ductility of Class 1 and Class 2 sections, which must sustain substantial inelastic strains to meet the corresponding design requirements. Meanwhile, there are major differences in the inelastic range between the mild-carbon and high strength steels, thus conclusions drawn by Hancock (1992) might not be applicable to Class 1 and Class 2 high strength steel sections.

More recently, Stewart (1995) performed a study on high strength steel W-shaped sections using finite strip methods with multi-linear material models. In his study, material properties obtained from standard tensile tests were employed in the idealization of multi-linear

material models. These multi-linear material models were used in a finite strip based local buckling analytical method. Based on this method, extensive study was carried out to obtain the local buckling strength and ductility of high strength steel W-shaped sections. The emphasis in his investigation was placed on whether the flange and web slenderness limits as given in the current design standard (CISC 1995) are applicable to high strength steel W-shaped sections.

The results from Stewart's (1995) analysis showed that the local buckling rules in the current CSA standards (CISC 1995) are not applicable to high strength steel W-shaped sections. New slenderness limits were proposed for a safe and efficient local buckling design of high strength steel W-shaped sections. In his proposal, these new slenderness limits are introduced in the form of interactive slenderness limits, which reflect the actual interdependence of the web and flange. Such interactive relationship between the web and flange slenderness limits, along with those of the current design standards (CISC 1995), are depicted in Figure 2.2. As shown in the figure, it is evident that the slenderness limits as given in the current design standards (CISC 1995) are not ideal. In some cases, such as that for 350W steel, it appears that the current design standards (CISC 1995) are somewhat too conservative. In other cases, such as that for 700Q steel, the current slenderness limits tend to lack conservatism. Thus the slenderness limits as given in the current design standards (CISC 1995) maybe inadequate for the local buckling rules of high strength steel W-shaped sections (Stewart 1995). In addition, more flexible slenderness limits for Class 1 sections were proposed (Stewart 1995) which are a function of the available ductility. However, this

proposal needed to be confirmed from experimental studies and this forms the initial drive of this current investigation whose objectives were previously described in Chapter 1.

2.5 Numerical Methods in Solving Local Buckling Problems

With the development of high speed digital computers, powerful analytical techniques, based primarily on numerical methods, have been used to study the local buckling characteristics of W-shaped sections. Numerical methods such as finite strip and finite element analyses, which are both energy-based formulations, are commonly used in such numerical analyses. The finite strip method involves a subdivision of a prismatic thin-walled structure into longitudinal strips joined at nodal lines. In the past, the finite strip method has been used by a number of researchers (Hancock 1978; Dawe and Kulak 1982). Applying the finite strip analysis, Hancock (1978) studied the local and lateral buckling of W-shaped beams. In this finite strip model (Hancock 1978), a linear elastic material response was assumed and residual stress effects were not included. In a later analytical model (Hancock 1986), effects of residual stress were taken into consideration by superimposing the residual stress, which was determined by factoring the measured residual strain with the value of Young's Modulus, onto the applied stress. Other studies using the finite strip method were presented by Plank and Wittrick (1974), Cheung (1976), GravesSmith and Sridharan (1978). These studies attempted to include lateral buckling modes, to solve problems with more complicated states of stress, or to increase the computational efficiency. In 1980, using the finite strip method incorporated with residual stress effects, Dawe developed techniques for the analysis of local buckling behaviour of thin-walled structural members which were

subjected to uniaxial loading in the direction parallel to the longitudinal axis of the member. Later Dawe and Kulak (1984) specialized this model to study local buckling behaviour of the W-shaped members under various combinations of axial and flexural loads. The results from their analytical model also led to the revision of CSA standards (CISC 1995) on local buckling rules. In their analytical technique, polynomial and Fourier series displacement functions were used in the transverse and longitudinal directions, respectively. With such displacement functions, this method may have proved difficult when analysing plate assemblies if shear force is present (Mahendran and Murray, 1986). Thus the finite strip method cannot be easily applied to complex problems when loading and boundary conditions become more complicated (Chin *et. al.* 1992). Despite the disadvantage of the finite strip technique, the results obtained from this method developed by Dawe (1981) were acceptable in comparison with the experimental results.

The finite element method has long been recognized as one of the most effective numerical techniques in solving local buckling problems of thin-walled structures under different loading and boundary conditions. In 1973, Rajasekaran and Murray studied the coupled local and lateral buckling behaviour in beam-columns. In their study, the finite element method accommodated a large variety of boundary conditions with the assumptions of linear material response and no residual stress effects. Their method gave good results for flange local buckling but web local buckling could not be predicted accurately. In the late 1970s, Akay, Johnson, and Will (1978) studied local buckling of beams under the assumption that, during buckling, straight lines remain straight across the flanges and normal to the web. Their

analytical results showed reasonable agreements with flange and web local buckling. Recent developments by Chin and Kitipornchai (1992) included finite element technique that is capable of predicting the complex buckling modes of thin-walled structures under any general loading and boundary conditions. A rectangular thin-plate element having four corner nodes with seven degrees of freedom (dof) per node and two mid-edge nodes with a single translational dof was used in their model. It has been demonstrated that results obtained from this finite element formulation agreed well with the experimental results in terms of flange or web buckling.

More recently, Abdel-Rahman (1997) developed a more powerful finite shell element which is applicable to both shell and plate local buckling problems. The "assumed strain" isoparametric shell element has nine nodes and each node contains five dof. In this finite element technique, not only the lateral displacement and rotations, but also the in-plane displacements were taken into consideration. Results from this formulation agree well with the experimental results of Abdel-Rahman (1997). The main purpose of this technique was to determine the local buckling behaviour of cold-formed steel, which possesses different characteristics of material behaviour and residual stress distribution from those of W-shaped sections. The stress-strain relationship of cold-formed steel reveals that there is no well-defined yield point and gradual yielding are always present. Also, in cold-formed steel the residual stress varies substantially across the thickness of the steel plate (Abdel-Rahman 1997). On the contrary, structural steel (hot-rolled or welded W-shaped sections) usually exhibits a well-defined yield point in the stress-strain relationship and residual stress varies

along the width of the web and flanges, but not across the thickness of the plate. Thus, changes have to be made to the computing procedure in order to incorporate the residual stress effects for a W-shaped section into the formulation and to represent the material properties for mild-carbon or high strength steels. Upon the availability of software and the sound results of this finite element technique, the formulation developed by Abdel-Rahman (1997) will be used and modified to determine the local buckling behaviour of W-shaped sections made of high strength steel.

2.6 Definition and Measurement of Ductility

Ductility is the measure of plastic deformation of a material, a structural member, or a structural system. The definition and measure of ductility may depend on the loading conditions, such as tension, compression, or bending. For example, steel material ductility may be determined from a tensile coupon test. From the stress-strain relationship, the material ductility can be determined by calculating the ratio, the ultimate strain over the elastic strain. However, the measure of material ductility may not indicate the ductility of a W-shaped member subjected to axial compression or bending, because of the different behaviour of the W-shaped member under such loading conditions. A W-shaped member subjected to axial compression may fail due to overall buckling of the member, or may be due to local buckling of flange and/or web plate elements. Similarly, a W-shaped member under bending may fail due to lateral-torsional buckling or due to section failure induced by local buckling of flange and /or web plate elements. Extensive experimental work had been done on W-shaped members by many researchers (Lay 1956, Galambos 1966, Dawe and

Kulak 1984, and Hancock 1993). The experimental work done by these researchers tended to be in favour of testing beams in the past. The common test is a simply supported and laterally restrained beam under a central point load causing moment gradient to the specimen. The widely accepted ductility corresponding to these testing programmes may be quantified most directly by measuring the available inelastic rotation, θ_p, as shown in Figure 2.3, over θ_e, for which the moment exceeds its design ultimate resistance , M_p. Under conditions of moment gradient, θ_p reflects the inelastic behaviour of a member and the θ_e is the elastic rotation at M_p over the same half-span of the beam. The quantified ductility, referred to as rotation capacity, R, is usually described in a non-dimensional form as $R= \theta_p/\theta_e$. This non-dimensional quantified ductility provides the convenience in assessing the amount of ductility required in the plastic design. In the past, different amounts of quantified ductility had been suggested for various design purposes. Yura et al. (1978) proposed an available rotation capacity of R = 3 for Class 1 sections and Kemp (1991) has suggested an available rotation capacity of R = 1 for Class 2 sections.

Dawe and Kulak (1981) considered that a Class 1 section has sufficient ductility if the strain in the compression flange of a beam reaches the strain-hardening range before local buckling occurs. This indicates that the compression flange has fully yielded and reaches the strain-hardening range. Therefore, based on testing beams under moment gradient, the measure of ductility by Dawe and Kulak (1981) was solely relied on the strain in the fully yielded compression flange. Under the condition that the strain in the compression flange reaches the strain-hardening range before local buckling occurs, the strain corresponding to the

compression flange can also be measured from testing stub columns. In a stub column test, web and flanges are subjected to uniform compression. When the strain in the compression flange reaches the strain hardening range, the flange of the stub column is also fully yielded, which is under the same condition as that of the compression flange in a beam test. Therefore the ductility of a Class 1 section can also be determined from measuring the strain in the flange of a stub column. From stub column test, the quantified ductility of a Class 1 section can be determined by calculating the ratio, the amount of inelastic strain over the elastic strain. Moreover, the ductility of a stub column can be transferred to rotation capacity of a beam with the same geometric configurations. This corresponding rotation capacity can be calculated based on the strain in the flange of the stub column and the depth of the beam.

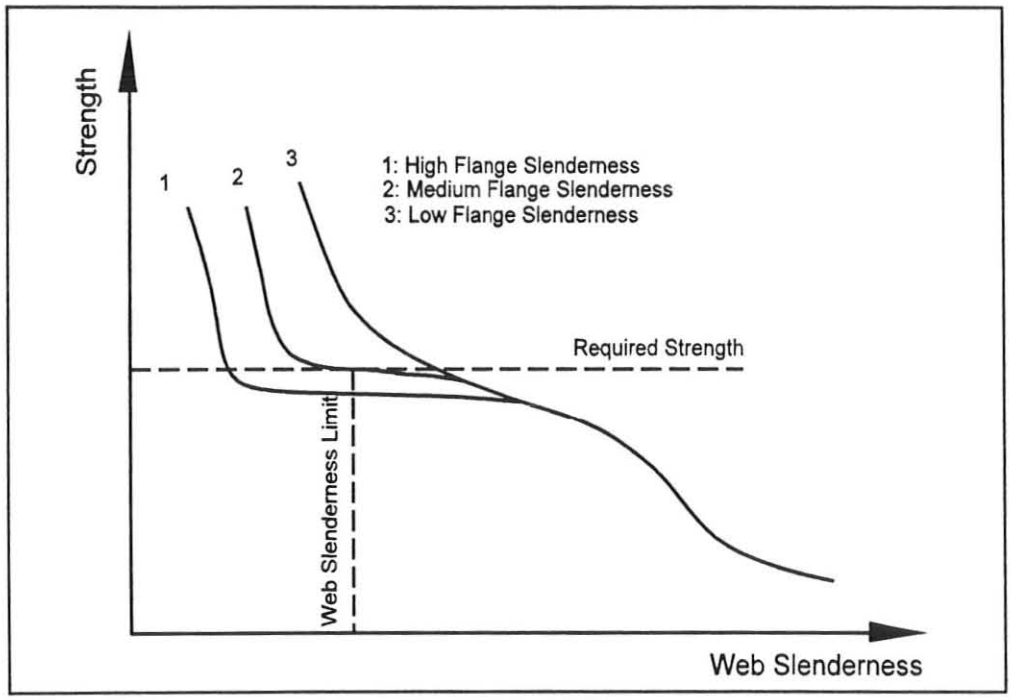

Figure 2.1 Effect of Web Slenderness on Strength as Flange Slenderness Varies (Schematic)

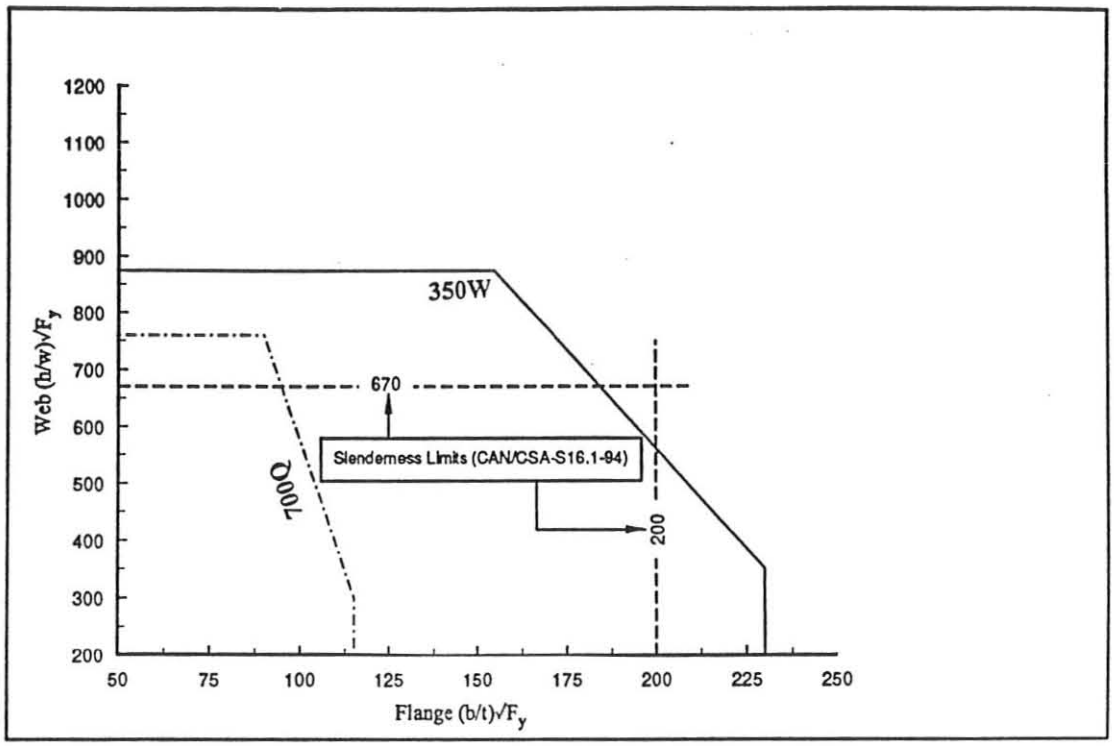

Figure 2.2 Proposed Slenderness Limits for Columns (Stewart 1995)

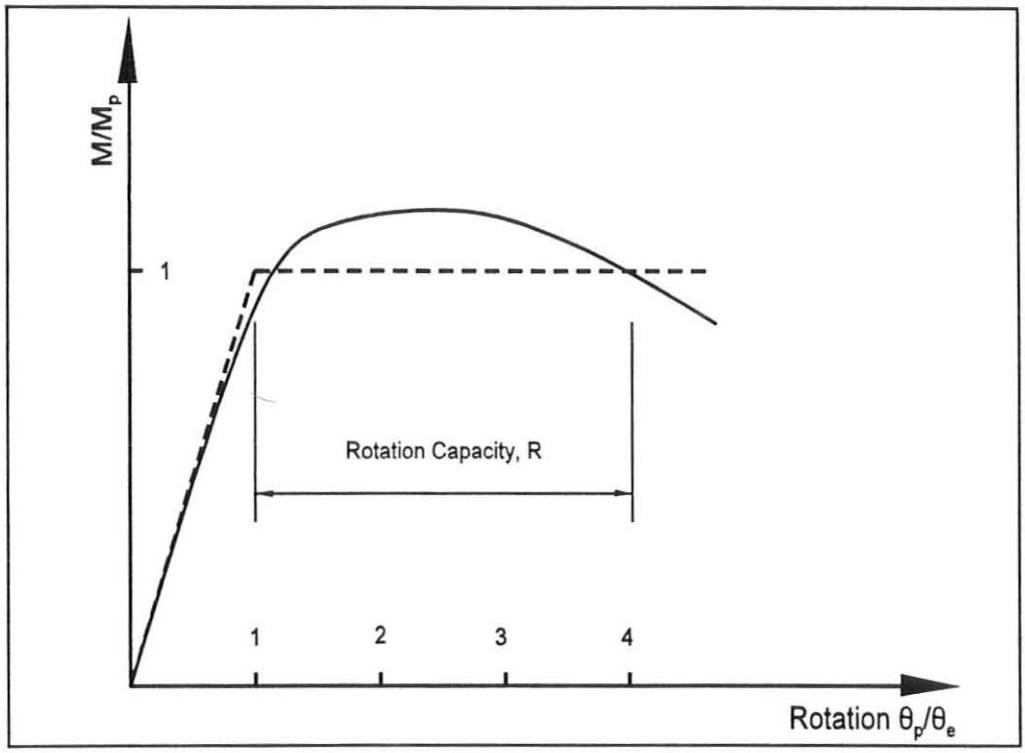

Figure 2.3 **Schematic moment-rotation curve of a beam under moment gradient**

Chapter 3

Material Properties of High Strength Steel

3.1 Introduction

Different grades of steel with different material properties are available in the market today. In Chapter 1, the general behaviour of mild carbon steel, and high strength steel was briefly discussed. Under uniaxial tension, mild steel undergoes elastic deformation, yielding with a definite yield plateau, strain-hardening, and followed by necking and rupture failure. The high strength steel undergoes elastic deformation, strain-hardening, followed by necking and rupture failure. Essential mechanical properties such as yield strength, ultimate strength, and final elongation over a certain length under tension are usually provided by the steel supplier with a mill certificate. However, since the high strength steel is a relatively new product and because of limited previous studies, insufficient information exists on the behaviour of such steel. Therefore an experimental evaluation of the properties and the behaviour of high strength steel is necessary in order to have better knowledge and understanding of the material behaviour of such steel. In this chapter, the details of the standard tensile test on high strength steel of different grades will be presented. From the results of the tensile tests, material properties of steels will be examined and stress-strain relationships will be obtained. From these stress-strain relationships, different material models will be derived for use in finite element modelling. Material models determined from the tensile tests give the ideal representation of the material behaviour for each grade of steel. Also, for the finite element modelling purposes, the distribution pattern of residual stress in welded W-shaped sections

will be reviewed. Based on the previous studies and results that exist in the literature, the idealized residual stress distribution pattern over the cross-section of a welded W-shaped section will then be determined. The idealized material behaviour and the effects of residual stress will be used in the finite element modelling part of the study presented in Chapter 5.

3.2 Tensile Testing of High-Strength Steel

Although many different steel grades having different mechanical, physical and chemical properties are available in the market today, the steel grades of 300W, 350W, 480W, and 700Q were selected for the current investigation. These steels were selected so as to consider a wide range of material behaviour among the available steel grades. Brief descriptions of each of these selected steel grades are presented as follows:

300W - this is the structural mild-carbon steel that is most commonly used for building construction in Canada. It is a weldable steel with a minimum specified yield stress of 300 MPa and a tensile strength between 450 and 620 MPa. Structural members in this steel grade are available in a wide variety of structural shapes, bars and plates. It is capable of providing significant elongation before rupture occurs, indicating a considerable amount of ductility.

350W - its mechanical properties are similar to those of 300W steel, however, the minimum yield stress is specified at 350 MPa. This steel is categorized as a high strength low-alloy steel. It is the normal steel that is used to manufacture hollow structural sections in Canada. Recently it has been introduced, by Algoma Steel

Inc., to produce W-shaped sections, which were originally made of the 300W grade steel.

480W - this is high strength low-alloy steel with minimum yield stress of 480 MPa and tensile strength between 600 MPa to 750 MPa. It is a typical high strength steel used in applications where weldability of the structural members and light weight structure are required.

700Q - this is a high strength quenched and tempered alloy with a minimum yield stress of 700 MPa and a tensile strength from 800 to 950 MPa. These steels are generally produced in plate form which are in turn used in high strength, light-weight assemblies such as industrial equipment and machinery. Applications sometimes include bridges and similar structures.

From the above selected steel grades, the coupons for tensile testing were made and, correspondingly, for this investigation the stub column specimens were fabricated from the same steel plates. Therefore, using the material models derived from the tensile tests, the analytical results from finite element modelling can be compared with the experimental results obtained from stub column tests. Details of the stub column tests and the finite element analysis will be further discussed in Chapter 4 and Chapter 5, respectively.

3.2.1 Tensile Coupons

Material properties of steel with different grades established in this study were based on tests on tensile coupons. The coupons were cut along the same direction as the plates cut for

fabricating the welded W-shaped stub columns. Dimensions of the tensile coupons were made according to the guidelines provided by the American Society for Testing and Materials (ASTM) Standards A370-92 (1994c). Coupons with a reduced cross-sectional area were selected to ensure that necking occurred in the reduced cross-section over which the strain gages were placed. Details of the tensile coupon dimensions are provided in Figure 3.1, in which it can be seen that the gage length used to calculate the elongated strain was 200 mm and the standard width of the coupons was 40 mm.

It was originally planned that each steel grade consisted of three identical tensile coupons in order to minimize the inconsistency in tensile tests. However, the steel supplier mistakenly fabricated only one tensile coupon for the steel grades of 350W, 480W, and 700Q steel, which were also used to fabricate the W-shaped stub columns. No additional tensile coupons were able to be produced from the same steel plates from which the stub columns were made. Facing the possible inconsistency and inaccuracy due to testing only one coupon from each grade, it was decided that three additional identical tensile coupons of these three steel grades would be made, but from different batches of production.

In total, there were 15 tensile coupons for steel grades of 300W, 350W, 480W, and 700Q. Three tensile coupons were for 300W steel, and four coupons were for each of the remaining selected steel grades. All tensile coupons were fabricated into the final shape, as shown in Figure 3.1, in the machine shop at McMaster University. Tensile coupons referred to herein as 300-1, 300-2, and 300-3 were of steel grade 300W and they were made from the same

steel plate from which the W-shaped stub columns of this grade were also fabricated. Coupons referred to herein as 350-1, 480-1, and 700-1 were of steel grades of 350W, 480W, and 700Q, respectively, and they were made from the same plates from which the stub columns associated with each of these steel grades were also produced. Coupons with labels of 350*, 480*, and 700* followed by numbers 1, 2 or 3 (ie. 480*-2) were the ones with the same steel grades as 350-1, 480-1, and 700-1, respectively, however with a difference. Even though these coupons had the same grades as those of 350-1, 480-1, and 700-1, they were actually made from steel plates of different batches. Thus the material characteristics obtained from 350*, 480*, and 700* coupons might not have the same material properties as the steel plates used to produce 350-1, 480-1, and 700-1 tensile coupons and the corresponding stub columns. In addition, it must be noted that the 480* coupons were made from an A516-70 steel plate stored in the laboratory. The material properties of A516-70 steel in the United States are similar to those of 480W steel in Canada (Stewart 1995). Therefore it was used to produce the 480* tensile coupons.

Residual stresses are always present in hot-rolled steel plates due to the different cooling rates in different portions of a steel plate during the steel producing process. Such residual stresses could be relieved when tensile coupons were made. However, additional residual stress could be introduced into a tensile coupon, depending on the way in which it was fabricated. All tensile coupons were supposed to be made from cold saw-cutting to minimize additional residual stress introduced to the tensile coupons. However, it appeared that the steel fabricator produced the 350* and 700* rectangular tensile strips by chopping off the

strips from steel plates, instead of using the cold saw-cutting method. The relief of residual stresses, in addition to the effect of possible impact loading, could result in an out-of-plane deformation in a tensile coupon. An amount of curvature (2 to 5 mm at the middle of the coupon, compared with the plate thickness of 6.4 mm) was measured with the 350* and 700* tensile coupons. Thus, possible gradual yielding in testing these tensile coupons could be expected. On the other hand, no curvature was observed in other tensile coupons. Therefore the results from these tests were expected to be more accurate.

3.2.2 Experimental Procedure

The tensile coupons were tested on a Material Testing System (MTS) with an axial load capacity set at 600 kN. As shown in Figure 3.2, this experimental setup consisted of two pairs of mechanical jaws, and devices for measuring the elongation of the coupon. The mechanical jaws were located within the loading platforms and were used to grip the tensile coupon. It can be seen that an 8" extensometer, a device with a linear voltage displacement transducer (LVDT), was placed on one side of the coupon. This longer extensometer had a gage length of 200 mm with the capacity of 75 mm in measuring elongation. It was intended to obtain data to study the overall behaviour of a coupon. Thus it was mounted on the coupon until the tensile test was completed. On the opposite side of the coupon, a 2" extensometer with a gage length of 50 mm was mounted. This extensometer was a more sensitive and accurate device in detecting elongation, but it had less capacity in measuring the overall lengthening of the coupon. The use of this extensometer was to acquire more accurate data in the elastic range so that a more accurate Young's modulus could be obtained.

Therefore, shortly after yielding occurred in each tensile test, the 2" extensometer was removed to avoid any possible damage caused from exceeding its measuring capacity. Both measuring devices were capable of transmitting the elongation of the coupon into voltages, which were then received by a data acquisition system and a computer. These voltages were multiplied by the corresponding calibration factors and then recorded by the computer. Thus the recorded data from the computer were the actual elongations in millimetres for each extensometer. The load applied on the coupon from the MTS loading machine was transferred and factored to the reading scale of kN in the computer system. All data were recorded in two second intervals. A real time display was made to visualize the stress-strain relationship during the test. This provided the convenience of monitoring the loading rate on the tensile coupon, and the overall performance of the test.

Prior to testing the width and thickness of each coupon at different locations along the section over which the extensometers were placed, were carefully measured. Such measurements were made within a tolerance of 1/100 of a millimetre and the average was taken from the above readings along the gage length. Variations for both the measurements of width and thickness were within 0.03 mm and they satisfied the tolerance required by ASTM (1994c) for the tensile coupons.

Before applying the axial load onto a tensile coupon, it was vertically aligned and centred with respect to the pulling jaws in order to avoid eccentricity with the coupon. The tensile coupon was then gripped on the machine by applying a small load on the pulling jaws. Prior

to each tensile test, the coupon was loaded, within the elastic range, at a relatively high rate of 7.6 mm (0.3 in) per minute until both ends of the coupon were fully gripped. This was done to avoid any possible slippage of the coupon along the gripping jaws during the actual test, especially at the initial loading stages. Then it was unloaded to the axial tensile load of approximately 2 kN required to grip the coupon firmly, and then it was ready to be loaded for the tensile test.

Upon loading, in the elastic range, the coupon could be loaded up to the proportional limit relatively fast. However, in order to obtain enough data points in the elastic range, the loading rate was set at 0.25mm (0.010 in) per minute. In the inelastic range the specimens were loaded at a rate of 0.89 mm (0.035 in) per minute until the test was completed. These loading rates were somewhat lower than that specified by ASTM (1992c), but they represented a better static behaviour of the tensile coupon (Stewart, 1995). All tensile coupons were loaded until rupture. Figure 3.3 shows some of the failed coupons after the tensile tests. All tensile coupons failed from rupture. In almost all of the coupons the rupture occurred within the domain of the extensometer gage length.

3.2.3 Observations and Test Results

The stress-strain relationship for each steel grade was derived from the applied load and associated elongation divided by the initial cross-sectional area and extensometer gage length, respectively. The initial cross-sectional area of a coupon was calculated from the measured width and the measured thickness prior to each tensile test. The resulting stress-

strain relationships for different steel grades are shown in Figure 3.4a to Figure 3.4d. In these figures, the curves with label 1, 2, and 3 (or *1, *2, and *3) correspond to the order in which the coupons were labelled and tested.

Figure 3.4a shows the stress-strain relationship for 300W grade steel. The stress-strain relationship in Figure 3.4a exhibits well defined elastic, yielding, strain-hardening, and necking ranges. As observed during tensile tests, tensile coupons of 300W grade represented the typical stress-strain relationship of mild-carbon or low strength steel as described in Chapter 1. However, it must be acknowledged that some unfortunate mistakes were made during the very first two tensile tests. An LVDT with measuring capacity of 25.4 mm (1 in) was mistakenly used for the first tensile test. Thus, there was no additional information, except for the ultimate strength, that could be obtained beyond the measuring capacity of the LVDT. Thus Figure 3.4a shows the results corresponding to specimens 2 and 3 only. Moreover, the 2" extensometer, which was intended to evaluate the stress-strain relationship more exactly in the elastic range, was improperly connected during the first two tensile tests. Consequently, the calculation of Young's modulus for the 300W steel relied solely on the data, associated with coupon 300-3, recorded from the 2" strain gage. Based on the results obtained from the 8" LVDT strain gage, the stress-strain relationship in the elastic range for coupons 300-1, 300-2, and 300-3 were the same. Therefore the Young's modulus calculated from the test on coupon 300-3 was considered reliable and acceptable.

Figure 3.4b shows the stress-strain relationships for 350W steel grade. The stress-strain

relationship of coupon 350-1 displays somewhat similar behaviour as did the 300W steel, except with a higher yield strength and ultimate strength, shorter yield plateau, and less overall elongated strain at rupture. Stress-strain curves associated with the 350* coupons showed the same relationship as that of coupon 350-1, except that there were no well defined yield plateaus. Perhaps the initial curvature, as described earlier, existing in the 350* coupons, accounts for such a difference.

Figure 3.4c shows the stress-strain relationships for coupons 480-1, 480*-1, 480*-2, and 480*-3. In this figure the stress-strain relationship of the 480-1 coupon, high strength low-alloy steel, had no obvious yield plateau. Instead, strain-hardening occurred immediately after the yield stress was reached. Results from coupon 480-1 showed that the yield and ultimate stresses were 600 MPa and 800 MPa respectively, which were much higher than the specified strengths. The percentage elongation over the 200 mm gage length was less than those of 300W and 350W coupons. However, the 480* coupons, which were made from A516-70 steel, had a lower yield stress than that specified and possessed the longest yield plateau among these selected steel grades. In addition, the 480* coupons had longer overall elongations than did the 350W steel. Furthermore, the test results from these 480* coupons are in agreement with the results obtained by Stewart (1995), who performed tensile tests on the coupons produced from the same steel plate. From these tensile tests, it was concluded that the steel grade associated with coupon 480-1 is much different than the steel grade associated with the 480* coupons. A516-70 steel did not display the material properties of 480W steel as expected and the source of the 480-1 coupon, which was claimed as 480W

steel by the supplier, was questionable.

Figure 3.4d shows the stress-strain relationships for 700Q steel, which is a high strength steel made from the quenching and tempering process. This grade steel behaved differently from those of mild-carbon steel and high strength low-alloy steel. Results from 700-1 and 700* coupons showed that steel of this grade had an obvious yield point but did not possess a well-defined yield and strain-hardening ranges. Compared with tensile coupons of other grades, the yield and ultimate stresses of this grade were very close to each other. All tensile coupons in this grade failed more quickly from rupture shortly after the ultimate strength was reached. Steel of this grade possessed the least percentage elongation over the gage length at failure. Thus it had the least material ductility in all steel grades considered in this study.

Stress-strain relationships for these four steel grades were plotted together in Figure 3.5 for better visual comparison. With the exception of 480-1 and 480* coupons, the experimental stress-strain relationships resulting from identical specimens were consistent. It was apparent that steel of all these four grades behaved linearly in the elastic range and slopes of the graphs appeared to be consistent to each other for all steel grades. Obviously the yield strength and the ultimate strength varies with the grade of steel. The lengths of the yield plateau for different steel grades varied from each other. Except for 480* coupons, the higher the steel strength, the shorter the yield plateau that was observed. The overall elongation of the coupons at rupture for each grade tended to decrease as the steel strength increased. After the ultimate strength was reached, failure from rupture occurred more

quickly in higher strength steel. This indicated that higher strength steel possessed less ductility and was more brittle, as mentioned previously.

The material properties were determined from these stress-strain relationships. A summary of the material properties corresponding to the steel grades considered in this study is presented in Table 3.1. As shown, the quantities calculated from the stress-strain relationships are the parameters E, f_y, ϵ_y, ϵ_{st}, f_u, ϵ_u, and ϵ_{rp}, which represent the material properties of Young's modulus, yield stress, ultimate stress, yield strain, strain-hardening strain, ultimate strain, and rupture strain, respectively. The ratios of f_u/f_y, ϵ_u/ϵ_y, and ϵ_{rp}/ϵ_y are also included in Table 3.1. The values of these parameters are the average from the tensile coupons of the same steel grade. Young's modulus, E, was calculated using linear regression based on the recorded data in the elastic range. The values of the Young's modulus corresponding to each steel grade are all larger than the generally accepted one, 200 GPa. The Young's modulus of these steel grades varies from 202 GPa for 700Q steel to 225 GPa for 480W (480* coupons) steel. It is evident that yield strengths, f_y, of all these steel grades except for 480W (480* coupons) steel, are higher than the corresponding specified strengths. The yield stresses of these tensile coupons are in the range from 335 MPa to 711 MPa, depending on the steel grades. The strain-hardening strain, ϵ_{st}, the strain level at the onset of strain-hardening, indicates the amount of plastic deformation that the steel can sustain. However, this strain-hardening strain was not applicable to 700Q steel, because there was no flat yield plateau in the stress-strain curves of this steel grade. The ultimate strength, f_u, of these coupons in each steel grade fall in the specified range, as indicated in Table 3.1. In

addition, the difference between yield and ultimate strengths depended on the steel grades and such differences can be interpreted as the ratio of f_u/f_y, the material reserve capacity. The ratio corresponding to each steel grade varied from 1.06 for the 700Q steel to 1.49 for 480W (480-1 coupon) steel. This reveals that the material reserve capacity for 700Q steel is comparatively low. On the other hand, the material reserve capacity of other steel grades are close to the same. The ultimate strain, ϵ_u, the strain at the stage where the ultimate strength was reached, measures the amount of strain that the steel can undergo prior to reaching the ultimate strength. Test results, as shown in Table 3.1, reveal that 300W grade steel possesses the highest ϵ_u and 700Q steel possesses the lowest. The rupture strain, ϵ_{rp}, the strain at which the coupon ruptures, is different from one steel grade to the other. For example, it varies from 0.1 for 700Q steel to 0.28 for 300W steel. The ratios of ϵ_u/ϵ_y, and ϵ_{rp}/ϵ_y represents the material ductility corresponding to the ultimate strain and rupture strain. The 700Q steel revealed the least material ductility and the 300W steel possessed the most. These differences between steel grades depended on, as discussed previously, the micro-structure of steel materials, which are affected from chemical constituents, presence of alloy, and physical treatments such as quenching and tempering.

3.3 Material Models for Different Steel Grades

In order to incorporate the stress-strain relationship into a finite-element model it is necessary to idealize the experimental stress-strain relationships. In material modelling, there are two common types of material idealization; bi-linear and tri-linear. Bi-linear modelling is generally the model of elastic and elasto-plastic idealization. Tri-linear modelling is usually

idealized with elastic, elasto-plastic, and strain-hardening ranges. Both of these material models were traditionally used in numerical analysis for mild-carbon steel, which had well defined yield point, yield plateau, and strain-hardening ranges. In Figure 3.6, the traditional idealized bi-linear and tri-linear models are shown (shown as conventional) with a schematic stress-strain relationship. It was clear that these two traditional material models did not accurately represent the actual material behaviour, especially the behaviour in the strain-hardening range. Also, as discussed earlier, the stress-strain relationship of high strength steel shows that strain-hardening occurred immediately after the yield stress was reached. Therefore the high strength steel material properties in the strain-hardening range have a great impact on the inelastic local buckling behaviour. In order to represent the material behaviour more accurately for both mild-carbon and high strength steel, multi-linear model was used to approximate the stress-strain relationship.

The multi-linear material models were derived based on the stress-strain relationship from tensile tests. These models are also shown from Figure 3.4a to Figure 3.4e accompanied with the experimental stress-strain curves for each corresponding steel grade. These models consist of line segments AB, BC, ..., EF, which are superimposed with the measured stress-strain curves. Each of these letters represents the significant co-ordinates for the idealization of the material model. As shown in Figure 3.4a, points A, B, and F, respectively, represent the yield point, co-ordinate at the onset of strain-hardening, and the point at which the ultimate stress is located. The yield point on the stress-strain curve was determined using the 0.2% offset method. Point B was located at the intersection of the actual stress-strain

curve and a line segment with a slope of approximately 1000, starting from point A. This slope is somewhat higher than the actual slope in plastic range. However, during the finite element analysis which will be discussed in Chapter 5, it was found that the material models with smaller slope than 1000 in segment AB did not give the reasonable results, compared with the experimental results. Therefore the slope of 1000 in segment AB was determined to use in the finite element modelling. Points C, D, and E represent the co-ordinates which equally divide the stress-strain curve between B and F, in terms of stress. Therefore point D is at the mid-stress level between points B and F. Points C and D are at the mid-stress level between points B and D, D and F, respectively. Similarly, material models for other steel grades can also be derived. All these material models are idealized to the actual material behaviour up to the point of ultimate strength. Material behaviour beyond the ultimate strength point was considered unstable because of the uncertainty associated with the necking and failure from rupture. However, for the completion of the material model representing the overall tensile stress-strain relationship, points G and H were added to approximate the stress-strain relationship beyond the ultimate strength. On the other hand, for the 700Q steel grade the assumed slope of 1000 did not intersect with the stress-strain curve. Therefore, point B was decided to locate at the ultimate stress level. As an exceptional case, points B to H are located at the same point on the stress-strain curve, therefore the material model of this steel grade was actually a bi-linear model. In all these material models, the stress and strain corresponding to the coordinates for points A to H were obtained from the stress-strain relationships for each steel grade and they are presented in Table 3.2. In Table 3.2, tangent modulus between the adjacent points were presented based

on the calculation of slopes of these line segments.

Even though a detailed multi-linear material model was derived, El-Ghazaly and Sherbourne (1985) indicated that the presence of the flat yield plateau in stress-strain relationship is misleading in a buckling analysis. Thus, a modified bi-linear and a modified tri-linear material model were also derived for the buckling analysis. Both the modified tri-linear and modified bi-linear material models were derived in a way to neglect the flat yield plateau. Based on the multi-linear models developed from the tensile stress-strain relationship, the tri-linear model was derived by connecting the line segment in the elastic range with AD and then DF to represent the material behaviour. For comparison purposes, a bi-linear model were modified by offsetting the line segment BC, which has largest tangent modulus in the strain-hardening range, to the yield point. These modified tri-linear and bi-linear material models are schematically shown in Figure 3.6, along with the traditional tri-linear and bi-linear models. All multi-linear material models derived from the corresponding tensile stress-strain relationships are compiled and shown in Figure 3.7, and these modified bi-linear and tri-linear models will be used in the finite element analysis presented in Chapter 5.

3.4 Treatment of Residual Stress

The way in which the W-shaped sections were fabricated results in built-in residual stresses. The residual stresses are caused by the uneven cooling rates at different portions of a section. The distribution pattern of residual stress in a W-shaped member is dependent on the method of fabrication, which introduces residual stress to the product unevenly. For W-shaped hot-

rolled sections, the flange tips and middle of the web would have cooled more quickly than the rest of the cross-section. Steel shrunk from cooling and this shrinkage of the warmer portion (i.e. junctions of web and flange) would likely exert a compressive force on the cooler flange tips and middle of the web. For a W-shaped section welded with flame-cut plates, tension along the flame-cut lines and compression in the middle of the plates are initially introduced from cutting. After welding to form a W-shaped section, the junction of the flange and web would have been heated and this caused less residual compression at this portion. However, such residual stresses are internal and they are in a self-balanced equilibrium state. Typical residual stress distributions in the flange and web of welded W-shaped sections are shown in Figure 3.8 (Galambos 1988).

It would be more practically sound and accurate to experimentally evaluate the distribution of residual stress on a welded W-shaped section. However, due to the time constraint in this study, the distribution and magnitudes of residual stress were assumed and idealized based on the experimental results from previous researchers (Galambos 1988 and Hancock 1991). Hancock (1991) investigated the residual stress of a welded W-shaped section with flame-cut plates. He found that, for a flange, the residual tension along the tips was 140 MPa. Also, the maximum residual compression in between the tip of a flange and the junction of web and flange was about 70 MPa. For a web, the residual stresses at the middle of the plate and at the junction of web and flange were 70 MPa (compression) and 140 MPa, respectively. The magnitudes of these residual stresses were dependent on the rate of flame cutting and welding. However, such information was not available for the specimens considered in his

study, thus these magnitudes were assumed to be applicable to the welded sections of this study. Based on the idealized distribution pattern of residual stress provided by Galambos (1988), a parabolic approximation was used for residual stress distribution over a welded W-shaped cross-section. Using this approximation, as shown in Figure 3.8, residual stresses over the cross-section of a welded W-shaped section could then be calculated from the above boundary values on web and flanges. Based on this idealization of the residual stress effects on such a welded W-shaped section, these calculated values will be incorporated in the finite element modelling part, which will be presented in Chapter 5.

Table 3.1 Material Properties of Various Steel Grades

Steel Grade		Material Properties									
		f_y (MPa)	ϵ_y	ϵ_{st}	f_u (MPa)	ϵ_u	ϵ_{rp}	f_u/f_y	ϵ_{st}/ϵ_y	ϵ_u/ϵ_y	ϵ_{rp}/ϵ_y
300W	Specified	300	-	-	380-450	-	-	-	-	-	-
	Tensile Test	335	0.0016	0.0174	498	0.1684	0.2751	1.49	10.88	105.25	171.94
		E = 209 GPa									
350W	Specified	350	-	-	480-550	-	-	-	-	-	-
	Tensile Test	406	0.0019	0.0082	542	0.1263	0.1912	1.34	4.32	66.47	100.63
		E = 209 GPa									
480W	Specified	480	-	-	450-550	-	-	-	-	-	-
	480W (Tensile Test)	590	0.0026	0.0026	814	0.0927	0.1443	1.38	1.00	35.65	55.50
		E = 215 GPa									
	A562-70 (Tensile Test)	454	0.0021	0.0265	591	0.1496	0.2364	1.30	-	71.24	112.57
		E = 225 GPa									
700Q	Specified	700	-	-	700-950	-	-	-		-	-
	Tensile Test	711	0.0035	0.0035	754	0.0606	0.0851	1.06	1.00	17.31	24.31
		E = 202 GPa									

Table 3.2 Significant Values for Various Material Models

Points	Material Properties					
	300W			350W		
	σ (MPa)	ε	E (MPa)	σ (MPa)	ε	E (MPa)
A	335	0.0016	E=209000	406	0.0019	E=209000
B	344	0.0168	E_{AB}=987	413	0.0088	E_{AB}=1014
C	375	0.0266	E_{BC}=3766	440	0.0173	E_{BC}=2952
D	416	0.0394	E_{CD}=2656	474	0.0309	E_{CD}=2494
E	457	0.0591	E_{DE}=1726	508	0.0515	E_{DE}=1647
F	498	0.1684	E_{EF}=393	542	0.1263	E_{EF}=455
G	491	0.2483	E_{FG}=n.a.	538	0.1665	E_{FG}=n.a.
H	384	0.2837	E_{GH}=n.a.	481	0.1912	E_{GH}=n.a.

Table 3.2 Significant Values for Various Material Models (cont'd...)

Points	Material Properties					
	480W			**480W - B** (same material as stub columns)		
	σ (MPa)	ε	E (MPa)	σ (MPa)	ε	E (MPa)
A	454	0.0021	E=225000	590	0.0026	E=215000
B	460	0.0334	E_{AB}=987	622	0.0064	E_{AB}=1053
C	488	0.0417	E_{BC}=3133	646	0.0146	E_{BC}=6341
D	522	0.0557	E_{CD}=1929	702	0.0236	E_{CD}=5889
E	556	0.0774	E_{DE}=1198	758	0.0409	E_{DE}=3006
F	591	0.1496	E_{EF}=374	814	0.0963	E_{EF}=957
G	580	0.2040	E_{FG}=n.a.	810	0.1232	E_{FG}=n.a.
H	516	0.2377	E_{GH}=n.a.	711	0.1443	E_{GH}=n.a.

Table 3.2 Significant Values for Various Material Models (cont'd...)

Points	Material Properties		
	700Q		
	σ (MPa)	ε	E (MPa)
A	711	0.0035	E=202000
B	719	0.0606	E_{AB}=998
C	721	0.0606	E_{BC}=n.a.
D	732	0.0606	E_{CD}=n.a.
E	743	0.0606	E_{DE}=n.a.
F	754	0.0606	E_{EF}=n.a.
G	748	0.0657	E_{FG}=n.a.
H	674	0.0863	E_{GH}=n.a.

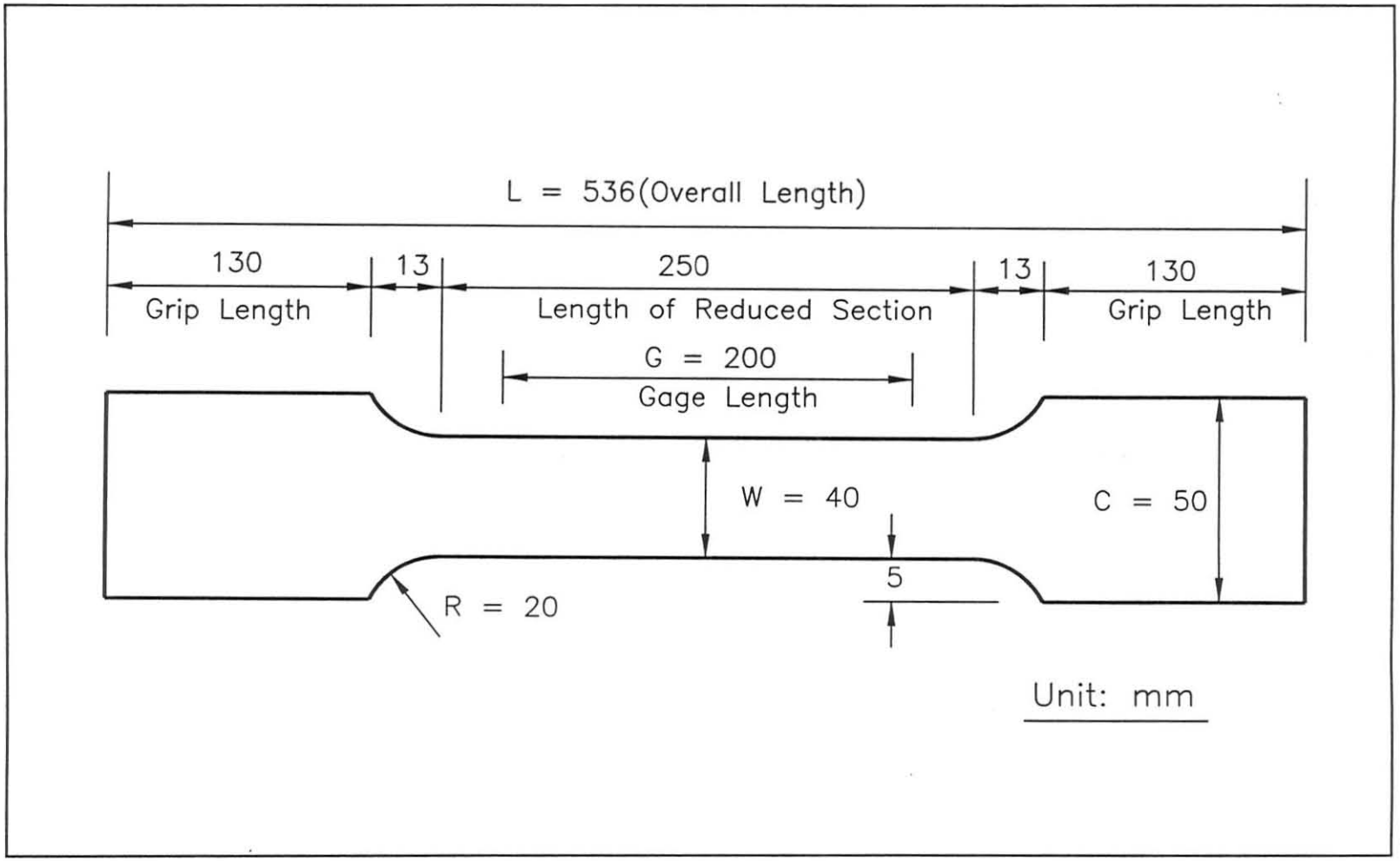

Figure 3.1 Dimensions of a Tensile Coupon

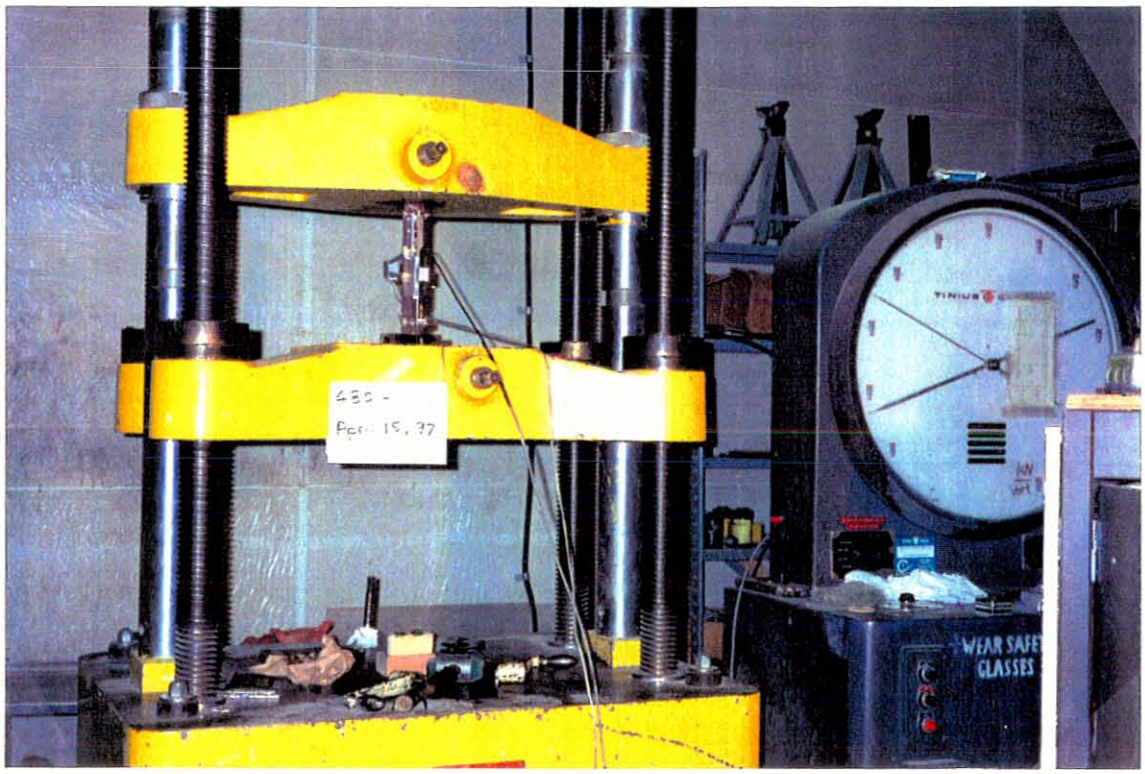

Figure 3.2 Experimental setup for tensile test

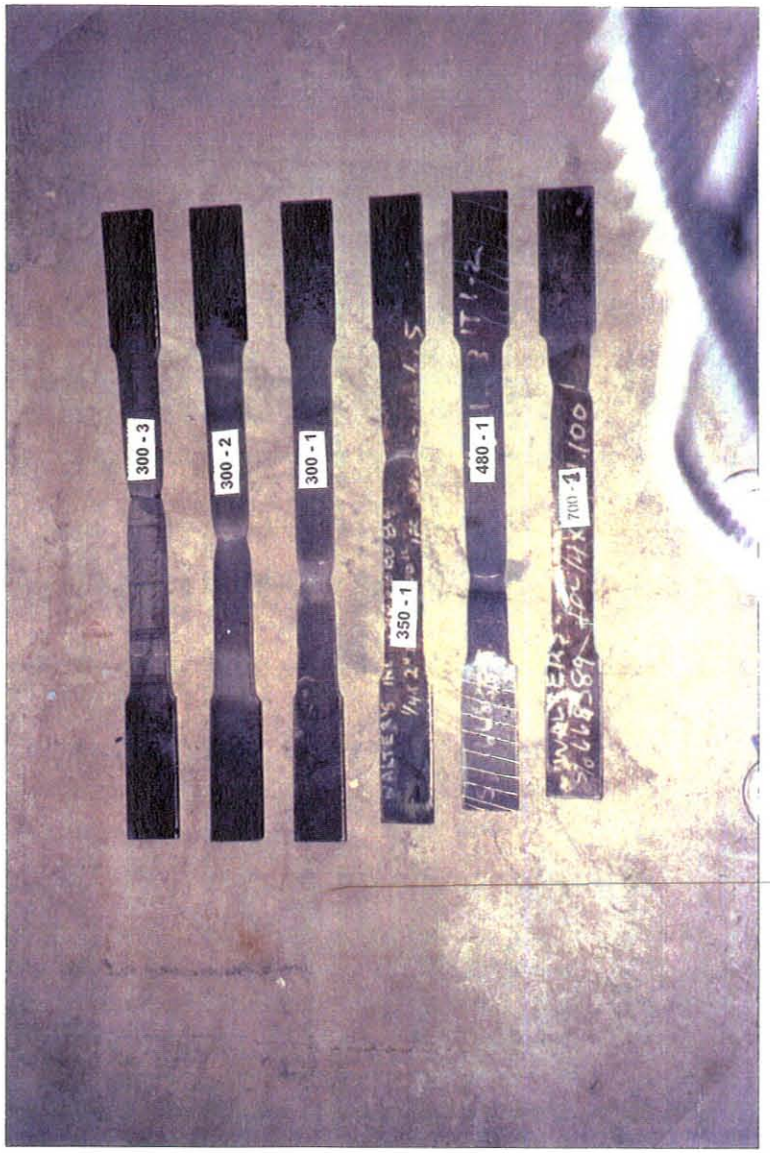

Figure 3.3 Ruptured tensile coupons

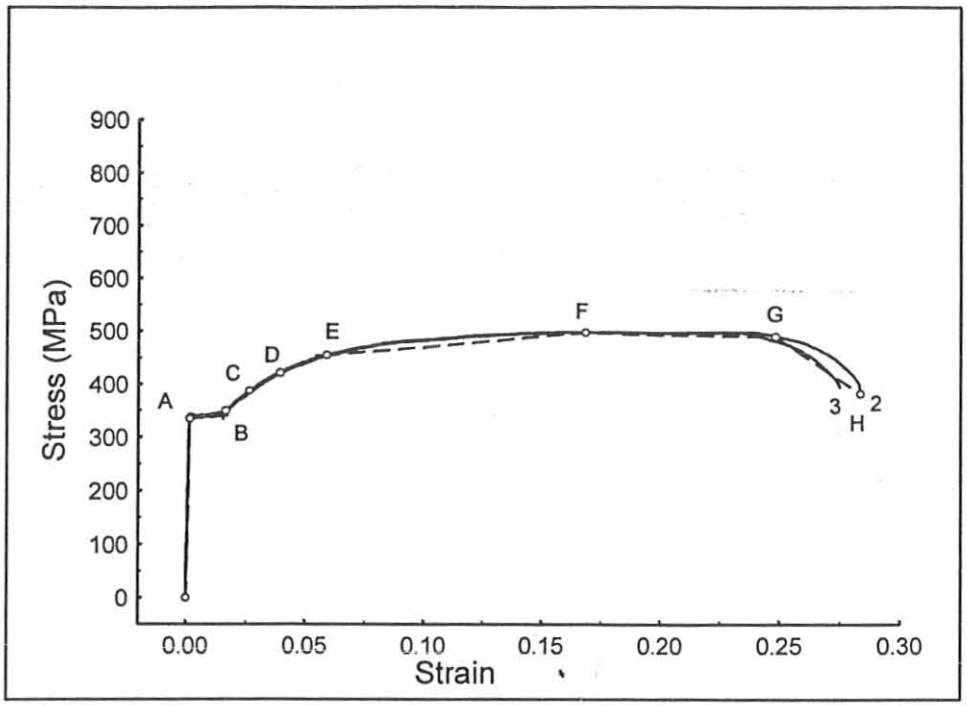

Figure 3.4a Stress-Strain Relationship of 300W Tensile Coupons

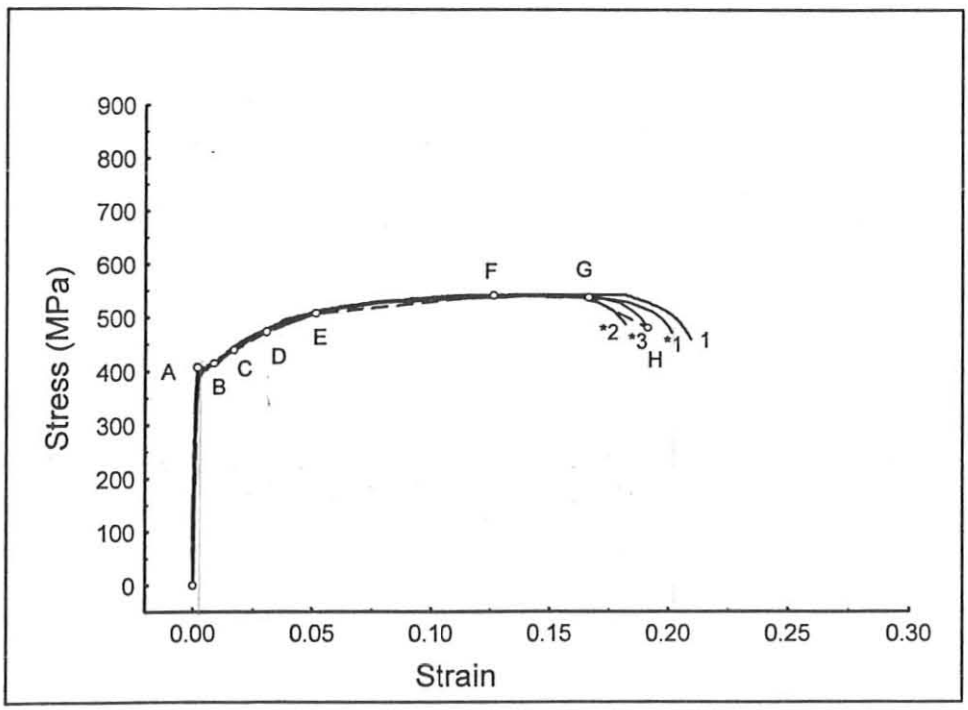

Figure 3.4b Stress-Strain Relationship of 350W Tensile Coupons

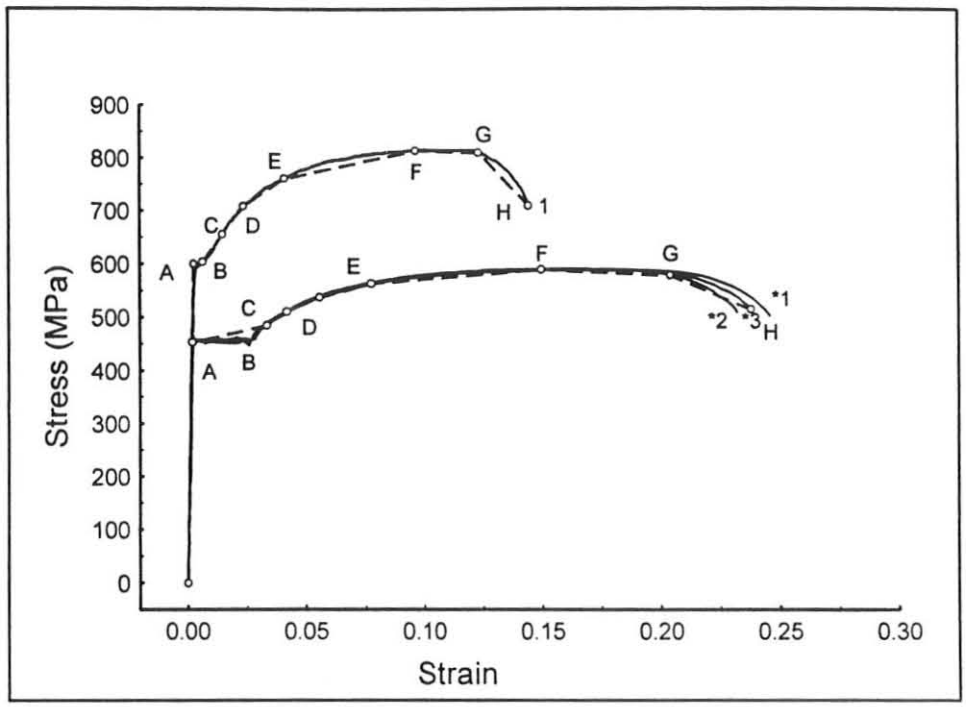

Figure 3.4c Stress-Strain Relationship of 480W Tensile Coupons

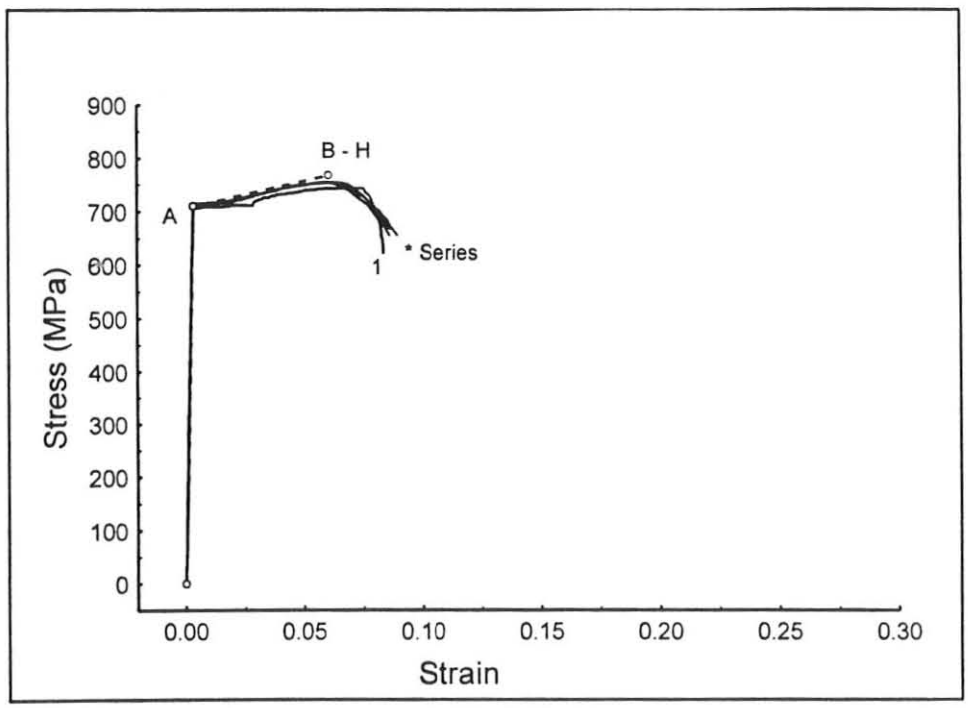

Figure 3.4d Stress-Strain Relationship of 700Q Tensile Coupons

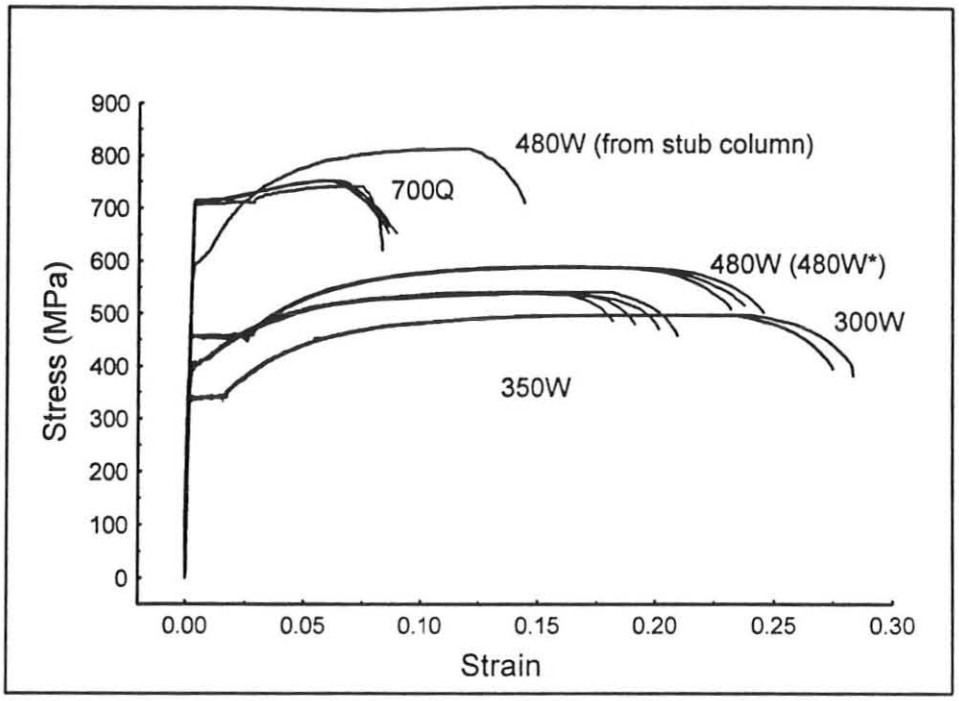

Figure 3.5 Stress-Strain Relationship of All Tensile Coupons

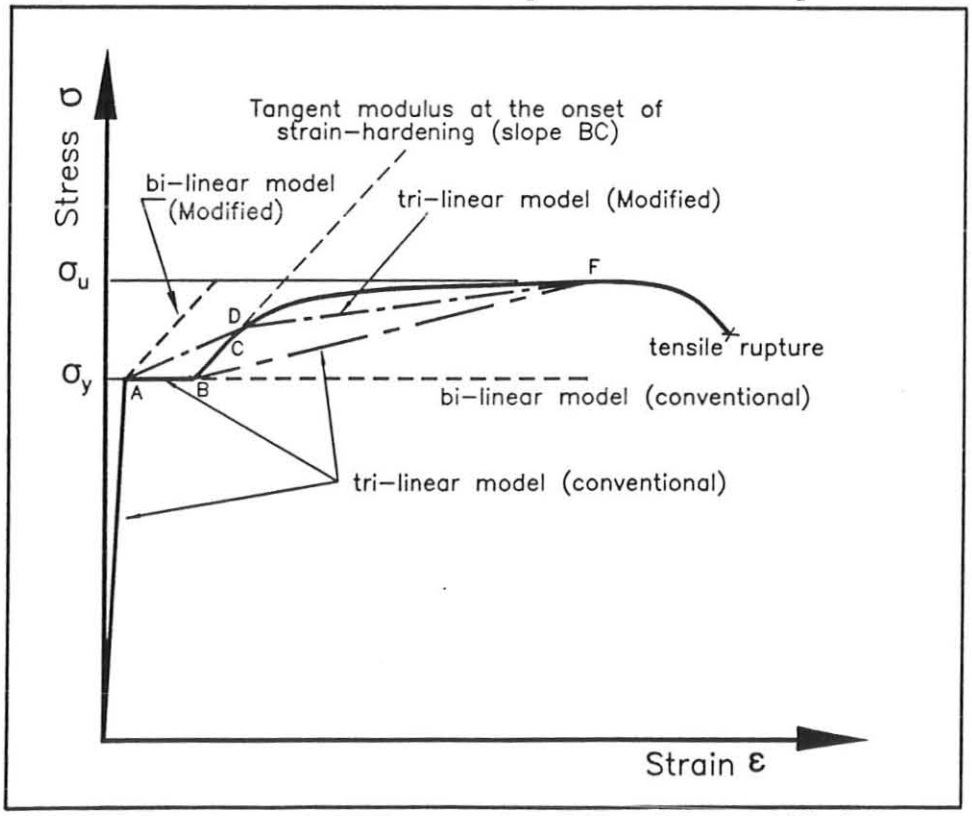

Figure 3.6 Schematic Bi-linear and Tri-linear Material Models

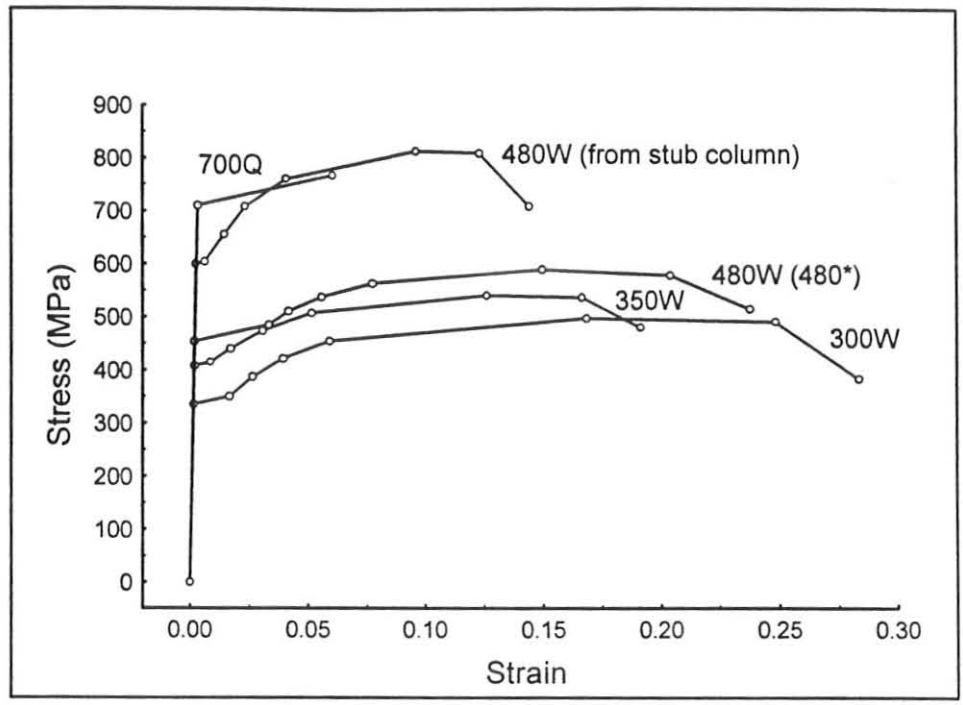

Figure 3.7 Material Models for Tested Tensile Coupons

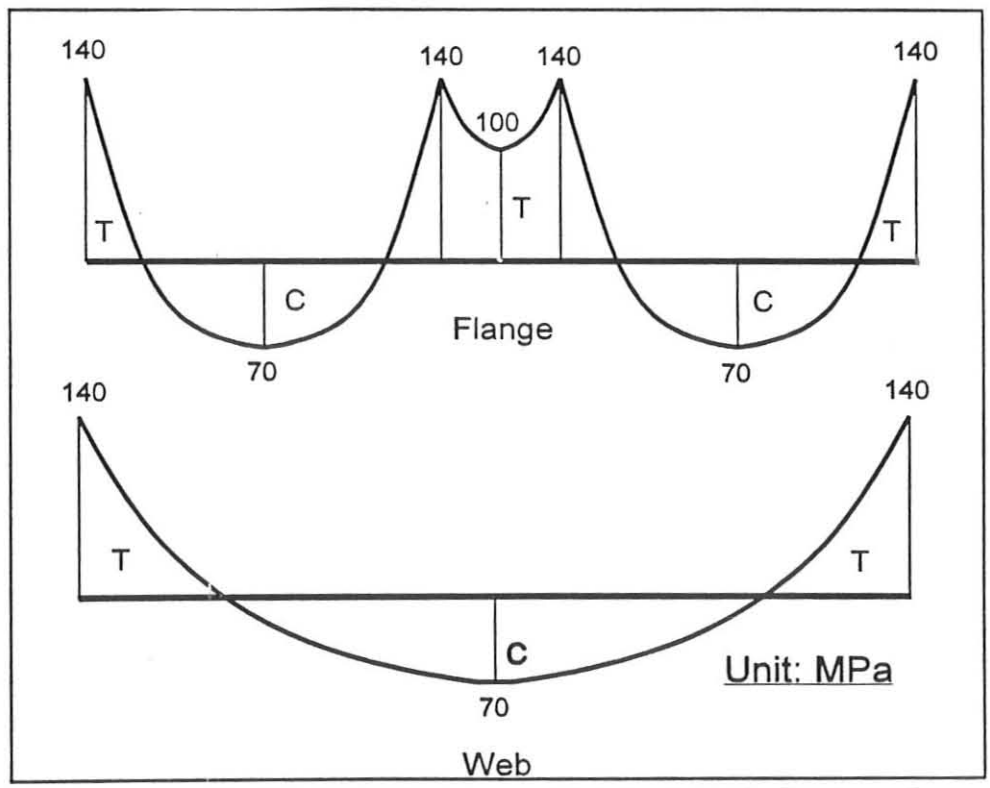

Figure 3.8 Idealized Residual Stress Distribution of a W-shaped Section Welded with Flame-Cut Plates

Chapter 4

Experimental Evaluation on Class 1 Stub Columns

4.1 Introduction

There are many ways to evaluate the local buckling behaviour of a W-shaped section. For example, conventional methods used by previous researchers (Haaijer 1958, Galambos 1965, Lay 1965, Dawe and Kulak 1984) included tests on stub columns, beam-columns, cantilever and simply supported beams. For Class 1 sections subjected to compression or flexural compression, the compression flange has the same behaviour regardless of the loading type. Since the interest of this study is concentrated on local buckling strain of the compression flanges of W-shaped sections, and high strength steels are more beneficial in column or beam-column designs, it is more practically sound to test a W-shaped section under compression. In addition, it is less complicated in the experimental set-up and more financially favourable in testing compression members than testing flexural members. Therefore, the stub column test was selected for the experimental part of this study.

When subjected to uniaxial compression, columns of W-shaped sections behave differently than tensile coupons because of the interaction between the web and flanges, and their susceptibility to local buckling. Class 1 sections are expected to exhibit substantial inelastic straining (ductility) prior to local buckling. In this chapter, the behaviour of Class 1 sections made of the steel grades presented in Chapter 3 will be investigated. Uniaxially compressed stub column tests were performed on Class 1 stub columns. The axial and out-of-plane

deformation behaviour of these stub columns will be of particular interest. The corresponding buckling load, ultimate load, and ductility of these stub columns (compression flanges) will be presented. Results obtained from this experimental evaluation will be used to verify the results from finite element modelling.

4.2 The Stub Column Specimens

There were a total of 13 stub column specimens tested under this study. One of the stub columns, the very first specimen, was made from a hot-rolled section of 300W steel. The estimated ultimate strength of this stub column was 2000 kN. This specimen was used as a trial test to evaluate the applicability of the experimental setup and to be familiar with the testing procedure. The remaining twelve specimens form the actual investigation. These specimens consisted of three identical specimens for each grade of 300W, 350W, 480W, and 700Q steels, which were fabricated and supplied by Walters Inc. in Hamilton, Ontario. The stub columns were of W-shape. The general configuration, and the dimensions of the stub columns are shown in Table 4.1.

As shown in Table 4.1, three of the identical stub columns of 300W grade were fabricated from a steel plate having nominal thickness of 9.5 mm (3/8 in). The remaining nine stub columns (three of the same size for each of the remaining steel grades) were fabricated from steel plates having a nominal thickness of 6.4 mm (1/4 in). Except for the trial hot-rolled section, in all of these twelve specimens, flange width was made equal to the web depth between flanges. All stub columns were designed for flanges at Class 1 limit for each grade.

Dimensions of flange width or web depth between flanges of Class 1 sections were determined based on the current CSA standard Class 1 limit ($b/t=145/\sqrt{F_y}$) described earlier in Chapter 1. The length of the stub columns for each steel grade was chosen to comply with the recommendations made by the Structural Stability Research Council (SSRC 1988). The selected length of stub columns was sufficiently short to avoid the overall instability effects, but sufficiently long to allow unrestrained development of local buckling and to eliminate the effects of frictional restraints at the ends on the plate strength. The web and both flanges were cut from the same plate corresponding to each grade. Care was taken to ensure that all component plates were cut from steel plates in the same orientation, in order to minimize anisotropic effects from the rolling direction (Hancock 1993). However, these component plates were fabricated from the flame-cutting method, thus additional residual stresses were introduced into these plate components. The specimens were welded by one pass of weldment on each side of the web, to produce approximate nominal weld leg lengths of 6 mm and 10 mm for plate components with nominal thicknesses of 6.4 mm and 9.5 mm, respectively. Dimensions of stub columns and the associated plate components are presented in Table 4.1, and also shown in Figures 4.1a to Figure 4.1d. For identification purposes the specimens were labelled using the corresponding steel grades followed by a number of 1, 2, or 3, representing the order of testing. For example, specimens 300-1, 300-2, and 300-3 were the specimens of 300W steel and specimen 300-1 was the first specimen of this grade to be tested.

The ends of the specimens were milled within the tolerance of ±0.13 mm(0.005 in) before

testing. This allowed proper seating on the supporting plates at both ends of the stub columns. With proper seating on the supporting plates, the possibility of eccentric loading to the stub column could be minimized and this also ensured that the applied load could be uniformly distributed over the entire cross-section of the specimen. The tolerance of ±0.13 mm at the parallel milled ends was the best that could be monitored in the machine shop at McMaster University. This tolerance was considered acceptable to allow stress to distribute evenly over a stub column when subjected to axial compression.

Initial imperfections of the flanges existed in all these stub columns. They were measured along the tips of the flanges at 30 mm intervals. The maximum initial imperfection of a stub column varied from 0.8 mm for stub columns of 700Q steel to 4 mm for stub columns of 300W steel. Initial imperfections associated with the stub columns of 300W steel could be visually noticed. The tips of the opposite flanges on one side of the web were bent towards each other, and about the junction of the web and flange. These initial imperfections with the 300W steel, along with other steel grades, were mostly caused from welding of the plate components. Welding introduced a massive amount of heat into the plate components, especially at the junction. During the cooling process, the tip of the flanges cooled down sooner than the portion at the junction. This caused the tips to bend about the junction of the web and flange. Overall, the larger the width of the flange, the greater the measured initial imperfection. Stub columns of 300W steel had the largest dimensions of all these stub columns, thus initial imperfections of this steel grade were found to be the highest among specimens.

4.3 Experimental Setup and Procedure

Overall Setup

Stub columns were tested using an experimental setup as shown in Figures 4.2a to Figure 4.2c. This closed loop experimental setup was restrained by two pairs of C channels on the top and the bottom, and by two vertical columns. The pair of C channels were bolted to the flanges of the W-shaped supporting columns using six bolts at each end. The stub columns are tested between two smooth supporting plates as shown in the figures. These supporting plates are referred to here as top supporting plate and middle supporting plate. The top supporting plate was first securely clamped, at both ends of the plate, against the C channels using two pairs of L-angles traversing the C- channels. The middle supporting plate was placed with two ends sitting on top of a roller and a pin. The roller and pin supports rested on top of two separate load cells as shown in Figure 4.2c. When a force is applied to the stub column through these plates, the supporting plates act like beams with a very short span. The plates were chosen to be sufficiently thick having a thickness of 114 mm (4.5 in) in order to minimize the deflection caused by the load transferred from the stub column. The calculated maximum deflection of these supporting plates when subjected to a central point load of 2400 kN, which was a much larger load than the maximum load applied to the stub columns, was less than 0.05 mm. This deflection on both of the supporting plates was considered negligible.

Two load cells having a capacity of 1600 kN each, were used to measure the total load applied to the stub column. The load cells were placed on top of two loading jacks. These

loading jacks were double-acting loading cylinders, which can be used as a displacement controlled loading jack. Each of the loading jacks was connected with two pairs of hydraulic hoses to two separate manually controlled hydraulic pumps. These loading jacks were rested on the bottom plate, which was supported by the bottom two C channels. The loading jacks were arranged in such a way that the deflection of the plate supporting the loading jacks could be minimized. As shown in Figure 4.2c, this was achieved by aligning the centre line of each loading jack to the web of each supporting C channel as closely as possible.

To ensure the overall applicability and safety of this experimental set-up, additional calculations on the strength (shear and/or bearing strength), and the corresponding deformations of the supporting C channels, supporting columns, bolts (A490) connecting the C channels and supporting columns were carried out. It was found that the deformations of these structural components of the experimental set-up were negligible and they could satisfactorily withstand a maximum load, 2400 kN, which may be transferred from the stub column. The largest estimated squash load, which is defined as the product of the cross-sectional area of the column, and the ultimate strength of the tensile coupons corresponding to each steel grade, was 2000 kN in all these thirteen stub columns. Therefore this experimental set-up was considered applicable and safe. This was also verified by a pilot test, which will be discussed in the subsequent sections.

Placement of LVDTs

Linear voltage displacement transducers (LVDT) were placed to monitor the flexibility, and the movements in the test reaction frames, and to record the axial deformation, and also the lateral deformations of the flanges at the mid-height of the stub column. During the pilot test three additional LVDTs were used to examine the possibility of uneven displacement at the supporting plates, and to measure the flexibility of the reaction frame. As shown in Figure 4.2c, one LVDT was placed on top of the supporting plate to measure the central deflection of the supporting plate. The other two LVDTs were placed (not shown in the figures) on the top flange of each supporting C channel. It was found, after the trial test, that the differences between the measurements of these two LVDTs were less than 0.1 mm. Thus it was considered that the top supporting end, including the supporting plate and two C channels, deformed evenly. Therefore, only the LVDT at the centre of the top supporting plate was used during the testing of the rest of the specimens. Due to the use of two loading jacks, and because of the separate control of the loading cylinders, there was a possibility that the loading cylinders raised unevenly and thus might be causing an eccentric loading to the stub column. To ensure that the middle supporting plate was raised evenly at both ends so that the stub column was compressed uniformly, two LVDTs were placed to measure the displacements of both ends of the plate supporting the lower end of the specimen (see Figure 4.2.c). The relative displacement between the upper and lower supporting plates, which is also the axial deformation of the stub column specimen, was obtained from the difference between the LVDT reading at the top of the upper supporting plate and the average reading of two LVDTs measuring the displacement of the middle plate supporting the lower end of

the stub column. Five other LVDTs were placed at the mid-height of the specimen. The placements of these LVDTs are presented in Figure 4.3. These LVDTs were used to monitor the out-of-plane displacements, and the rotations at the mid-height, which are associated with the local buckling behaviour. One of these five LVDTs was located at the middle of the web to observe the web buckling and the remaining four were positioned at the tip of the flanges to detect the flange buckling.

Placement of Strain Gages

Strain gages were used to obtain the local strains of a specimen, which will be used to study the local buckling behaviour of compression flanges. They were also used for aligning of each specimen in order to avoid eccentric loading to the specimen during each test. The strain gages were selected to have a maximum measuring capacity of 10% strain, so that the stress-strain relationship beyond yielding could be determined. Thus, inelastic local buckling of compression flanges could be detected. Strain gages were placed symmetrically about the mid-height of the specimen and in the direction along the length of the stub column. They were glued onto the specimen as a pair, in the opposite positions at the tip of one of the flanges, as shown in Figure 4.3. Utilizing the doubly symmetric characteristics about the major and minor axes of a W-shaped section when subjected to uniform compression, only four strain gages were used with each specimen in order to minimize the number. Both pairs of strain gages were set at the tip of the flanges diagonally about the centroid of the cross-section. Such an arrangement can be used to ensure the symmetric behaviour by aligning the specimen properly. It can also be used to determine the local buckling behaviour of the

compression flanges based on the information obtained from at least one pair of the strain gages.

Data Acquisition

Signals from the LVDTs, the strain gages, and the load cells were received as voltages by the data acquisition system. Using the computer with the LABTECH NOTEBOOK software, the voltages were transferred to actual readings, such as displacement in mm and load in kN, by multiplying each signal input by a corresponding calibration factor. The real time relationships of axial load versus average axial deformation, and average axial stress versus lateral deformations and local strains, at the mid-height of the specimen, were displayed on the computer screen. This provided the convenience of observing the local buckling behaviour and monitoring of the whole test. Two sets of data were recorded by the computer. One set was recorded at an interval of every one second for the purpose of real time display on the screen, and the other set was recorded by keyboard control so that only the significant data points in this experimental study were acquired at appropriate time intervals.

Test Procedure

A pilot test on a stub column of 300W grade was performed to examine the adequacy, applicability and safety of the whole experimental setup. The experimental ultimate load of this stub column was 1830 kN. The measurements of the deformations at the top supporting plate, and at the C channels were in the vicinity of the values calculated earlier. The results

from this pilot test experimentally proved that this test setup was satisfactory and it could resist a load exceeding 1830 kN. The maximum squash load of the remaining twelve specimens was less than 1830 kN and thus they were tested using the same experimental setup without further modifications.

Initial alignment of the specimen within the test setup was an important step in the stub column testing procedure. As discussed earlier, proper alignment allows the applied load to be evenly distributed over the cross-section of the specimen. Initially the stub column was carefully aligned geometrically, by allowing its centroid to coincide with the centre of the steel plate supporting the lower end of the column. The centre of this supporting plate was also located at the middle of the span between the pin and roller supports. After this initial alignment, the plate was raised very slowly by applying hydraulic pressure to both of the loading jacks. Both loading jacks were raised at the same incremental displacement simultaneously. When the specimen was in contact with the top supporting plate, the seatings at both ends of the specimen were carefully checked, by using a filler gage of 0.13 mm (0.005 in). The column was then loaded within the proportional limit, up to the average axial stress of approximately 100 MPa. In order to ensure that the axial stresses were essentially uniform, differences between the strains obtained from the strain gages at the flange tips were calculated, and checked against the pre-set strain tolerance of ±5% of the average strain. If this criteria was not met, the specimen was unloaded and shifted slightly over the centre of the supporting plate, and then was loaded again. This procedure was repeated until this predetermined strain tolerance criterion was met. Once satisfying the

alignment tolerance, the specimen was unloaded to a load of 2 kN to secure the specimen and maintain the acceptable alignment. This procedure ensures a concentric loading of the stub columns.

After the specimen was aligned, the actual test could proceed. The test load was applied to the stub column slowly, using the displacement control method. The incremental displacement, or the axial deformation of the specimen, was controlled by monitoring the real time display of the relative displacements between the top and bottom supporting plates. In order to obtain sufficient data points in the elastic range, the incremental displacement was set at 0.04 mm in this range. After yielding, which was evident by the non-linearity in the load-deformation curve, the incremental displacement was set at 0.08 mm before the peak load was reached. Beyond the peak load, a larger incremental displacement of 0.1~0.15 mm was used. The data recorded by the keyboard control method were taken about one minute after each incremental displacement was reached. This provided sufficient time to allow stress to redistribute within the cross-section and along the length of the specimen. The data recorded by the keyboard activated control method constituted the final experimental results.

4.4 Experimental Observations

Figure 4.4 shows some of the specimens removed after the tests. All specimens eventually experienced local buckling failure. It was also observed during each test that all stub columns could sustain average axial stresses higher than the corresponding material yield stress. The experimentally observed maximum loads of all the specimens were lower than the calculated ultimate or squash load. The calculated ultimate loads here are simply the

cross-sectional area x the ultimate strength of each corresponding steel grade. These calculated ultimate loads were used as a guideline only for the tests. After the plastic range was reached, gradual yielding was observed from the average axial stress to average axial strain curves on the real time display. The specimens did not fail rapidly after the peak load was reached. Instead, they failed gradually and this proved the desired ductility possessed by the Class 1 compression flanges. More specific experimental observations associated with the specimens of each steel grade will be described in following subsections.

300W Grade Steel

Figures 4.6A, 4.7A, and 4.8A show the experimental results corresponding to the 300W steel grade stub columns. Stub columns of this 300W grade could withstand the average applied axial stress exceeding the material yield stress of 335 MPa, which was determined from the tensile test. Prior to reaching this yield stress, the real-time average axial stress versus average axial strain relationship showed that all the specimens of this grade started to behave non-linearly when the applied average stress reached approximately 250 MPa. Gradual yielding was observed in all these three stub columns and no well-defined yield plateau was noticed. After gradual yielding, strain-hardening was observed up to about 0.02 strain, where the maximum average stress of approximately 400 MPa was reached. Beyond the peak stress, stress tended to decrease gradually and this behaviour differed from the behaviour observed during the tensile test. Recall that the tensile coupon tests showed that the tensile stress decreased rapidly beyond the ultimate stress until rupture.

In all these three specimens of 300W steel grade, local buckling was observed in the vicinity

of peak stress. The first indication of local buckling with one half sine wave near the mid-height of the specimen occurred shortly after the peak stress was reached. As the local buckling with one half-sine wave started to propagate, at an average stress level of approximately 340 MPa beyond the peak stress, the local buckling shape with three half-sine waves was observed in all three specimens. The buckling shapes at the flanges of all three specimens showed that flanges buckled towards each other on one side of the web and, on the other side of the web, they buckled away from each other. These buckling forms at both sides of the web occurred at the same height of the column. On the other hand, no local buckling of the web was observed when local buckling first occurred at the tips of the flanges. However, as the local buckling propagated along the tips of the flanges, local buckling of the web was also noticed. Since this experimental study was intended to concentrate on the local buckling behaviour of the compression flanges of W-shaped sections, the buckling behaviour of the web component will not be further discussed.

Unfortunately, perhaps due to the end conditions, the first local buckling in all these three specimens did not occur exactly at the mid-height of the columns, but rather in the vicinity of the mid-height. Specimens 300-1 and 300-3 showed that the first local buckling occurred at the location approximately 20 and 30 mm, respectively, above the mid-height of the column. The first local buckling of specimen 300-2 was located at about 30 mm below the mid-height of the column. Thus the data obtained from the LVDTs and strain gages, which were all placed at the mid-height of the specimens and were intended to detect the local buckling of the flanges, might not provide accurate information in studying the local buckling behaviour of the stub columns. However, the half sine buckling wave length of the

buckling shape was observed to be quite large, which indicated that flange buckling propagated to the mid-height of the specimen shortly after being initiated. Therefore, information obtained from the LVDTs and strain gages on these specimens were deemed to still be useful in studying the local buckling behaviour.

Strain gages glued at the mid-height of the specimen were used to determine the local buckling strength based on the strain reversal method, which will be discussed later in this chapter. It was expected that the average axial stress to strain curves would show the linear relationship of these two parameters before the yield stress was reached. In the real-time displays, some of these curves showed non-linear behaviour at a stress level as low as 200 MPa. This undesired early non-linear behaviour observed from the average axial stress-strain curves was possibly caused by the initial imperfections with the specimens.

350W Grade Steel

Figures 4.6B, 4.7B, and 4.8B show the experimental results corresponding to the 350W steel grade stub columns. Stub columns of this grade behaved somewhat similarly to that of 300W grade steel described previously. Three specimens could easily sustain the material yield stress of 406 MPa, which was obtained from the tensile test. Non-linear characteristics were revealed from the real time relationships between the average axial stress and average axial strain in these specimens when the average stress exceeded 300 MPa. Rather than a well-defined yield plateau, gradual yielding was observed. Upon the completion of gradual yielding, strain-hardening was observed up to the approximate strain of 0.20~0.25, where the maximum stress was achieved. The average axial stress of the specimens of this grade,

similar to those of 300W grade steel, tended to decrease gradually beyond the peak stress.

In the vicinity of the maximum average stress of these three specimens, visual local buckling was noticed. A half sine wave occurred in specimen 350-1 exactly at the mid-height of the stub column and the half wave length of the buckle shape started to propagate beyond the peak stress. No other half sine waves were observed throughout the test on this specimen. Data obtained from the LVDTs and strain gages located at the mid-height of the specimen provided excellent information with which to study the local buckling behaviour of the compression flanges of the stub columns in this steel grade. On the other hand, the first half sine wave in specimen 350-2 was located 30 mm below mid-height, which was observed shortly after the peak average stress, 461 MPa, was reached. As the first buckled half sine wave started to propagate, a second half sine wave was observed at about 25 mm above the mid-height of the specimen at a stress level of about 420 MPa. The crest of the first and second half sine waves was approximately symmetric about the mid-height of the specimen and this led to very small lateral displacements at the mid-height of the specimen. However, strain reversal on the convex side of the buckled flange was detected by the strain gages. The explanation for this is that the first and second half sine waves were not exactly symmetric about the mid-height and they did occur simultaneously. Specimen 350-3 had the first half sine wave at about 60 mm above the mid-height of the stub column, which occurred shortly after the peak stress was reached. This half sine wave started to propagate even though the average stress decreased. At an average stress level of approximately 390 MPa, a second sine wave was observed at the mid-height of the specimen. The length of the second half sine wave was considerably shorter than that of the first half sine wave. This second buckled

sine wave occurred almost at the end of the test on specimen 350-3. Therefore the data obtained from the LVDTs and strain gages located at the mid-height of this specimen were insignificant in determining the local buckling load, because the lateral displacement at the mid-height and the strain reversal were detected at a stage much later than when the first flange local buckling actually began.

The buckled shapes of the flanges of all three specimens of this grade showed that if one tip of a flange buckled towards the major axis of the cross-section, the opposite tip of the other flange buckled in the same direction. At the same height where the flanges buckled towards each other, the other side of the same flange tended to buckled away from the major axis of the cross-section. This showed that, when subjected to uniform compression, the flanges of the stub column of this grade behaved symmetrically about both the major and minor axis of the cross-section. This behaviour is similar to that of specimens of 300W steel grade, which were discussed in the previous section. In the real time display, the curves corresponding to the average axial stress and local strains showed very little or no strain deviation from each other in the range prior to reaching the yield stress. This indicated that the specimens of this grade possessed few imperfections and were in agreement with the measurements on imperfections prior to each test.

480W Grade Steel

Prior to the discussion of the experimental observations on the stub columns of this steel grade, it must be noted again that the source of this steel grade was questionable. The results from the tensile test (Chapter 3) revealed that the steel used in the fabrication of these stub

columns possessed much higher yield stresses than the specified yield strength of 480 MPa. As described previously in this chapter, the dimensions of the stub columns, which were designated as Class 1, were pre-determined solely based on a function of $\sqrt{F_y}$. Without knowing the yield stress of the steel plate prior to the assembly of the stub columns, an F_y value of 480 MPa was used in the calculations of the flange and web dimensions as shown in Table 4.1. However, in view of the larger material yield strength, these stub column specimens could possibly fall in the category of Class 2 sections. Unfortunately, with such an abnormally high yield strength compared with the specified value, it was considered that the results obtained from this category could not correctly represent the W-shaped sections of the 480W steel.

Figures 4.6C, 4.7C, and 4.8C show the experimental results corresponding to 480W steel grade stub columns. All these three specimens could sustain an average axial stress higher than the material tensile strength of 590 MPa. However, prior to reaching the yield stress, substantial non-linear deviation in the real time display of the relationship between the average axial stress and the average axial strain was observed. The explanation of this early non-linear behaviour is that local buckling may have occurred at the stage before the yield stress was achieved.

Visually local buckling was first observed, in all these specimens, in the range where the yield stress was reached. However, none of these specimens had a local buckling wave near the mid-height, and the half buckled sine waves did not propagate as much as those of the stub columns made from 300W and 350W steels. In all these stub columns, local buckling

with two half sine waves was later developed at average axial stresses beyond the peak stress. Specimen 480-1 had both local buckling waves above the mid-height. Therefore the LVDTs located at the mid-height of this specimen could barely detect any lateral deformations. Specimen 480-2 had the first buckling wave occur 35 mm above the mid-height and the second buckling wave 40 mm below the mid-height. Specimen 480-3 had the first and second buckling waves occur at locations similar to those of specimen 480-2. There were small lateral deformations at the mid-height of these specimens. Therefore information obtained from these devices at the mid-height of these two specimens were insufficient for the purposes of studying the local buckling behaviour.

Strain gages located at the mid-height of these specimens experienced a similar discrepancy in detecting the occurrence of local buckling. Some of the strain gages, however, revealed that strain reversal occurred at higher stresses, which were near the maximum stress that the specimen could sustain. However, in all three specimens, the strain gauge based occurrence of local buckling at the flange were not in agreement with local buckling that was visually observed during the test, which was shortly after the yield stress was reached. As explained previously, it could be that the strain reversal was not detected until the local buckling wave has propagated to the location where the strain gages were placed.

700Q Grade Steel

Figures 4.6D, 4.7D, and 4.8D show the experimental results corresponding to the 700Q steel grade stub columns. Stub columns of this steel grade had the highest yield strength in this experimental study. Specimens in this category could sustain the applied average axial stress

greater than the material yield stress of 711 MPa, which was determined from the tensile test. Prior to reaching the yield stress, the real-time relationship between the average axial stress and average axial strain displayed that there was only trivial non-linear behaviour. This indicated that the effects of imperfections and residual stress associated with these specimens may be insignificant. Compared with the behaviour observed from the tensile test, the axial stress-strain curves showed no sharp yield point. Instead, gradual yielding was observed. After the stage of gradual yielding, strain-hardening with relatively low modulus of strain-hardening was noticed. Similar to the behaviour of stub columns from other steel grades, specimens of this group did not fail rapidly after the maximum stress was reached, but failed slowly in a rather gradual decrease in the average axial stress.

Visually, local buckling was observed in the vicinity of the maximum average axial stress, which was about 780 MPa. The local buckling behaviour of the stub columns in this grade differed from those of other grades, of which the buckling behaviour was discussed previously. Stub columns of other grades tended to display symmetric local buckling and they showed that if the tips of the flanges on one side of the web buckled towards each other, on the other side of the web at the same height of the stub column, the tips of the flanges buckled away from each other. The stub columns of 700Q steel did not behave in this way. Rather, the buckling shapes on the flanges were very erratic and were not symmetric. On the same side of the web, one tip of a flange buckled into as many as four half sine waves and the tip of the opposite flange buckled into only two half sine waves. The first buckling waves in specimen 700-1 and 700-2 tended to be symmetric about the centre-line of the web, but the subsequent buckled half sine waves showed unsymmetric forms. The first buckling

half sine waves in specimen 700-3 had unsymmetric buckled shapes, which showed that the tips of the flanges on the same side of the web buckled in the same direction. This unsymmetric local buckling behaviour could be caused by friction effect at the ends of the stub column. Compared with stub columns of other steel grades, stub columns of this steel grade had the shortest length and smallest cross-section area, and they were subjected to the highest axial compression. Therefore stub column of 700Q steel may have the most severe friction effect and this effect could have extended throughout the whole length of the specimen. In addition, this friction effect differed from one specimen to the other, depending on the degree of eccentric loading. Therefore, compression flanges might have been subjected to nonuniform compression and this could have caused that specimen 700-3 had the unsymmetric buckled shapes.

As discussed earlier, measurements from the LVDTs and strain gages relied heavily on the actual location where local buckling occurred. If local buckling started at some location other than the mid-height, then at least it should propagate to the mid-height of the specimen. Specimens 700-2 and 700-3 had the first local buckling start closer to the mid-height than did specimen 700-1. Therefore the information obtained from specimens 700-2 and 700-3 were more satisfactory to study the local buckling behaviour than that acquired from specimen 700-1.

4.5 Experimental Results

Average Axial Stress and Average Axial Strain Relationship

In summary, the average axial stress and average axial strain relationships for the stub columns under consideration are shown in Figure 4.5A to Figure 4.5E. The results from the stub columns of each steel grade exhibit somewhat similar average stress-average strain relationship up to the maximum average stress, an average stress level where most visual local buckling was first noticed. Beyond the maximum load, these average stress-strain curves of the specimens made from even the same steel grade started to deviate from each other, even though they have the same geometric dimensions. The explanation for this may be that the stub columns of the same grade may have different initial imperfections and the end conditions were different in each test. The behaviour beyond the maximum load tended to be less stable, and it was difficult to maintain consistent incremental displacements using the manually controlled hydraulic pumps.

The average axial stress and the average axial strain relationships of all the stub columns in this study, as described previously, showed that the compression flanges of Class 1 stub columns could sustain an average stress above the material yield stress and they appeared to be quite ductile. These relationships also revealed that the stub columns tended to yield gradually rather than to yield with a sharp yield point associated with the tensile coupon tests, as described in Chapter 3.

The Ductility of Compression Flanges of a Stub Column

The method to quantify the ductility of compression flanges of stub columns may be analogous to that used in quantifying the ductility of beams under a central point load causing moment gradient to the specimen, as described in Chapter 1. Here the ductility associated with the specified strength is quantified by measuring the available inelastic strain, ε_p, as shown in Figure 4.5A, over ε_y. It can be seen that in the plastic range, a certain amount of average stress exceeds its yield stress obtained from tensile tests. Since gradual yielding was observed in all these stub column tests and the yield stress obtained from tensile tests are usually higher than the associated specified yield stress, parameters corresponding to the specified yield stress will be considered in quantifying the ductility of compression flanges of the stub columns. Under conditions of uniform axial compression, ε_p reflects the inelastic behaviour of the compression flanges and ε_y is the yield strain, at the stress level of the specified yield stress, of the specimen. The quantified ductility, using the symbol D, is described in a non-dimensional form as $D=\varepsilon_p/\varepsilon_y$. In addition, two other terms D_u and D_1, which were the quantified compression flange ductility associated with the ultimate load and the local buckling load, respectively, can also be defined in a similar way. Instead of ε_p, strains corresponding to the ultimate load and local buckling load were respectively used in determining the quantities of D_u and D_1. Based on these definitions, the quantified ductility associated with the compression flanges of the stub columns were found and presented in Table 4.2. Results showed that the ductility associated with the ultimate load and local buckling load were relatively low compared with the ductility associated with the specified strength of each streel grade. The 350W steel revealed that it had considerable ductility and

the amount of ductility was comparable with that of the 300W steel, which was used to determine the b/t limits in the current design standard (CSA 1995). The compression flange ductility associated with the 480W and 700Q steel were lower than those of 300W and 350W steel. In terms of compression flange ductility, the Class 1 b/t limit ($b/t = 145/\sqrt{F_y}$) defined from the 300W steel may also be applied to the 350W steel. On the other hand, the compression flange ductility of the stub column associated with the 700Q steel was calculated to be 5.6, and this is much lower than that of the 300W and 350W steel. Therefore, the b/t limit defined in the current CSA standard (1995) may not be directly applicable to this steel grade. The applicability of this b/t limit ($b/t = 145/\sqrt{F_y}$) to the 480W steel was questionable because the material yield strength obtained from the tensile test was not compatible with the minimum specified yield strength.

Local Buckling Stresses

The out-of-plane displacements, or lateral displacements, and local strains started to deviate when local buckling occurred at the mid-height. In most of the tests, the locations of local buckling did not occur at the mid-height of the specimens. Thus local buckling could not be detected until the local buckling wave has propagated to the mid-height. Most local buckling occurred in the vicinity of the mid-height of the specimen and it was inaccurate to use data obtained from the LVDTs and strain gages, which were all located at the mid-height of the specimens. Unfortunately there were no other useful data to detect the local buckling and in addition, the location of local buckling in the inelastic range is uncertain and it was difficult to predict prior to each test. One can attach many strain gages on the tips, along the longitudinal direction of the flanges, to detect the local buckling behaviour. But it is an

impractical and very expensive way to study the local buckling behaviour. It was considered acceptable to use the information on the out-of-plane displacements and the local strains to determine the local buckling load, unless local buckling started too far away from the mid-height of the specimen.

The average axial stress versus the lateral displacement curves for each specimen are plotted in Figures 4.7A to Figure 4.7D. It can be observed that some of these lateral displacement mode shapes of "identical" specimens from the same grade are not consistent. This inconsistency depended largely on where local buckling occurred. It can be explained in that the location of local buckling depended on the initial imperfections of the specimen and the residual stress introduced to the specimen during the fabrication process. This discrepancy resulted in the inaccuracy in determining the local buckling load from considering the relationship between the average axial stress and lateral displacements.

The average axial stress versus local strain curves for each specimen are shown in Figures 4.8A to Figure 4.8D. It can be seen that some of the curves, before the yield stress was reached, started to behave non-linearly and this indicated the possibility of local buckling. However, no visual local buckling was observed during the test when this happened. This early non-linear behaviour can be explained through the initial imperfections of the specimen.

The local buckling stress for each specimen was determined from the relationship between average axial stress and local strain, or the relationship between the average stress and lateral

displacements. From the average stress-local strain relationship, the buckling stress can be determined using the strain reversal method, which was based on the average stress-local strain curves corresponding to the strains placed on the convex side of the buckled flange. The buckling stress from the strain reversal method was determined from the point at which the maximum strain occurred. The buckling stress can also be determined from a relationship between the average stress and lateral displacements. Based on such relationships, conventionally the inflection point method could be employed. The buckling stress derived from this method is defined as the stress corresponding to a point with a maximum rate of increase of the lateral deflection with respect to the stress; i.e. minimum slope (Schlak 1968). However, in most cases, no minimum slope was observed in the range from the yield stress to the ultimate stress. Using the conventional inflection point method, it could be concluded that the ultimate average stress was also the local buckling stress of these stub columns. Based on experimental observations, most local buckling occurred before the ultimate average stress was reached. Therefore the inflection point method was not used in this study. Instead, the local buckling stress was determined from the relative lateral displacement of the opposite flanges. It was assumed here that local buckling has been initiated when this relative displacement reached half thickness of the flange, provided that the corresponding strain was not greater than the ultimate strain. In case local buckling did not occur at the mid-height of the specimen, or that the corresponding strain was beyond the ultimate strain, the ultimate stress was determined to be the local buckling stress. The buckling stresses obtained from the strain reversal method and the proposed method varied from each other. Different buckling stresses based on these two methods were due primarily to plate imperfections, inferring that strain reversal possibly occurred prematurely. The

buckling stresses obtained from these two methods are presented in Table 4.2. It was found that the buckling stress of each stub column is also, more or less, the same as the peak stress of the corresponding specimen. Meanwhile, the buckling stresses were all greater than the corresponding material yield stress. This indicated that local buckling occurred in the inelastic range.

Table 4.1 Dimensions of Stub Columns

Steel Grade	Dimensions (mm)		
	Flange (**b**)	Web (**w**)	Length (**L**)
300W (t = 9.5 mm)	159.5	159.5	540.0
350W (t = 6.4 mm)	98.4	98.4	335.0
480W (t= 6.4 mm)	84.1	84.1	300.0
700Q (t= 6.4 mm)	69.6	69.6	280.0

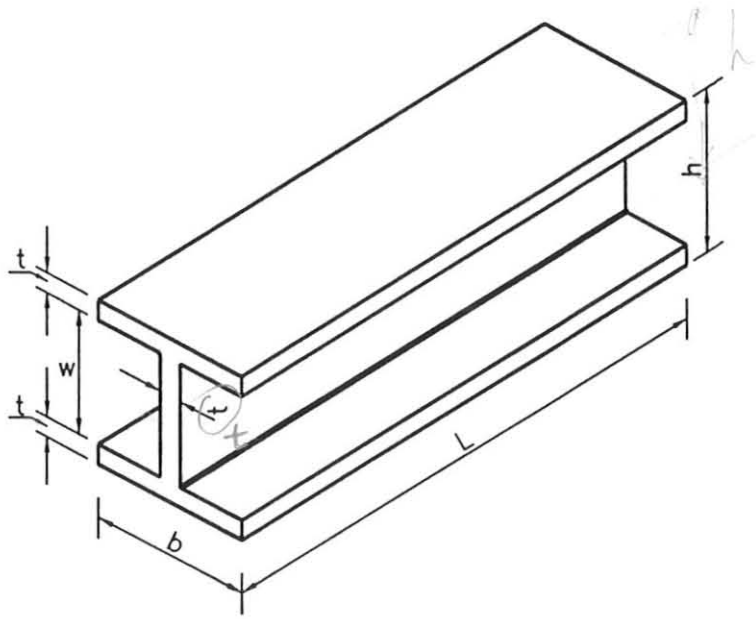

Table 4.2 Experimental Results from Stub Column Testing

Steel Grade	Specimen	Properties						
		f_{buckle} (MPa)		f_u (MPa)	Reserve Capacity f_u/f_y	Ductility		
		Relative Displacement Method	Strain Reversal Method			D_u	D_l	D
300W	300-1	385	383	385	1.15	3.3	3.0	8.8
	300-2	383	383	383	1.14	3.4	3.4	13.3
	300-3	370	391	392	1.17	4.3	3.5	14.9
Average		379	386	387	1.15	3.7	3.5	12.4
350W	350-1	420	464	470	1.16	5.0	3.5	19.6
	350-2	N.A.(1)	459	462	1.14	4.0	3.8	12.1
	350-3	472	N.A.(1)	472	1.16	4.9	4.9	14.0
Average		446	462	468	1.15	4.7	4.1	15.2
480W	480-1	690	N.A.(1)	699	1.18	3.1	2.6	5.5
	480-2	N.A.(1)	N.A.(1)	668	1.13	1.9	1.9	3.5
	480-3	N.A.(1)	659	669	1.13	2.0	1.5	3.8
Average		690	659	679	1.15	2.3	2.0	4.3
700Q	700-1	741	N.A.(1)	747	1.05	2.2	1.6	4.0
	700-2	770	761	774	1.09	4.6	3.1	6.9
	700-3	720	764	765	1.08	3.3	1.4	5.9
Average		738	762	762	1.07	3.4	2.1	5.6

Note: (1) Local buckling stress was unable to be detected because local buckling occurred off the mid-height of the specimen, resulting in neither strain reversal nor deviations being detected by the strain gages and the LVDTs, respectively.

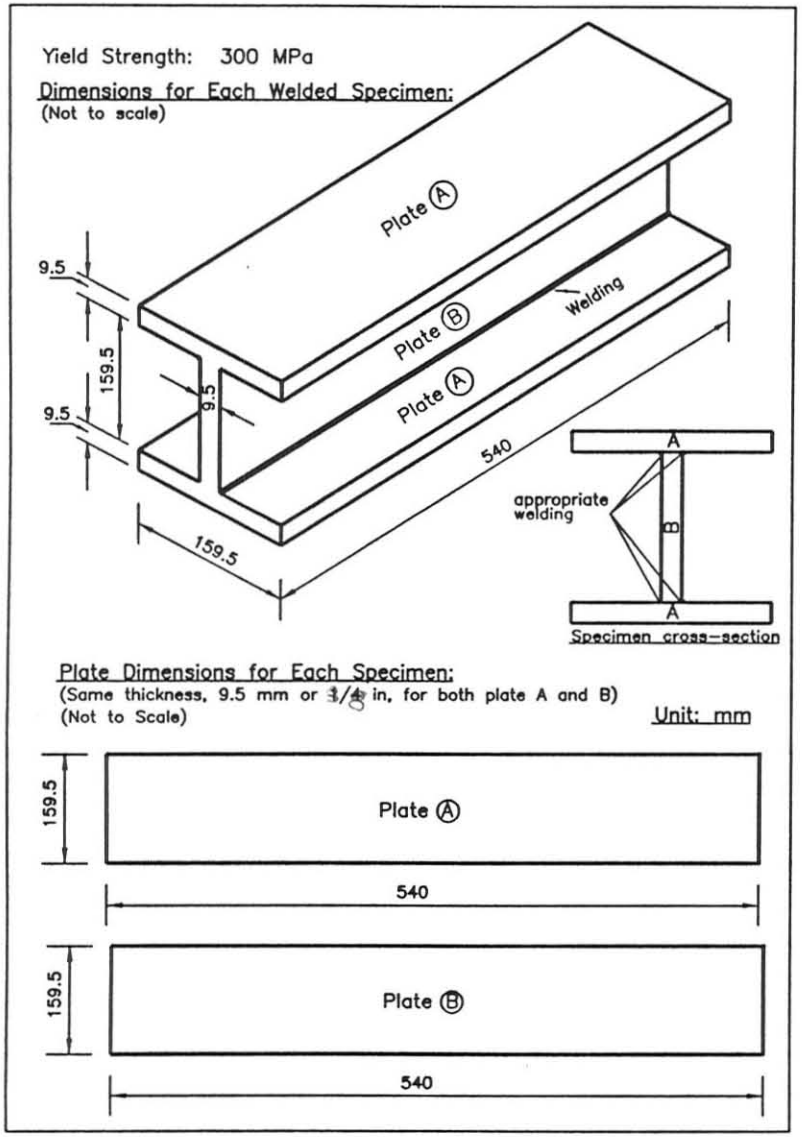

Figure 4.1a Stub Column Dimensions of 300W Steel

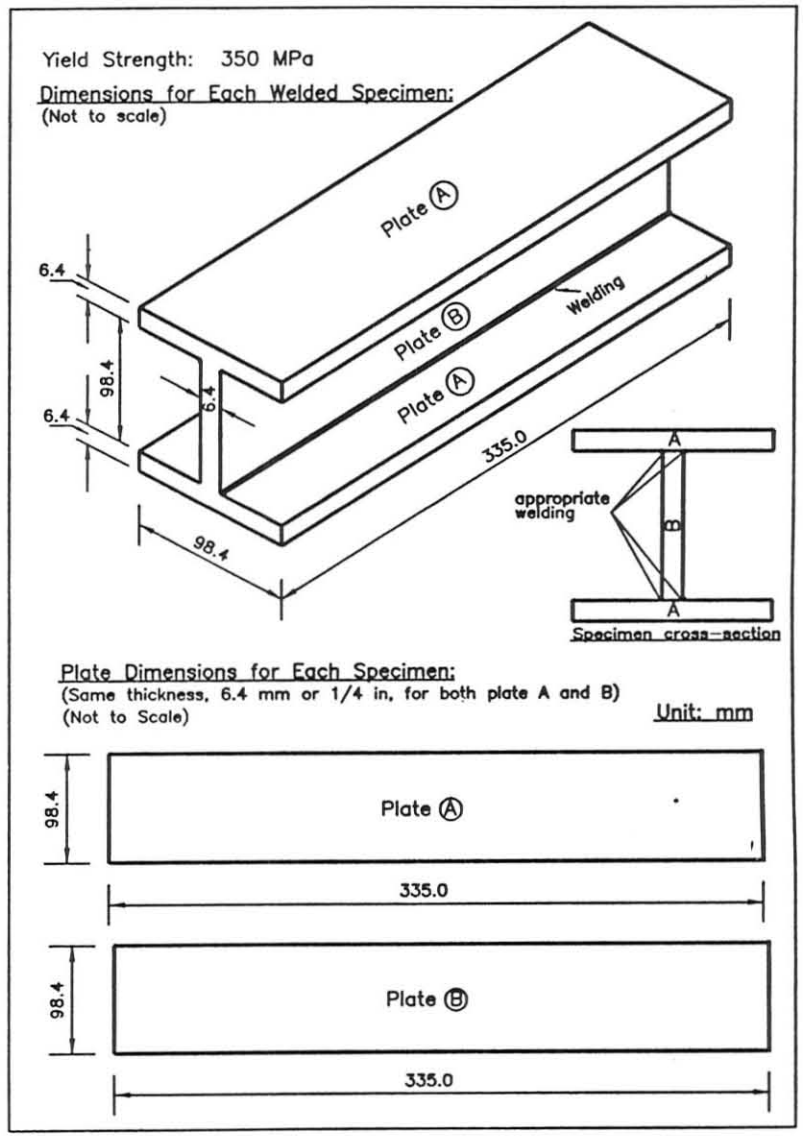

Figure 4.1b Stub Column Dimensions of 350W Steel

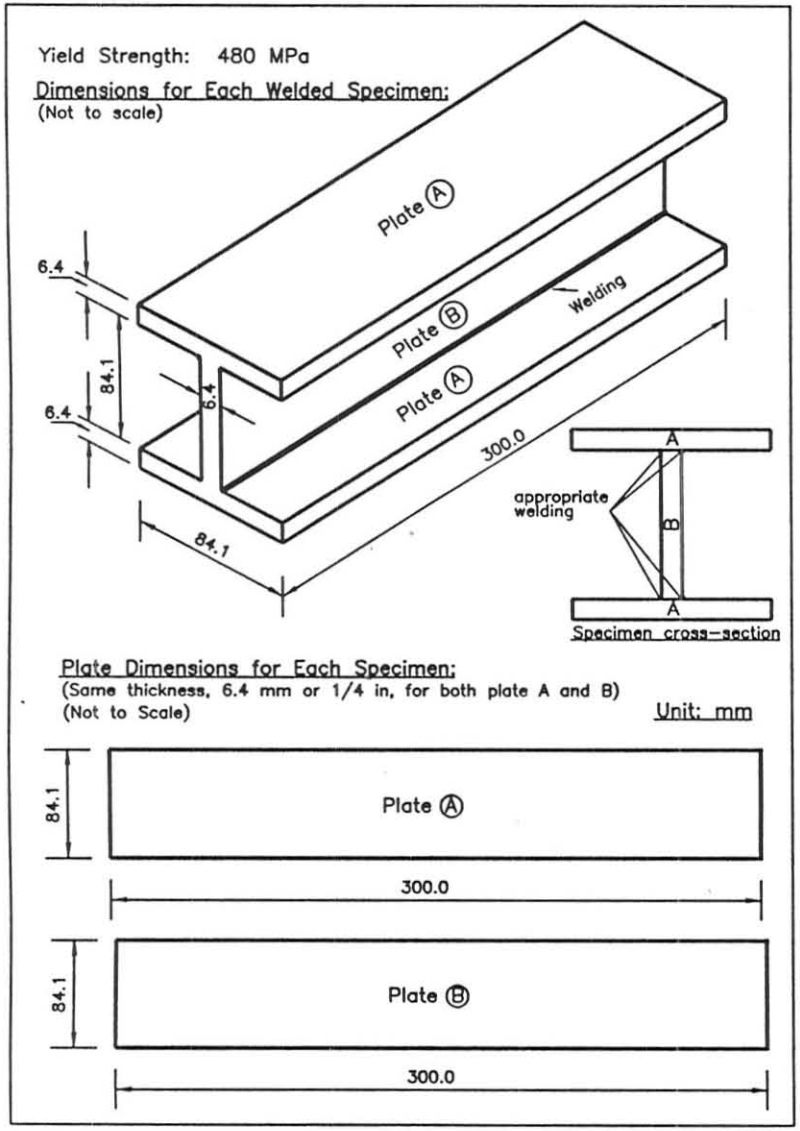

Figure 4.1c Stub Column Dimensions of 480W Steel

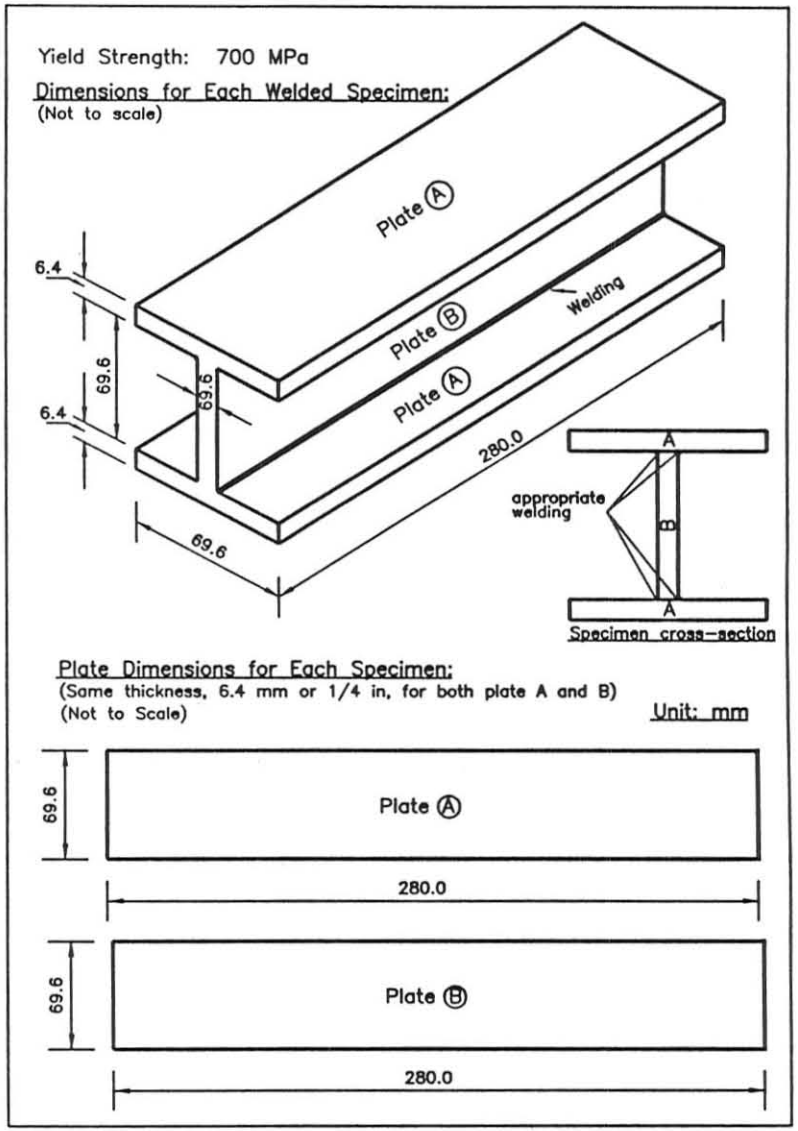

Figure 4.1d Stub Column Dimensions of 700Q Steel

Figure 4.2a Experimental Setup

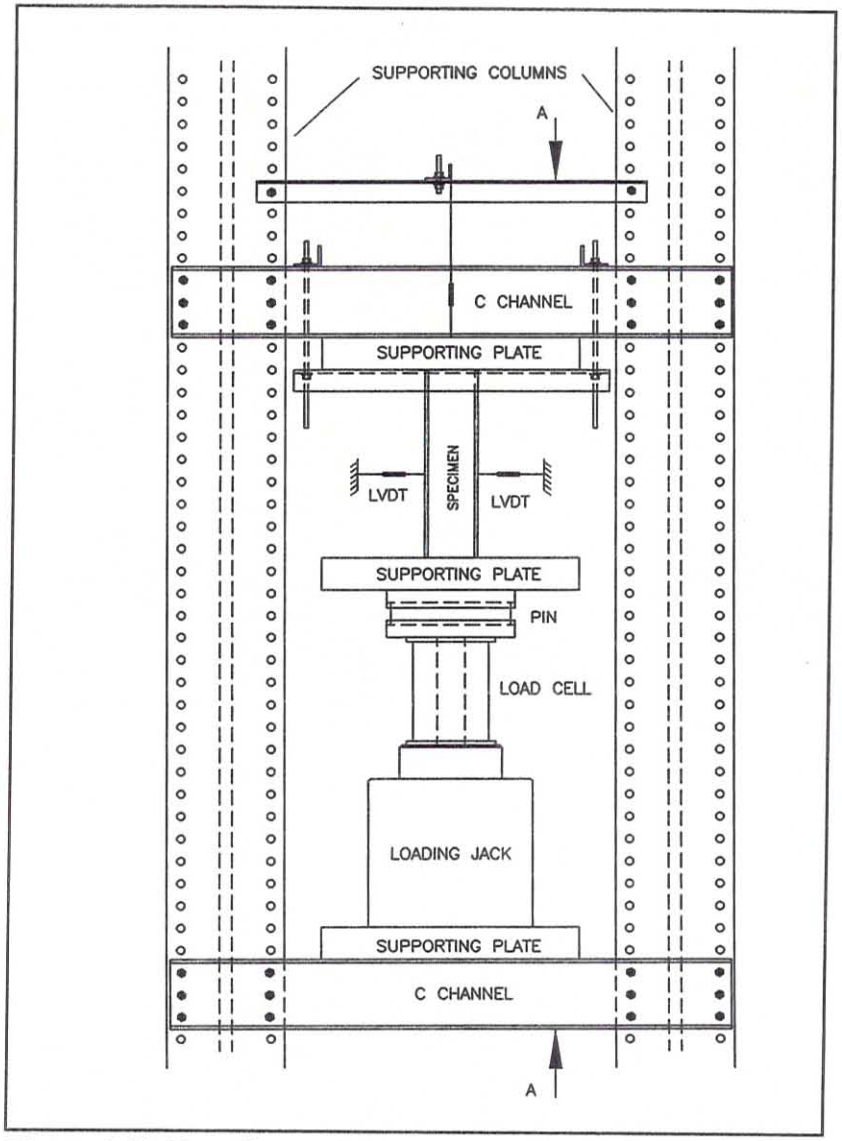

Figure 4.2b Experimental Setup - Front View

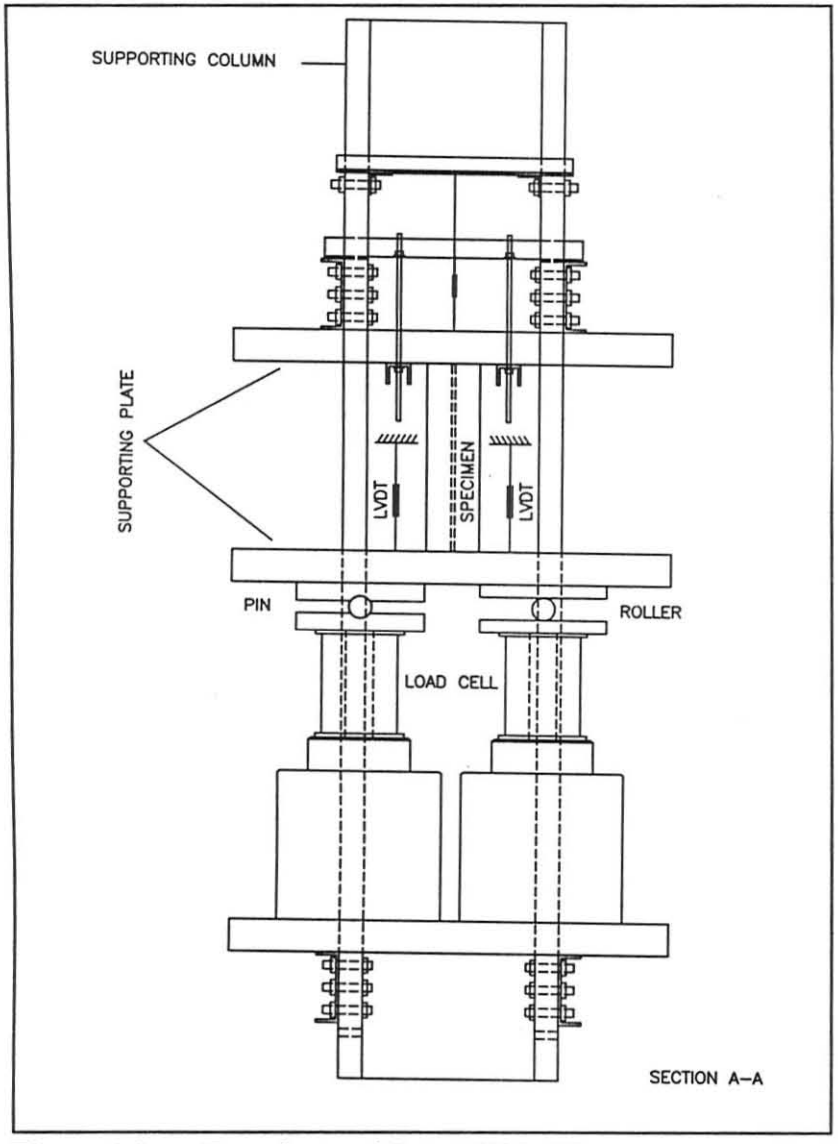

Figure 4.2c Experimental Setup (Side View at **A-A** Section)

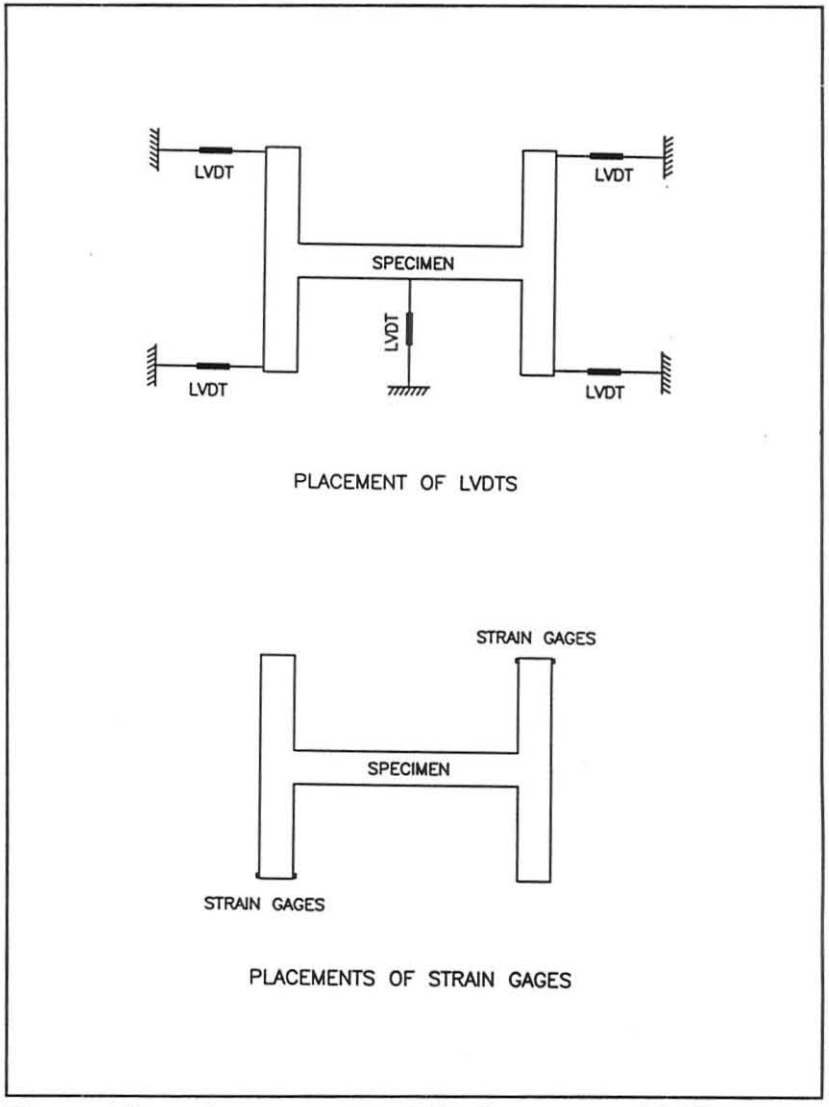

Figure 4.3 Arrangements of Strain gages and LVDTs at Mid-Height of a Specimen

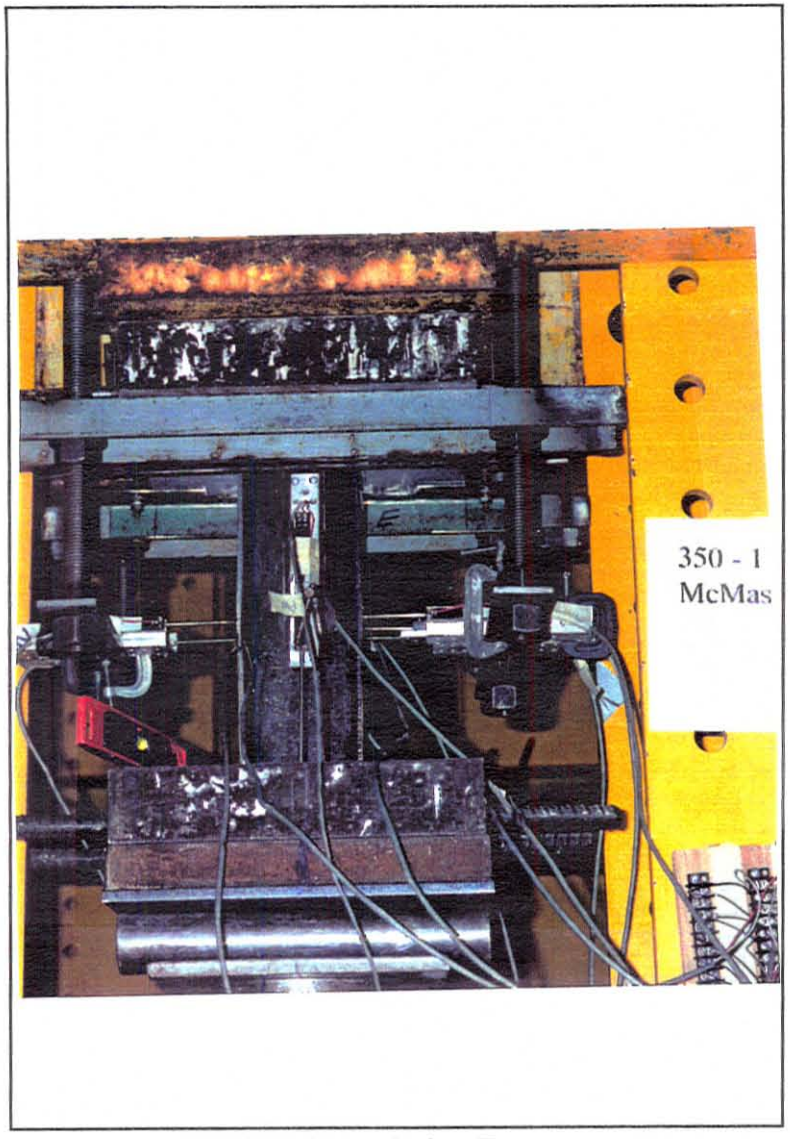

Figure 4.4 Stub Column during Test

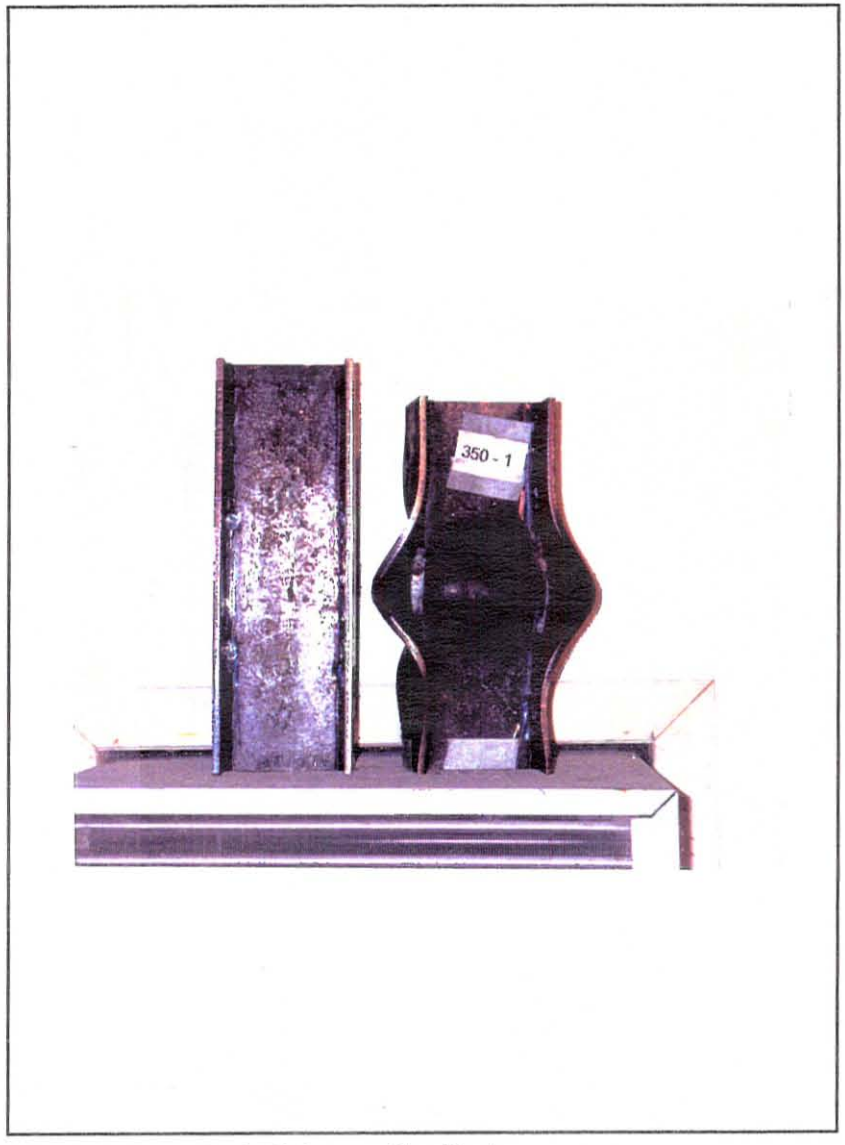

Figure 4.5 Stub Column after Test

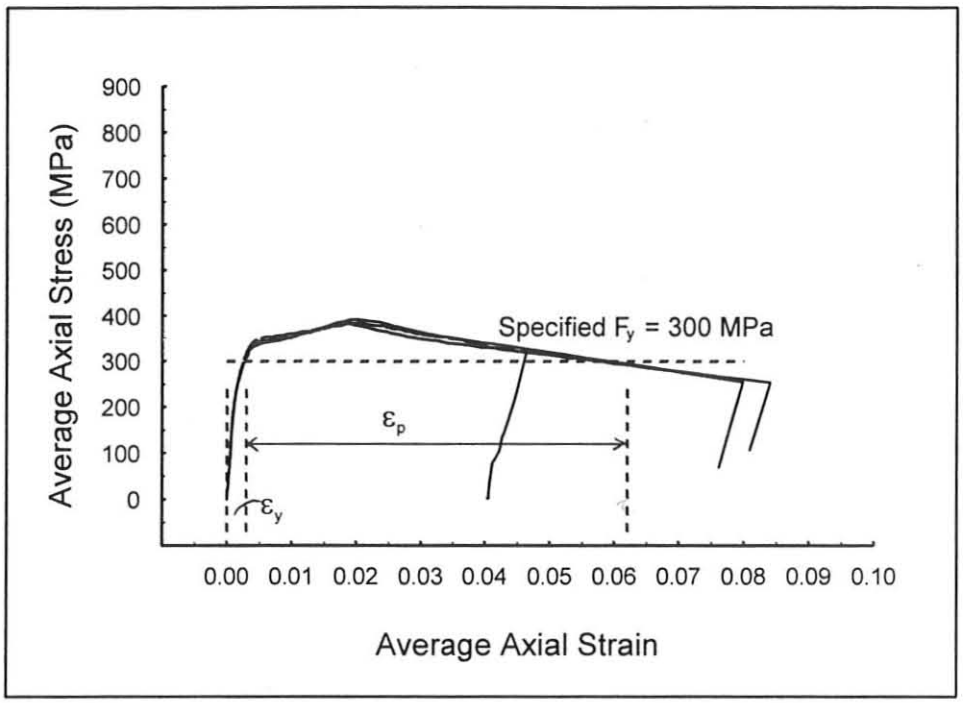

Figure 4.6A Axial Stress and Axial Strain Relationship of 300W Steel

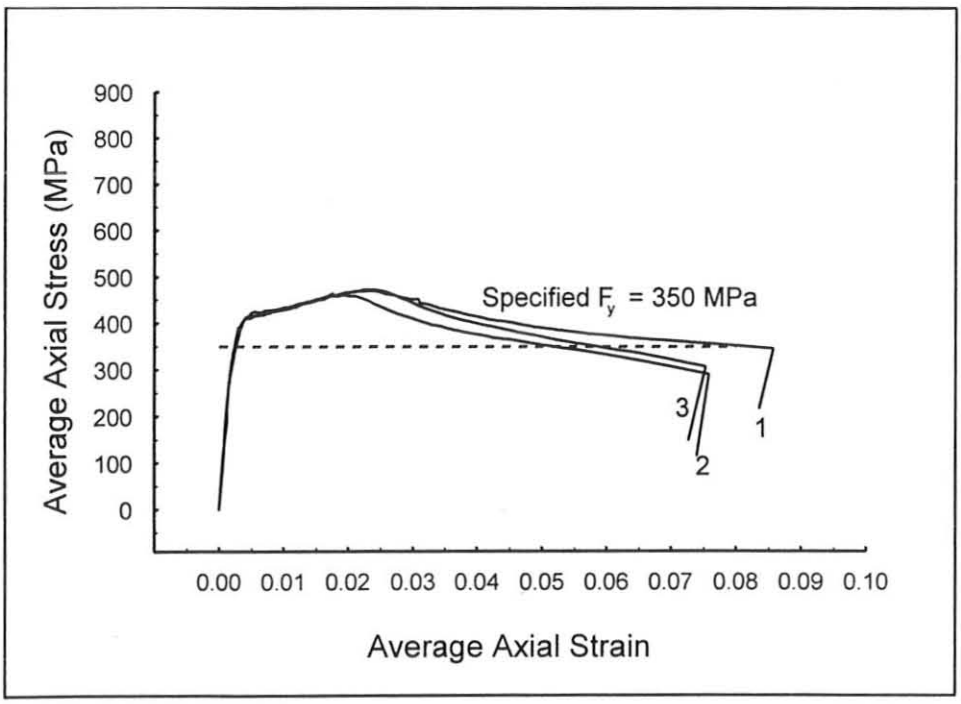

Figure 4.6B Axial Stress and Axial Strain Relationship of 350W Steel

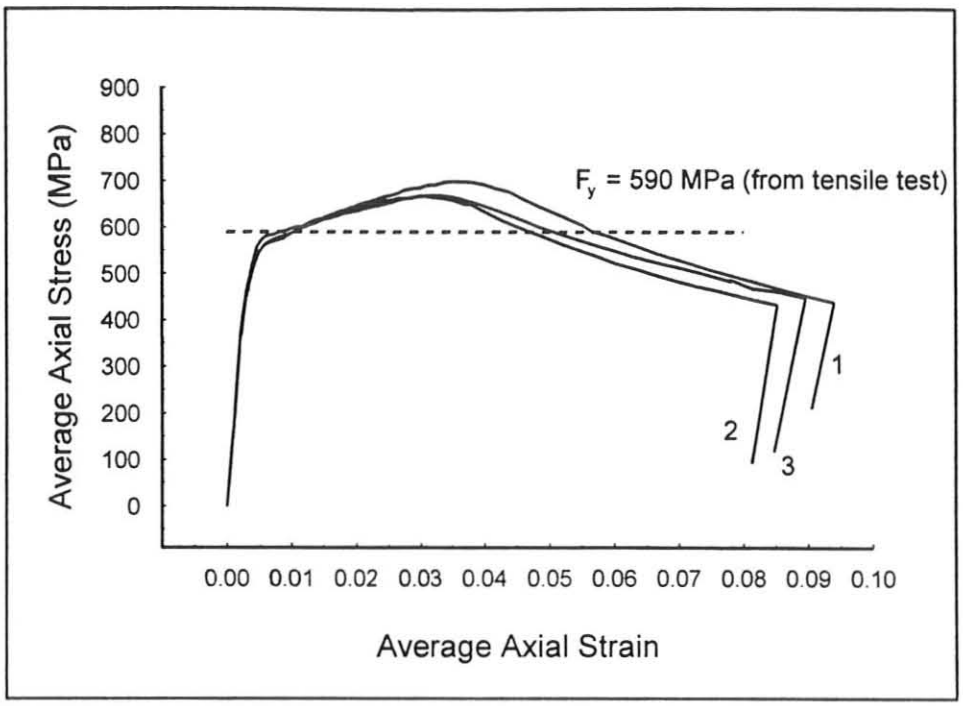

Figure 4.6C Axial Stress and Axial Strain Relationship of 480W Steel

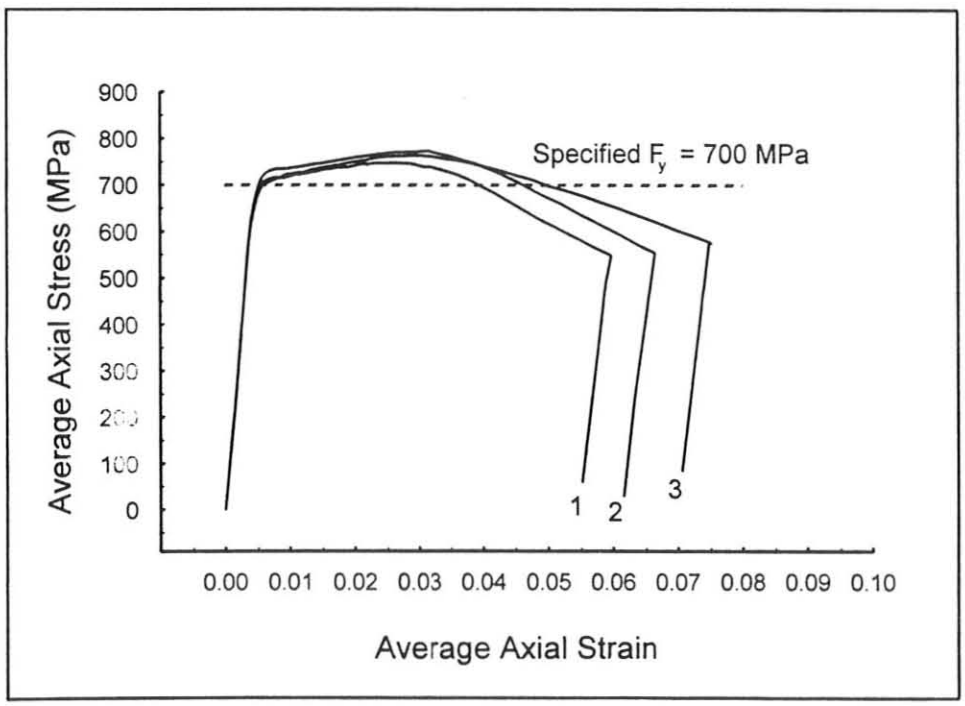

Figure 4.6D Axial Stress and Axial Strain Relationship of 700Q Steel

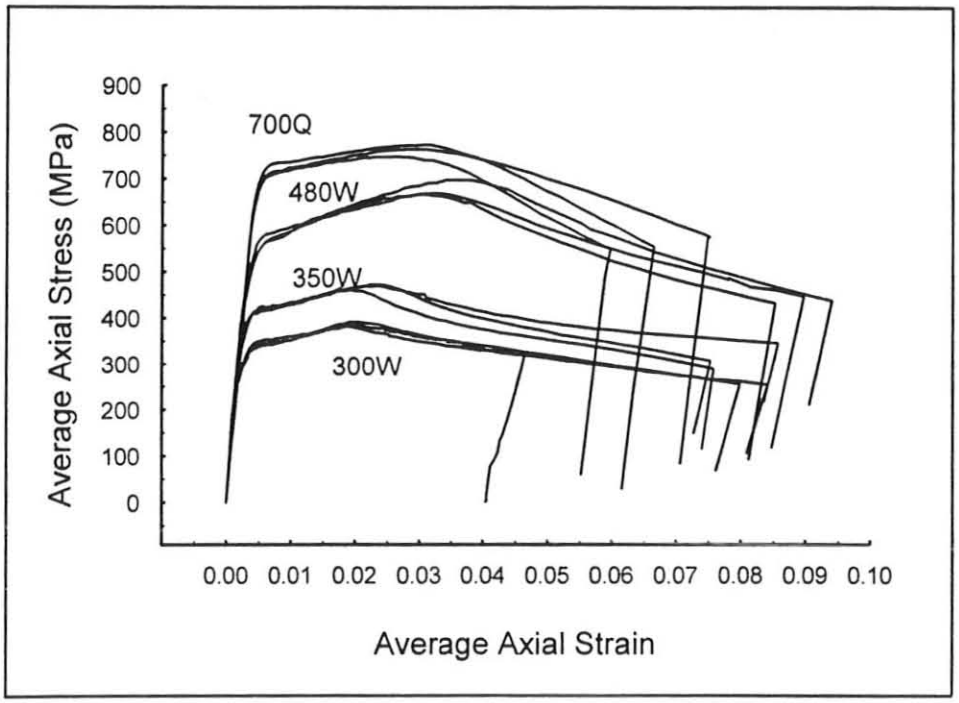

Figure 4.6E Axial Stress and Axial Strain Relationship of All Specimens

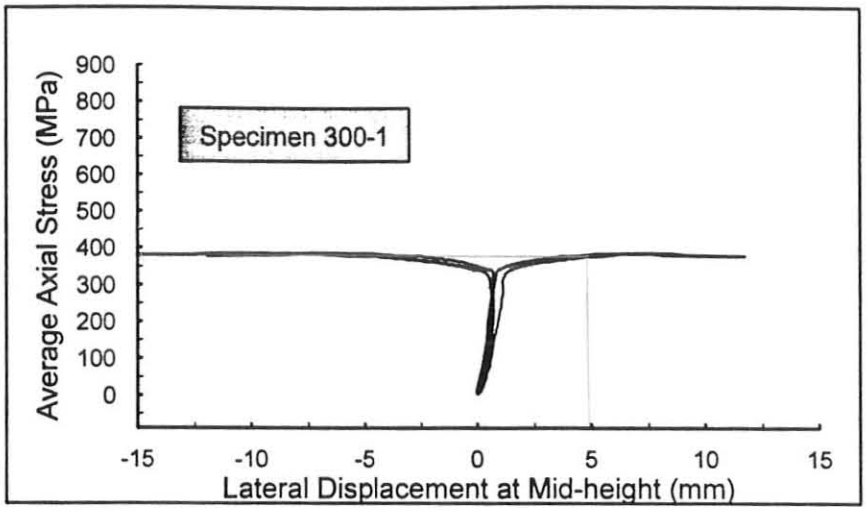

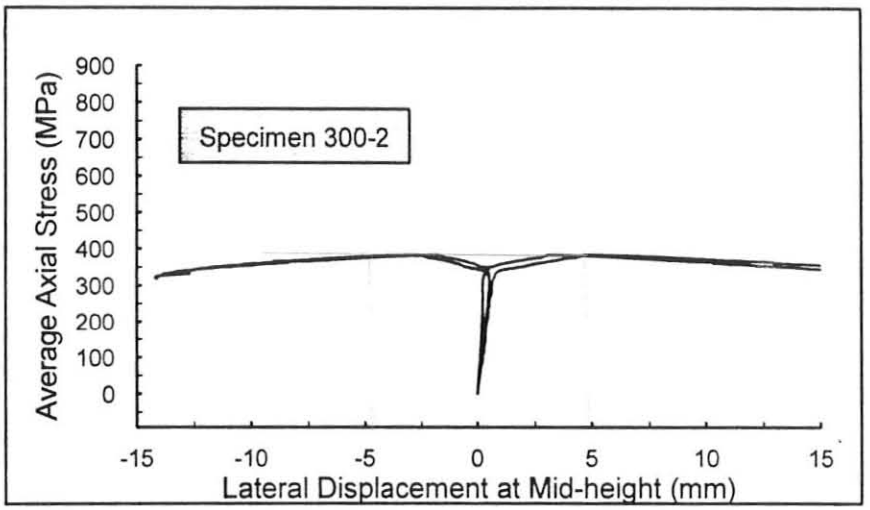

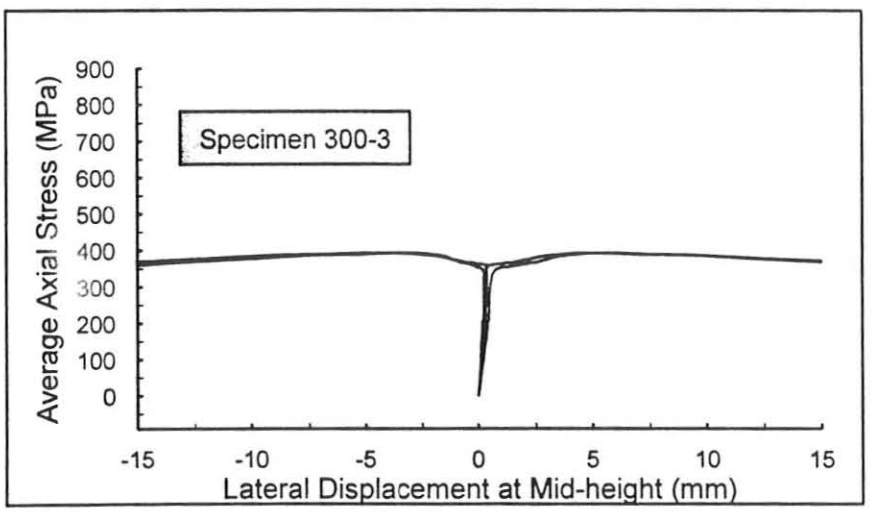

Figure 4.7A Relationships of Average Stress and Lateral Displacement at the Mid-height of Specimens (300W Steel)

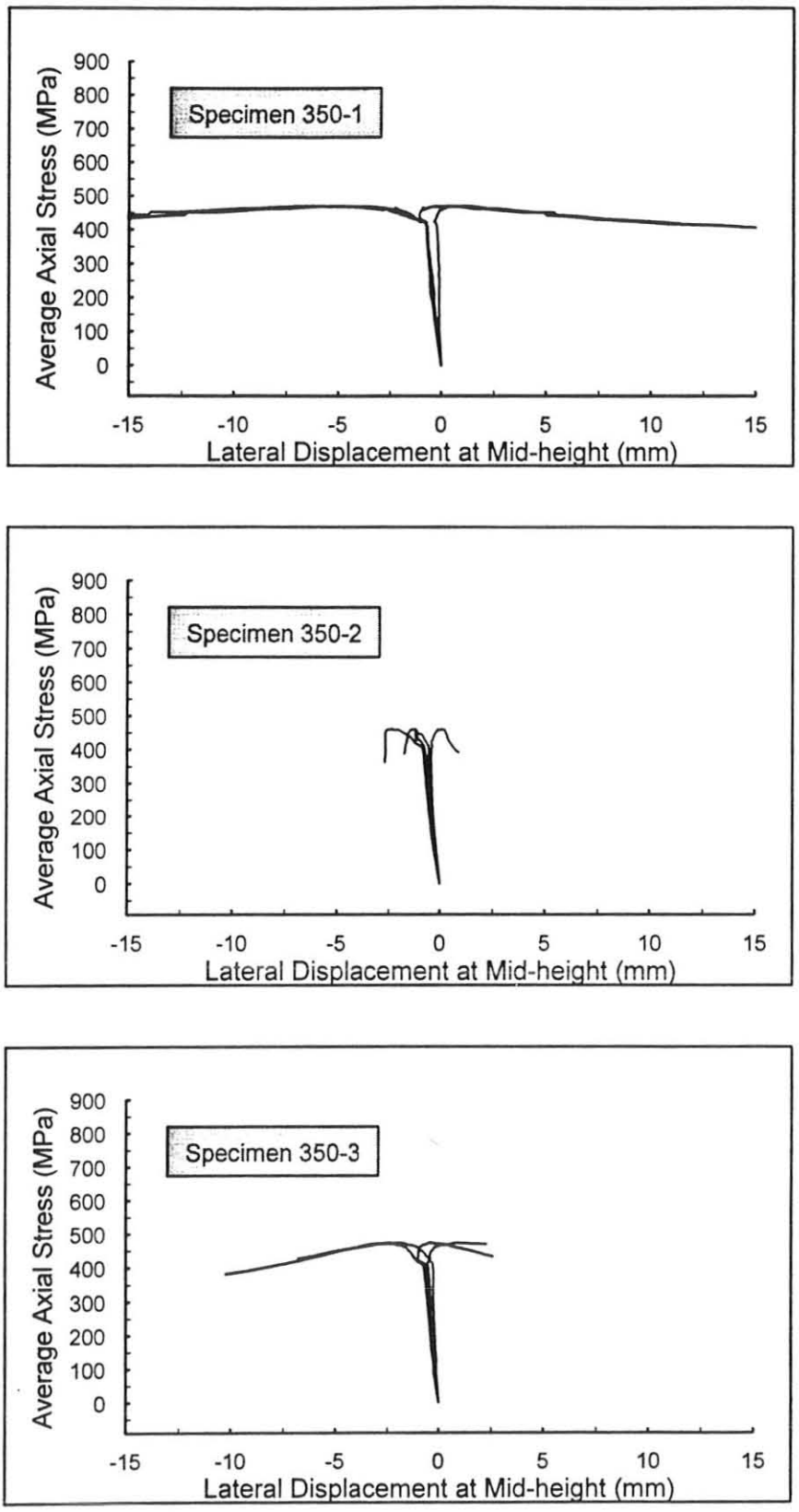

Figure 4.7B Relationships of Average Stress and Lateral Displacement at the Mid-height of Specimens (350W Steel)

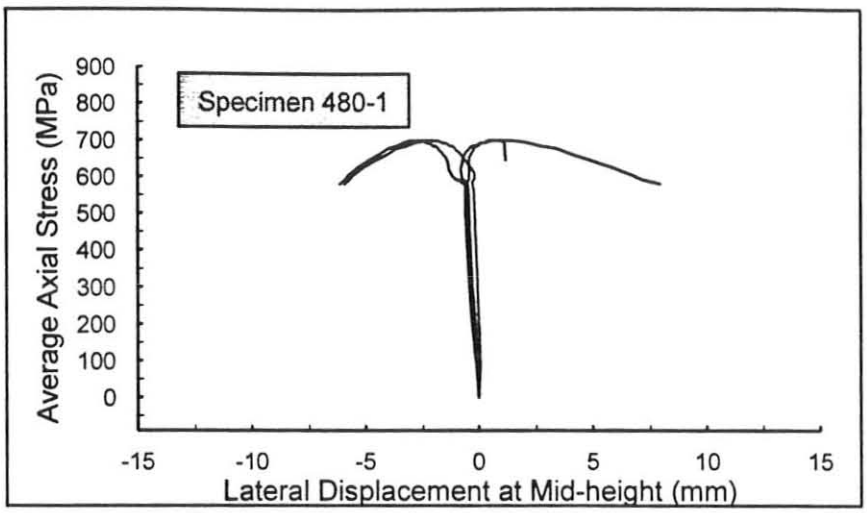

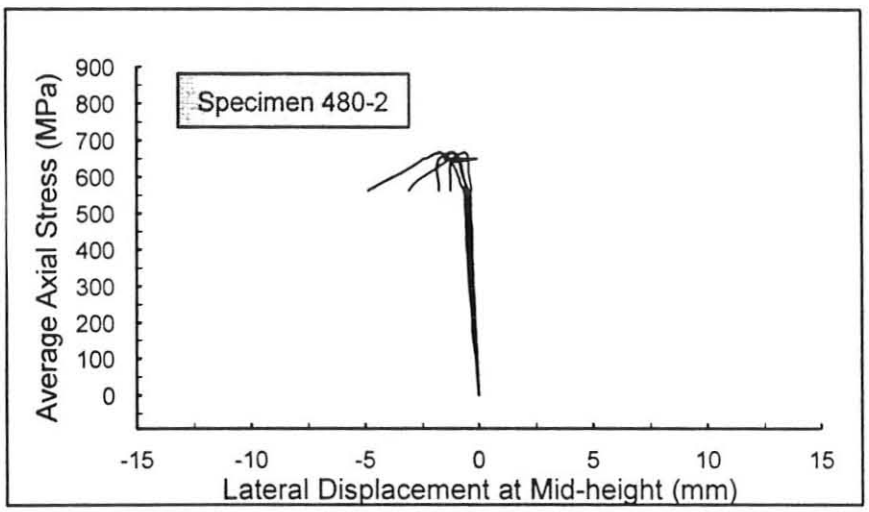

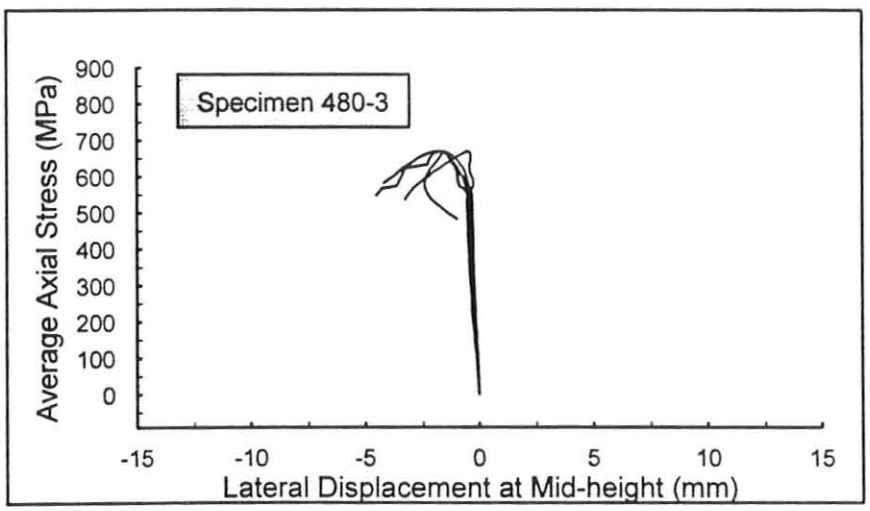

Figure 4.7C Relationships of Average Stress and Lateral Displacement at the Mid-height of Specimens (480W Steel)

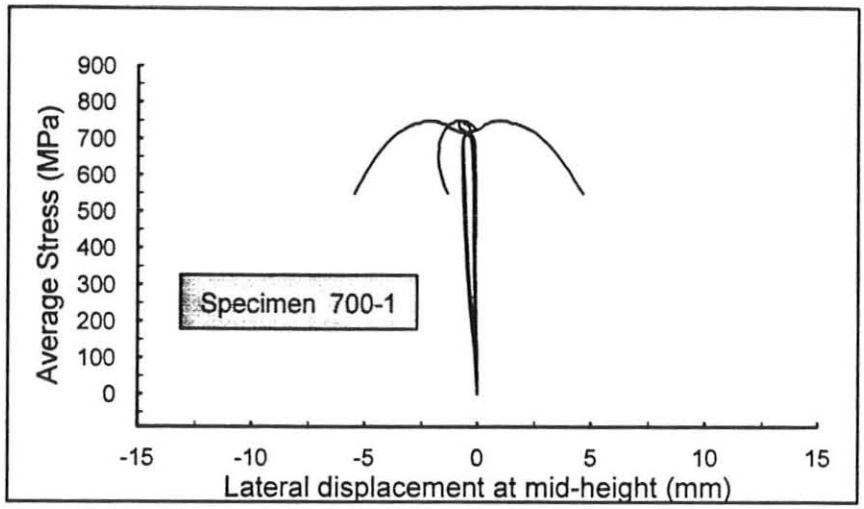

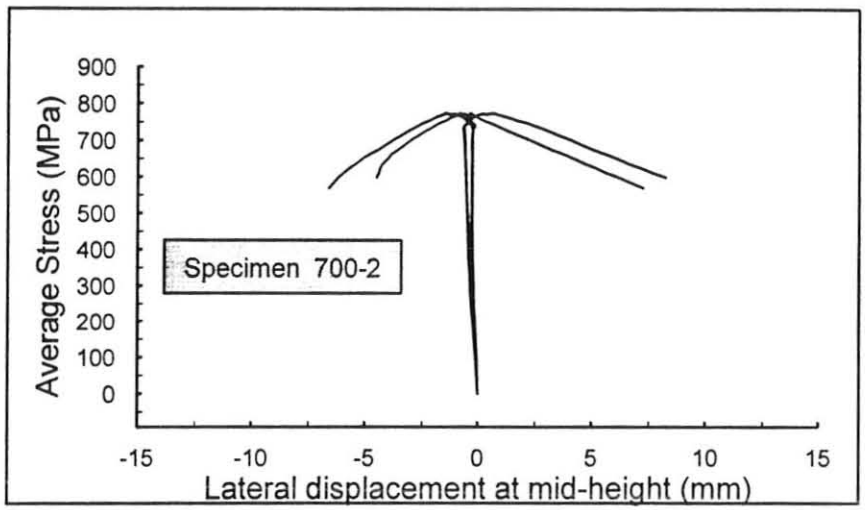

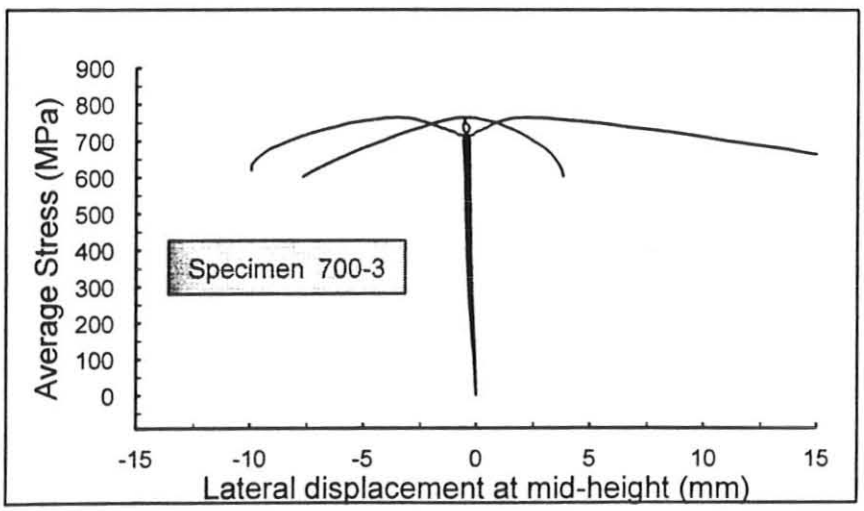

Figure 4.7D Relationships of Average Stress and Lateral Displacement at the Mid-height of Specimens (700Q Steel)

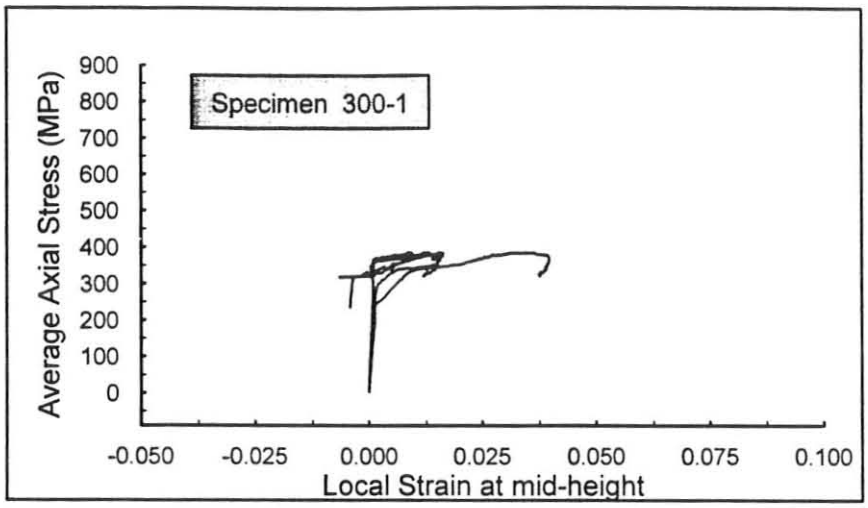

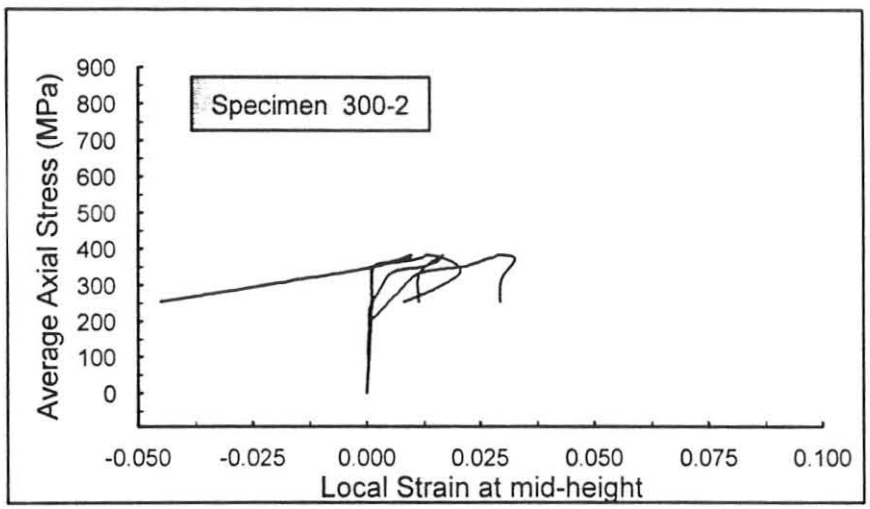

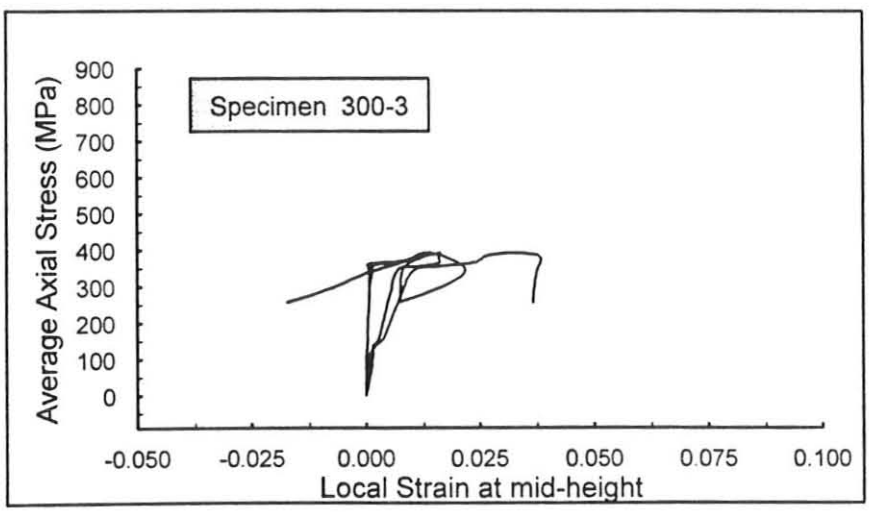

Figure 4.8A Relationships of Average Stress and Local Strain at the Mid-height of Specimens (300W Steel)

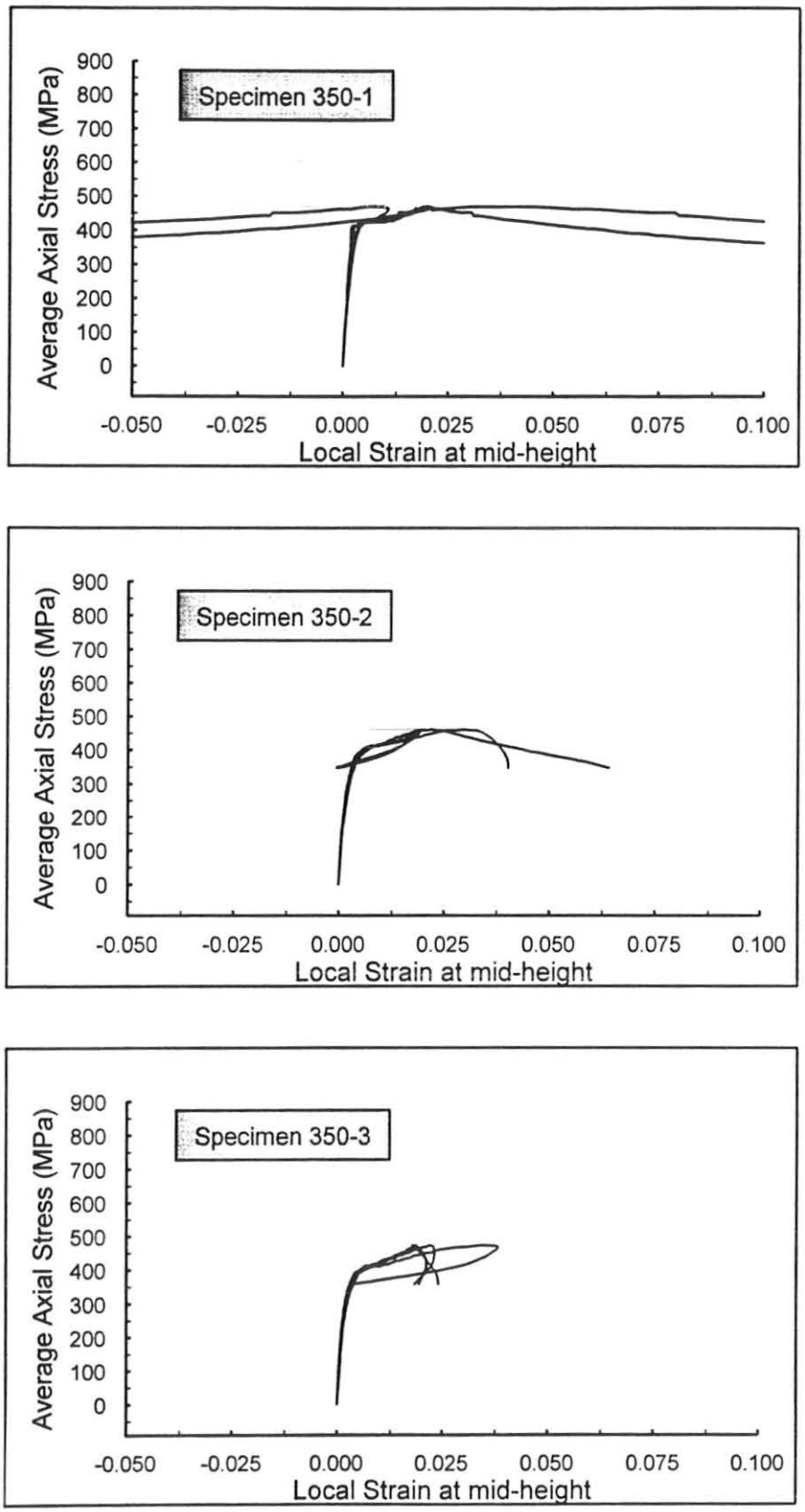

Figure 4.8B Relationships of Average Stress and Local Strain at the Mid-height of Specimens (350W Steel)

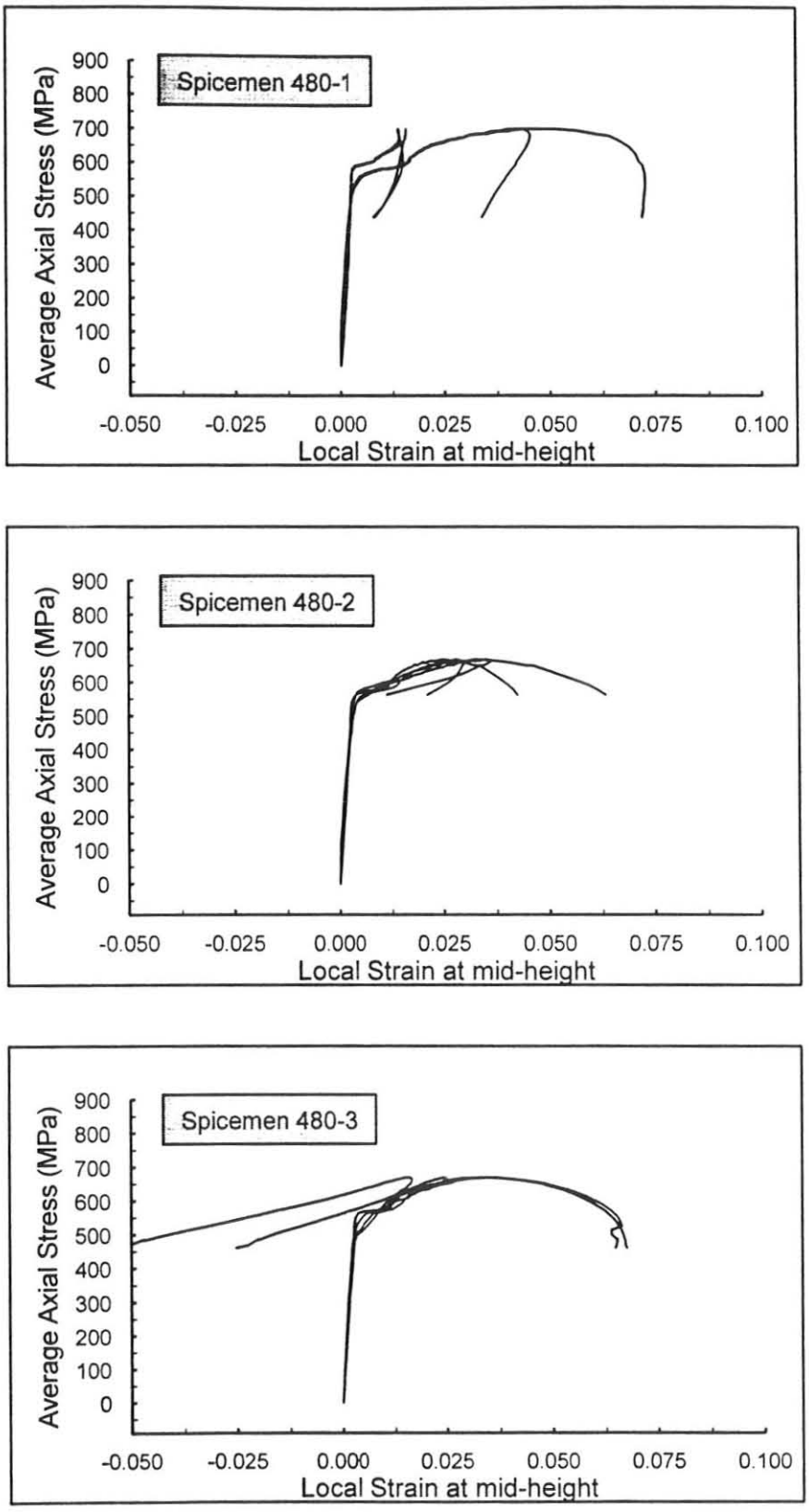

Figure 4.8C Relationships of Average Stress and Local Strain at the Mid-height of Specimens (480W Steel)

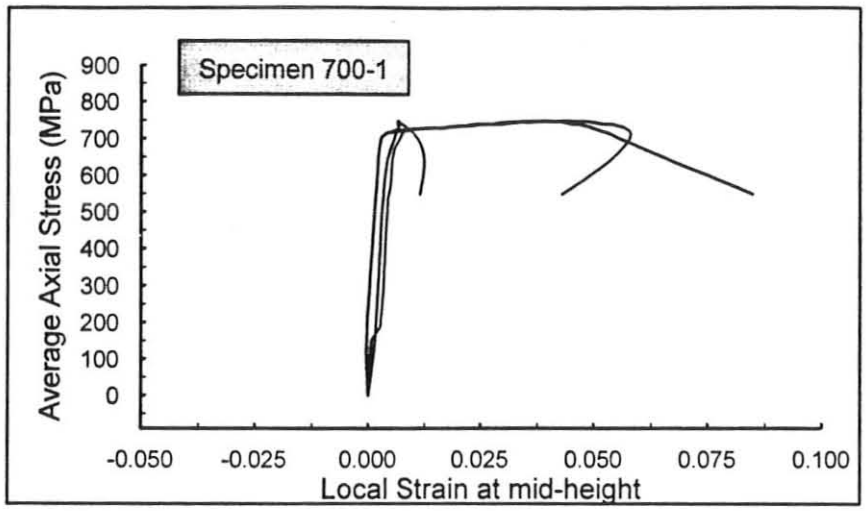

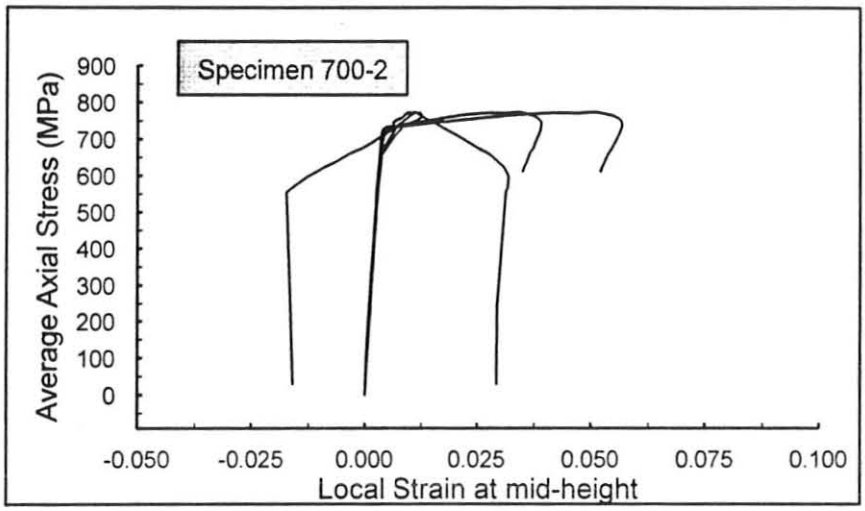

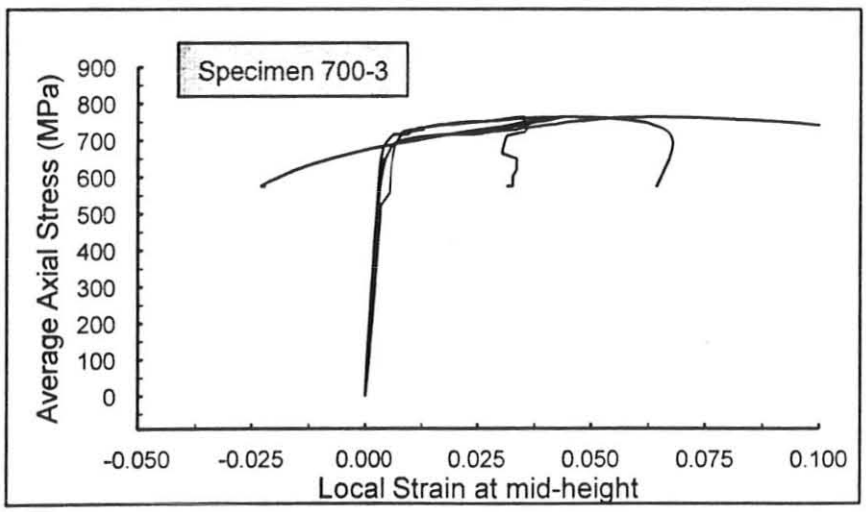

Figure 4.8D Relationships of Average Stress and Local Strain at the Mid-height of Specimens (700Q Steel)

Chapter 5

Finite Element Analysis

of W-shaped Steel Compression Members

5.1 Introduction

In Chapter 3, experimental stress-strain relationships for various steel grades, including high strength steel were presented. Based on these results various analysis models for stress-strain relations, such as, the multi-linear model, the modified tri-linear model, and the modified bi-linear model have been derived in Chapter 3. In the first part of this chapter a finite element analytical model will be developed to study the local buckling behaviour of steel W-shaped sections. This model is based on the idealized analytical material models, and incorporates an idealized distribution of residual stress for the cross-section. The finite element mesh is created using a 9-node shell element. Results obtained using this analytical model will be compared and verified with the experimental results acquired from the stub column tests, which were presented in Chapter 4. The material model that best correlates with the experimental results will be determined. In the second part of this chapter, this selected material model will only be considered for further studies on the local buckling behaviour of high strength steel W-shaped sections. This study on local buckling behaviour will concentrate on the compression flange buckling of W-shaped sections, with varying flange width-to-thickness (b/t) ratios, but constant web width-to-thickness (w/t) ratio. Results obtained from this parametric study will be compared with the current design standards (CISC 1995) expectations, in order to determine whether the standard is applicable to the

high strength steel W-shaped sections.

5.2 Modelling of High Strength W-shaped Members in Compression

In this section, a finite element method based analytical model will be constructed to study the local buckling behaviour of W-shaped stub column members in compression and to determine the ultimate load of these members. The variations in the material properties, material analysis models, residual stresses, and initial imperfections will be incorporated in this finite element modelling. The accuracy of the proposed FE analytical model will be verified with experimental results obtained on steel W-shaped stub columns in Chapter 4.

5.2.1 The Assumed Strain Shell Element and its Applications

The local buckling of W-Shaped members in compression involves not only the in-plane displacements, but also the lateral displacements and rotations. Therefore, the finite element analysis model to study the local buckling behaviour of compression flanges of a W-shaped steel section must use the shell element, because the lateral deformations, rotations, and the in-plane displacements are taken into consideration in such elements. Shell elements based on independent interpolations for the translational and rotational degrees of freedom (dof) were first introduced by Ahmad, et al. (1970). Such shell elements are independent of any shell theory and they are most suitable for modelling and studying moderately thick structures. However, for thin and for moderately thick structures, a new efficient, accurate, "assumed strain" isoparametric shell element has been recently developed by Abdel-Rahman (1997). This finite element, as shown in Figure 5.1, consists of nine mid-surface nodes.

Each node has five dof, consisting of three mid-surface displacements and two rotations of the mid-surface normals as the nodal dof. In this element, the method of "assumed strain" was used to eliminate the transverse shear and membrane locking problems associated with the other shell elements. The "assumed strain" method implies that the transverse shear strains and the membrane strains are not directly evaluated from the displacement and rotation fields of the element. Instead, the transverse and the membrane strains throughout the element's mid-surface plane are re-interpolated by introducing auxiliary quadratic, consistent strain fields. However, the original strain fields and the auxiliary strain fields can be linked through a set of pre-defined "sampling points" in each element. At these sampling points, zero transverse shear is obtained for the thin shell, when such strains are evaluated from the original displacement and rotation fields of the elements (Huang and Hinton 1986). A detailed description of this 9-noded finite element formulation can be found in the study performed by Abdel-Rahman (1997).

The verifications of applying this finite element to solve shell and plate problems have been carried out extensively by Abdel-Rahman (1997). One of the verification problems involve application of this "assumed strain" finite element and comparison of the results obtained from the finite element analysis with the corresponding experimental results performed on cold-formed steel stub columns. In this verification study, a quarter section of a stub column (due to symmetry) was used in the finite element modelling. The FE model used the idealized material properties and idealized residual stresses that were developed by Abdel-Rahman (1997). Also, the displacement control method was employed to acquire a uniform

displacement condition at the loading ends of the compression member. Figure 5.2 shows the axial load to axial strain relationships, which were from the experimental and the finite element analysis (Abdel-Rahman 1997). It shows excellent correlation between the experimental results and those obtained from the finite element analysis. With such excellent agreement with the experimental results acquired from Abdel-Rahman (1997), the "assumed strain" shell finite element was adopted for use in the finite element modelling of high strength steel W-shaped sections. Details of the finite element modelling of such W-shaped sections will be discussed in the subsequent sections.

5.2.2 Finite Element Mesh and Boundary Conditions

In the finite element modelling, an appropriately discretized finite element mesh must be determined and boundary conditions corresponding to the problem under consideration need to be proposed. In the first part of this study the dimensions of the finite element mesh are deemed to be the same as those of the experimental stub columns described in Chapter 4. Therefore the stub columns used for finite element modelling also comply with the recommendations made by the Structural Stability Research Council (SSRC 1988). That is, as described previously, the column is short enough to eliminate the overall buckling mode, but long enough to retain residual stress. Therefore, the finite element mesh was determined based on the dimensions of the stub columns tested in the experimental part of this study.

The W-shaped section is subjected to uniform compression and the W-section is symmetric about both its minor and major cross-sectional axes. Therefore a W-shaped section

theoretically has symmetric behaviour when subjected to such loading conditions. Thus, a quarter of the W-section was used for the finite element modelling for the columns of the selected steel grades in this study. Various trial analyses consisting of a different number of meshes were carried out to determine the final mesh for this study. The purpose in selecting an appropriate mesh size for a quarter of the column is to ensure the continuities of stress and displacement across the boundaries connecting the adjacent elements, and to minimize computing efforts. During the trials of selecting the proper mesh size, it appeared that the stress at a node between the adjacent elements were difficult to match, especially at the inelastic range stress levels. Thus, a tolerance of ±5% discontinuity was set to determine a suitable mesh for acceptable continuities of both stress and displacement. A final mesh was selected based on the dimensions of the stub columns of 300W steel grade, and the associated material properties. Figure 5.3 schematically shows the selected mesh, where it can be seen that there are seven and four elements along the width of flange and web, respectively, while five shell elements have been used along the longitudinal directions of the quarter of the column. With such an element arrangement, there are a total of 55 elements and correspondingly 253 nodal points. All elements in the web and flange have the same length in the longitudinal direction. The widths of all the elements across the flange are equal, and this width was calculated by dividing the flange width by the total number of elements (seven) across the flange width. Also, the widths of all the elements across the web were also of the same dimensions, and this width was determined by taking half the web width divided by the number of elements (four) in the web. The stub columns of 300W steel grade had the largest dimensions of all these specimens. Thus, this selected finite element

discretization was assumed to be applicable to the modelling of stub columns of other grades as well.

Figure 5.4 shows the boundary conditions used for the finite element model. Unless otherwise shown, all nodal dof for all nodes were set to freely displace and rotate. The boundary conditions at the top of the loaded end are assumed to be the simply supported conditions. Displacements in the X and Z directions are restrained, but free displacement in the Y-direction and free out-of-plane rotations are allowed. As shown in Figure 5.4, due to the symmetric nature of a stub column, symmetric boundary conditions were imposed at the symmetry lines of the quarter column. Such boundary conditions ensure that rotations about the centerline and in-plane displacement across the centerline are not realized. Since Figure 5.4 clearly shows all the boundary conditions, no further discussion on boundary conditions is warranted.

5.2.3 Material Model and Residual Stresses

Even though the finite element analysis results obtained by Abdel-Rahman (1997) showed a high degree of correlation with the experimental results, Abdel-Rahman's study concentrated on the local buckling behaviour of cold-formed steel compression members. The cold-formed steel possesses different characteristics of material properties and residual stress distribution from those of the structural steel W-shaped sections. The stress-strain relationship of cold-formed steel shows that there is no well-defined yield point, and gradual yielding is always present. Thus, Abdel-Rahman (1997) idealized the material behaviour

using an elastic segment, and three plastic segments to represent the stress-strain relationship. In addition, the residual stress in cold-formed steel varies considerably across the thickness of the steel plate (Abdel-Rahman 1997). On the other hand, the structural steel W-shaped sections, for example mild carbon steel, exhibit a well-defined yield point in the stress-strain relationship. Also, the residual stress in W-shaped structural steel sections varies along the width of the web and flanges, but not significantly across the thickness of the plates. Since the original finite element computer code used by Abdel-Rahman (1997) was intended to incorporate the material properties and residual stress possessed by cold-formed steel into the analysis, this may not be directly applied to the study of local buckling of structural steel W-shaped sections. Therefore, it became necessary to modify the original finite element computer code to accommodate the characteristics of the material properties and residual stress distribution associated with the structural steel W-shaped sections. Modifications in the computing code implemented during the current investigation include the addition of two plastic segments to the material model in order to more accurately represent the material behaviour of structural steel. Instead of the linearly varying residual stress across the thickness of a plate component of a cold-formed steel section, a parabolic approximation for the distribution of residual stress across the web and flange width, which had been described earlier in Chapter 3, was incorporated into the computing code. Verification of such changes made in the finite element programming code will be carried out with concerns about whether the original finite element technique can properly incorporate the parameters representing the multi-linear material model. Prior to the finite element modelling of the stub columns, verification of the modified finite element program was carried out. This

verification was intended to test whether the multi-linear material model was properly incorporated into this finite element computer code. A simply supported plate subjected to tension was used to verify the changes. A multi-linear material model was used to represent the stress-strain relationship of the steel plate. Figure 5.5 reveals that the stress-strain relationship obtained from finite element modelling exhibits elastic, plastic, and strain-hardening behaviour exactly the same as the specified stress-strain relationship. From the results of modelling a simply supported plate, it was considered that the modification in the finite element program was correct. Therefore the modified finite element computer program was used for modelling the tests on stub columns. The proposed material models and the idealized residual stresses, which were developed and presented in Chapter 3, were used in the finite element modelling. Proposed material models included the modified bi-linear mode, modified tri-linear model, and multi-linear material model. The idealized residual stress varying across the width of the web/flange was assumed to have a parabolic distribution as shown in Figure 3.8.

5.2.4 Geometric Imperfections

Geometric imperfections may exist in plate components of W-shaped steel sections. The imperfections on the stub columns described in Chapter 4 were measured prior to the tests, and were found to be in the vicinity of 1 mm or less, except that the stub columns of 300W steel had maximum initial imperfection of 4 mm. These measured initial geometric imperfections can be incorporated in the finite element modelling. Also, in the finite element modelling of buckling problems, in order to initiate the local buckling mode of an individual

plate component of such sections, it is necessary to impose a disturbance which may be a geometric imperfection. The predicted buckled form of a plate component of a stub column consists of a half sine/cosine wave in the transverse direction, and one or a set of half sine waves in the longitudinal direction of the column (Abdel-Rahman 1997). Therefore, geometric imperfections of a half sine wave in the longitudinal direction, and a half sine/cosine wave in the transverse direction of a plate component were assumed in this study. Figure 5.4 schematically shows the geometric imperfections based on these assumptions. In Figure 5.4, it can be seen that half cosine and sine waves in the transverse direction were assumed with the flange and web, respectively. Also, a half sine wave in the longitudinal directions of both the web and flange was assumed. The largest geometric imperfections are located at the tips of the flange and the central point of the web. Therefore, the distribution of such assumed imperfections of a flange and web can be calculated at all nodal points using the following equations:

$$\textit{Flange Imperfection:} \quad \delta = \delta_0 \cos(\pi x/b_f) \sin(\pi y/L) \tag{5.1a}$$

$$\textit{Web Imperfection:} \quad \delta = \delta_0 \sin(\pi z/b_w) \sin(\pi y/L) \tag{5.1b}$$

where δ_0 is the imperfection amplitude at the tips of the flange and at the centre of the web, at the mid-height of the column, b_f and b_w are the width of flange and web respectively, and L is the length of the column. This distribution of initial geometric imperfection was used during the modelling of all the stub columns. Depending on the measured imperfections, various amplitudes associated with the initial imperfection were used for stub columns

depending on the dimensions of the stub column and the steel grades. For example, amplitudes used for the stub columns of 300W and 700Q steel grades were 4 mm and 0.4 mm, respectively.

5.2.5 Control Method and Loading Mechanism

In order to obtain the load-displacement (average applied stress-average strain) relationship beyond the ultimate load level, and to study the post-buckling behaviour, a displacement control method was used in the finite element modelling. However, the displacement control algorithm built into the finite element computer code used in this current study allowed the incremental axial displacement at only one node of the finite element mesh. Therefore, a special technique must be used to provide uniform incremental compressive displacement over the whole loaded end of the stub column, so that the quarter column can be modelled in a more realistic way (a member subjected to uniform displacement, simulating the experimental condition). Therefore, it was necessary to use rigid plate elements and rigid truss elements at the top end of the quarter column which provided a uniform incremental displacement loaded end condition. As shown in Figure 5.3, the rigid plate elements and the plate elements of the quarter column are connected through the rigid trusses. This arrangement in the finite element modelling ensures that the incremental displacement incurred at one node in the rigid plate can be transferred evenly to the nodes located at the loaded end of the quarter column. In order that the loaded end of the quarter column receive the same incremental displacement as that of the control node in the rigid plate, the rigid plate elements and rigid truss elements are deemed to have very large values of Young's

modulus. Therefore the deformations of the rigid plates and rigid trusses are negligible. Also, the ends of the trusses connected to the loaded end of the stub columns are free to rotate. Conversely, the ends of the trusses connected to the rigid plate are restrained from rotating. Such boundary conditions of the trusses are compatible with the boundary conditions of the loaded end of the stub column. In addition, it ensures that, under uniform incremental displacement throughout the analysis, the nodal points at the loaded edge of the quarter column can be maintained flat and straight in the same plane. With such boundary conditions, the model simulates the tests on stub columns, where the supporting plates had flat contact with the ends of the stub column.

As mentioned previously, a displacement controlled method was used in this finite element analysis. The displacement algorithm allows only one control node within the finite element mesh. The node 277 at the junction of the web and flanges, as shown in Figure 5.3, was selected as the control node. Based on the results of trial analysis, the incremental displacement of 0.05 mm was selected for every solution step. This small incremental displacement was to minimize the undesired disturbance, referring to the sudden drop in stress, that was noticed on the stress-strain curve when larger increments were used. Depending on the dimensions of the stub column and the steel grades, this incremental displacement allowed 40~120 solution steps to reach the ultimate load, and 250~450 steps to complete one analysis.

5.3 Comparison of Analytical Results with the Stub Column Tests

Based on the finite element model described in the previous section, analyses incorporating the proposed material models, which are the modified bi-linear, modified tri-linear and multi-linear models, were carried out. The finite element models had the same dimensions as the experimental stub columns of each steel grade. In this section, the analytical results will be compared with the test results in terms of the relationship between average axial stress and strain, local buckling behaviour, and ductility of these sections, and thus the compression flanges. In the experimental study on stub columns presented in Chapter 4, each selected steel grade consisted of three identical specimens. However, results obtained from these identical specimens were not the same, thus the average buckling stress, ultimate load, reserve capacity, and ductility were used to compare with the analytical results. In addition, in graphical comparison, only one specimen was selected to best represent the average overall behaviour of each steel grade. From these comparisons, the material model that best correlates with the experimental results will be selected to study the strength and compression flange ductility of high strength W-shaped steel sections with various b/t ratios.

Relationship of Average Axial Stress and Average Axial Strain

Figure 5.6 (A) shows the relationship between the average axial stress and strain of the 300W steel stub column, accompanied by the experimental results. It can be seen that results from the tri-linear and multi-linear models associated with this steel grade do not appear to correlate well with the experimental results. In these two models, little strain-hardening was observed in the average stress-strain relationship. On the other hand, the bi-linear material

model seems to correlate better with the test results. Using the bi-linear material model, the analytical results reveal a similar slope during strain-hardening to that from the experimental study. The ultimate load corresponding to each of these three material models are located in the vicinity where the ultimate load associated with the stub column test is located. It can thus be said that in modelling the stub column of 300W steel, analytical results obtained from the bi-linear material model correlate better with the experimental results.

Figure 5.6 (B) shows the average axial stress-strain relationship of the 350W steel corresponding to three different material models and that obtained from the test on stub column 350-3. Similar to the modelling of 300W stub columns, average stress-strain relationships obtained from the modified tri-linear and multi-linear models are quite similar. The average stress-strain relationship obtained from the bi-linear model shows a better correlation with the experimental result. Unlike the bi-linear model of 300W steel, which shows the ultimate load calculated from analytical modelling is slightly larger than that from testing, the ultimate load calculated for 350W is lower than the experimental one. The ultimate load associated with each material model is also located in the vicinity of the strain where the ultimate load from testing is positioned. Compared with results from testing stub column 350-3, the bi-linear material model reveals better analytical results in the finite element modelling.

Figure 5.6 (C) depicts the average axial stress-strain relationships of the results obtained from finite element analysis and those from testing the stub columns of 480W grade steel.

As mentioned in Chapter 3, the material models used in finite modelling for 480W steel were solely based on the results of only one tensile coupon associated with the stub columns of this steel grade. It was possible to have some uncertain test results from a single tensile test, thus it might result in some disagreements between the results from the stub column testing and those from finite element modelling. In Figure 5.6 (C), it can be seem that none of the relationships derived from these three proposed material models show good correlation with that from testing the stub columns of this steel grade. The average stress-strain curve associated with the bi-linear material model reveals that the ultimate load is higher than that from testing. On the other hand, the stress-strain curves associated with the tri-linear and multi-linear material models show that the ultimate stresses are approximately the same as those from the stub column testing. However, it must be acknowledged that there was a sudden drop, shortly after the yield stress is reached, in the stress-strain curves corresponding to the tri-linear and multi-linear material models. This disturbance was possibly caused, in the finite element modelling, by the low value of tangent modulus at the onset of strain hardening range corresponding to the tri-linear and multi-linear material models. It was considered that this disturbance was abnormal and unrealistic with regard to the material strain-hardening behaviour. Therefore this sudden drop was deliberately removed in order that the stress-stain relationship, beyond the yield stress, represents a more realistic strain-hardening behaviour.

Figure 5.6 (D) shows the average stress-strain relationship corresponding to 700Q steel stub columns. In finite element modelling, as described earlier, only the modified bi-linear

material model was used to model the stub columns of this steel grade. To reiterate, applying the material modelling procedures to the 700Q steel experimental stress-strain relationship would have resulted in similar material models (essentially a bi-linear model) regardless of the modelling procedure. This is due to the unique material stress-strain relationship possessed by 700Q grade steel. The average stress-strain relationship obtained from the analytical model exhibits very little strain-hardening and rapid drop in stress beyond the ultimate stress. The ultimate average axial stress appears much lower than that from the experiment. It was considered that the overall behaviour does not agree with the experimental results. This disagreement reveals, as experienced during the trial modelling, that the use of a relatively small tangent modulus in the strain-hardening range would yield inaccurate results.

Relationship between Average Axial Stress and Lateral Displacement

Figures 5.7 (A) shows the relationship between average axial stress and lateral displacement corresponding to the modified bi-linear model, modified tri-linear model, and multi-linear model of 300W steel, respectively. From the output of the analytical model, the maximum lateral displacement was located at the mid-height of the stub column, meaning that the maximum lateral displacement occurred at node 1 and 221 of the flange, and node 243 of the web. Therefore lateral displacements corresponding to these three nodes were used to study the local buckling behaviour and to determine the local buckling load. In addition, the average axial stress and lateral displacement relationship of the tested specimen, best representing the overall average behaviour of the stub columns of this steel grade, was also

included in these figures. As described earlier, the average axial stress-strain relationship from the bi-linear material model represented a better correlation with the test results. Therefore, the relationships obtained from the tri-linear and multi-linear material models will be discussed in lesser detail. In Figure 5.7 (A)-I, the stress to lateral displacement relationships obtained from the bi-linear model was depicted. It can be seen that the lateral displacement obtained from the analytical model tends to deviate more gradually than that of the stub column testing results. Overall, the results obtained from the analytical model correlated quite well with the experimental results. In addition, these relationships show that the lateral displacement at the centre of the web started to deviate later than at the tips of the flange. This indicated that, for a stub column with dimensions as presented in Chapter 4, the flange is more susceptible to compression local buckling than web local buckling. In Figure 5.7 (A)-II and III, the stress to lateral displacement relationships show similar behaviour to that obtained from the bi-linear material model. However, since the ultimate axial stresses associated with these two models were lower than that from the bi-linear material model, the stress to lateral displacement curves are relatively lower than those from the bi-linear material model.

Figures 5.7 (B)-I, II, and III show the relationships between the average axial stress and the lateral displacement associated with the 350W steel. Similar to the results of the modelling for 300W steel, maximum lateral displacements occurred at the same nodes as those of the 300W steel model. Figure 5.7 (B)-I represents this relationship obtained using the bi-linear material model. It shows that results obtained from this model correlate well with the

experimental results, except that the ultimate average stress from the stub column test is higher. It can also be seen that the web tends to be stiffer to resist local buckling. The relationships corresponding to the tri-linear and multi-linear model, shown in Figures 5.7 (B)-II, and III, respectively, reveal that the curves have a similar pattern to those from the bi-linear model. However, these curves are lower than the experimental ones because the ultimate stresses obtained from these models are relatively lower than those corresponding to the test results.

Figures 5.7 (C)-I, II, and III show the average stress to lateral displacement relationships corresponding to the 480W stub columns. The output of the analytical model shows that maximum lateral displacements occurred near the end of the stub column, rather than the mid-height of the column. Therefore the lateral displacements corresponding to the nodes with maximum deviation were used to determine these relationships and to determine the local buckling load. The lateral displacements obtained from the stub column tests were based on the measurement of the LVDTs located at the mid-height of the column. However, the most laterally deformed part of the flange of the specimen was not located at the mid-height. Therefore, as described previously in Chapter 4, results from the LVDTs could not be used to study the local buckling behaviour accurately. All these figures show results similar to those of the stub column tests, except that analytical models exhibit more lateral displacements. Moreover, it was observed that, from the relationships of all three material models, lateral deformation on the flange of these stub columns began earlier than the web, indicating that the web is stiffer to withstand local buckling under uniform compression.

Figure 5.7 (D) shows the stress to lateral displacement relationship corresponding to the 700Q steel. It appears that the flange and web started to deviate when the yield stress was reached. Results from the analytical model did not correlate well with the experiment results. It was observed that, in the experimental study of stub column testing, flange buckling did not occur in symmetric fashion. However, Figure 5.7 (D) shows that one tip of the flange buckled towards the centerline of the web, and the other buckled away from the centerline of the web. This represents symmetric buckling behaviour of the flange and it is different from what was observed from the experimental studies.

Buckled Shapes

As discussed previously, the bi-linear material model best represents analytical results associated with the average axial stress-strain relationship, and the average stress to lateral displacement relationship. Therefore, only the buckled shapes of each analytical model associated with the bi-linear material model are plotted, as shown in Figures 5.8 (A) to (D). For the finite element modelling purposes, initial imperfections were imposed with each analytical model corresponding to each steel grade. Since these initial imperfections were unsymmetric, it is expected that the modelled stub columns would not buckle in a symmetric form. Therefore, the lateral displacements at nodes 1 and 221, which were both at the mid-height of the column, were expected to be different. The deformed/buckled shape at various stress levels are shown in these figures. It can be seen, in Figures 5.8 (A)-(B), that models corresponding to 300W and 350W buckled into three half sine waves and maximum lateral displacement occurred at the mid-height of the modelled column. However, the model

corresponding to the 480W steel buckled near the loaded end. As shown in Figures 5.8 (C), very small amounts of lateral displacement at the mid-height were obtained. Therefore, the nodal points with the most lateral displacement were selected to determine the local buckling load. Figures 5.8 (D) show the buckled shapes corresponding to the 700Q steel. It appears that the model buckled in one half sine wave and the half sine wave is relatively short, meaning that the local buckling does not propagate as much as those of other steel grades.

Discussion of Analytical Results

Results from the finite element modelling are summarized in Table 5.1. In Table 5.1, f_u and f_l are the ultimate average stress and the average stress at local buckling, respectively, corresponding to different material models under consideration. f_y is the material specified yield strength or average specified yield strength for the stub column. D_u, D_l, and D are the compression flange ductilities (represented by average strain of a stub column) corresponding to the ultimate average stress, local buckling state, and at the specified yield strength level of the descending branch, respectively. These quantities were defined in the same way as that described in Chapter 4. In Table 5.1, the values of D_u and D_l are much less than that of D for all these steel grades. For example, results associated the bi-linear material model of 350W steel show that the values of D_u and D_l are both 4.3, but the value of D is 15. This indicates that 350W steel had substantial deformation capacity beyond the average ultimate stress and local buckling stress before the stress reduces to the minimum specified yield stress level. Therefore it is more meaningful to use the value of D to consider the compression flange ductility of a W-shaped section. The correlation between the

experimental and analysis material model results was established based on the ratio of the experiment result to the analytical result. From these response ratios, an overall mean response ratio was obtained by calculating the average of these ratios corresponding to f_u, D_u, D_l, and D. The mean value associated with the bi-linear material model for 300W and 350W steels are 0.92 and 1.01, respectively, which were quite close to unity. This indicates that the analytical results obtained from the bi-linear material model correlate well with the experimental study, when considering the reserve capacity and ductility of the stub column. The mean values associated with the tri-linear and multi-linear material models are both greater than unity and the difference between the mean value and unity is larger than that associated with the bi-linear material model. The mean value associated with the different material models for the 480W steel are not close to unity, and they vary from 1.35 for the bi-linear model to 1.58 for the multi-linear model. This indicates that the analytical results moderately correlate with the test results, in comparing the mean values of the 300W and 350W steels. The mean value for the 700Q steel is 8.66, which is much higher than unity. This shows that the analytical results of the 700Q steel correlated poorly with the experimental results. This poor correlation was possibly caused by the relatively low tangent modulus chosen at the onset of the strain-hardening range.

Overall, the analytical results associated with the bi-linear material model corresponding to all these steel grades best correlated with the experimental results. Based on b/t ratios associated with Class 1 sections defined in the current standards (CSA 1995), the analytical results show that the Class 1 section had variable reserve capacity. For a Class 1 section,

700Q has very little reserve capacity and, on the other hand, 300W and 350W steel had a considerable amount of reserve capacity beyond the specified yield strength. Observing the compression flange ductility values, 350W steel has a similar amount of ductility to that of the 300W steel. Therefore, it can be considered that the b/t ratio defined in the CSA standard for a Class 1 section is applicable to the 350W steel. Results associated with the 480W steel were based on the results of a tensile coupon with abnormally higher yield stress than the specified yield value. Therefore results obtained from the analytical model cannot be used to determine the applicability of the CSA standard to this steel grade. Compared with the results corresponding to the 300W and 350W steel, results related to the 700Q steel showed that a Class 1 section of this grade has very little reserve capacity and lesser ductility. Therefore, the current CSA standards may not be applicable to the 700Q steel grade.

5.4 Strength and Ductility of W-shaped Sections with Various b/t Ratios

As discussed previously, the analytical results associated with the bi-linear material model correlated better with the experimental results. Therefore the bi-linear material model was selected to further study the strength and ductility of compression flanges of W-shaped sections having various b/t ratios. Due to the uncertainty of the 480W steel (as described previously), only 300W, 350W and 700Q steels were considered in this investigation. Four b/t ratios were selected based on the current CSA standard (1995) as guideline, and they are presented in Table 5.2. Two of these four b/t ratios were in the range of Class 1 section, more specifically, one was chosen at the Class 1 limit and the other was selected within the Class 1 b/t limit. One of remaining two b/t ratios was chosen at the limit of a Class 2 section

and the other had the b/t ratio by taking the average of the b/t limits of Class 1 and Class 2 sections. The rationale for selecting these b/t ratios was to determine whether the high strength steel section with b/t limits in this range can be incorporated into the current design standards. The analytical model used in this analysis was the same as that used to compare with the experimental results. The average axial stress-strain relationships of these selected steel grades were compiled and plotted in Figures 5.8 (A) to (C). Results from the finite element modelling were summarized as presented in Table 5.2.

Figures 5.8 (A) and (B) show the average axial stress-strain relationships associated with the 300W and 350W steel, respectively. From these figures, it appears that relationships of the 350W steel exhibit similar behaviour to that of the 300W steel, except that 350W steel has higher ultimate average stress. All stress-strain relationships exhibit strain-hardening and these relationships of both steel grades show that the ultimate average stress and the associated strain tend to decrease as the b/t ratio increases. Stress beyond the ultimate average stress decreases gradually. This indicates that the W-shaped sections of these two steel grades have considerable amounts of ductility. Figure 3.9C shows the relationship between the average axial stress and strain of the 700Q steel. Unlike the behaviour of 300W and 350W steel, the stress-strain relationship of this steel grade shows very little or no strain-hardening behaviour. Stress tends to drop more rapidly beyond levels exceeding the ultimate stress.

In Table 5.2, the reserve capacity and the compression flange ductility (represented by

average strain) associated with the corresponding b/t ratios are presented. The 300W steel, which was used to establish the b/t limits in the current design standards, exhibits a considerable amount of ductility and reserve capacity. However, note that the current Class 1 limits were established based on a compression flange ductility demand of 10.4 (Dawe and Kulak 1981), and 300W Class 1 limit exhibits that D_u and D values are 4.1 and 13.8, respectively. It can be seen that the ductility and reserve capacity decrease as the b/t ratio increases. The 350W steel, which has been recently introduced to the industry to replace the 300W steel, also reveals considerable ductility and reserve capacity. In addition, the amount of ductility and reserve capacity are quite similar to that of the 300W steel. Therefore, it can be considered that the b/t limits in the current design standards are applicable to the 350W steel. On the other hand, the 700Q steel reveals very little compression flange ductility and reserve capacity. For sections with b/t ratios of 6.0 and 6.4, the corresponding ultimate stress was even lower than the yield stress. Based on these analytical results, it can be concluded that the b/t limits in the current design standards are not applicable to 700Q steel.

Table 5.1 Ductility and Reserve Capacity (Experimental and Finite Element Results)

Steel Grade	Results	Properties					
		f_u/f_y	f_l (MPa)	D_u	D_l	D	Mean
300W	Experimental Average	1.28	382	3.7	3.5	12.4	
	Model 1: Bilinear	1.34	399	4.1	3.7	13.8	
	Test / Bilinear	0.96		0.90	0.92	0.90	0.92
	Model 2: Tri-linear	1.21	362	3.2	3.2	7.2	
	Test / Tri-linear	0.94		1.14	1.03	1.72	1.21
	Model 3: Multi-linear	1.15	346	3.4	3.4	7.3	
	Test / Multi-linear	0.90		1.09	0.99	1.69	1.17
350W	Experimental Average	1.28	454	4.7	4.1	15.2	
	Model 1: Bilinear	1.28	447	4.3	4.3	15.0	
	Test / Bilinear	1.00		1.08	0.95	1.01	1.01
	Model 2: Tri-linear	1.24	432	3.9	3.9	8.8	
	Test / Tri-linear	1.04		1.18	1.04	1.73	1.25
	Model 3: Multi-linear	1.23	431	3.9	3.9	9.3	
	Test / Multi-linear	1.04		1.18	1.04	1.64	1.23
480W	Experimental Average	1.28	675	2.3	2.0	4.3	
	Model 1: Bilinear	1.20	706	1.5	1.5	3.0	
	Test / Bilinear	1.07		1.58	1.35	1.40	1.35
	Model 2: Tri-linear	1.14	675	1.3	1.3	2.7	
	Test / Tri-linear	1.12		1.76	1.51	1.58	1.49
	Model 3: Multi-linear	1.13	669	1.2	1.2	2.6	
	Test / Multi-linear	1.13		1.91	1.63	1.66	1.58
700Q	Experimental Average	1.19	750	3.4	2.1	5.6	
	Model 1: Bilinear	1.01	708	0.2	0.2	1.7	
	Test / Bilinear	1.18		18.76	11.45	3.25	8.66

Table 5.2 Ductility and Reserve Capacity of W-shapes with various b/t Ratios

Steel Grade	b/t ratio	Properties		
		f_u/f_y	D_u	D
300W	7.7	1.38	5.1	21.7 (estimated)
	8.4	1.34	4.1	13.8
	9.1	1.31	3.5	16.8
	9.8	1.28	3.1	12.0
350W	7.2	1.29	4.7	17.0
	7.8	1.28	4.3	15.0
	8.5	1.26	3.6	12.2
	9.1	1.25	3.2	10.7
700W	5.0	1.01	0.2	1.7
	5.5	1.01	0.1	1.7
	6.0	1.00	0.1	N.A.
	6.4	0.99	0.1	N.A.

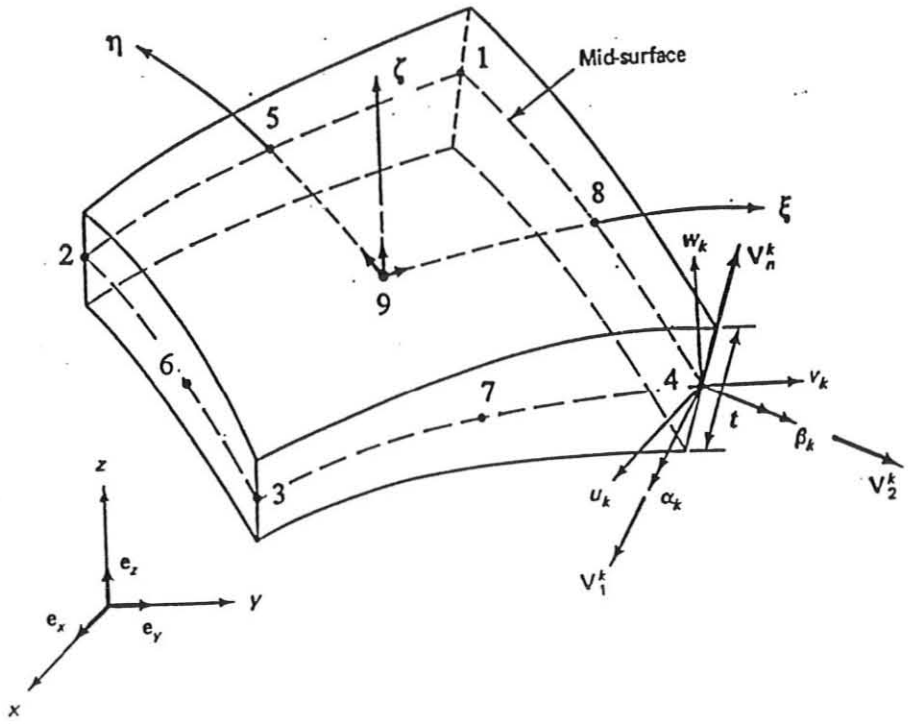

Figure 5.1 The 9-node Shell Finite Element (Abdel-Rahman 1997)

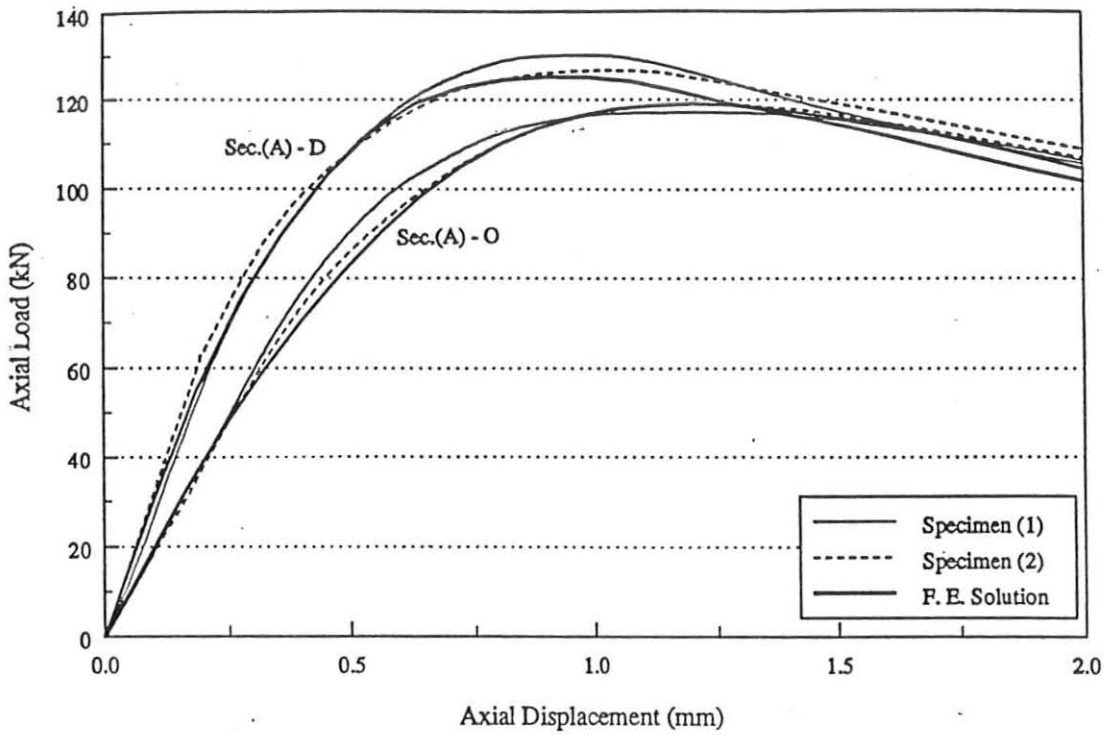

Figure 5.2 **Experimental and Finite Element Analysis Predicted Response (Abdel-Rahman 1997)**

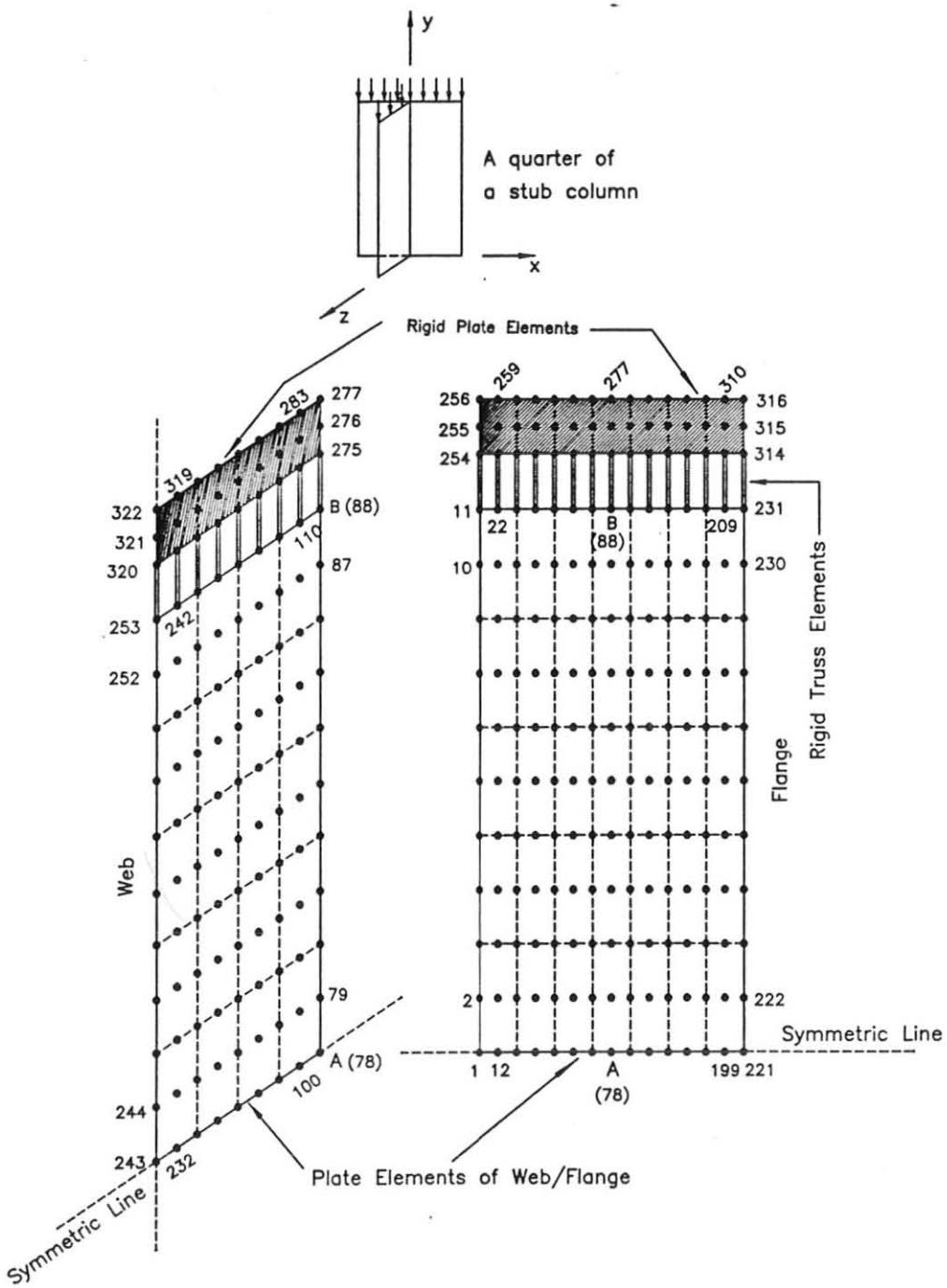

Figure 5.3 Finite Element Mesh of a Quarter of a Stub Column

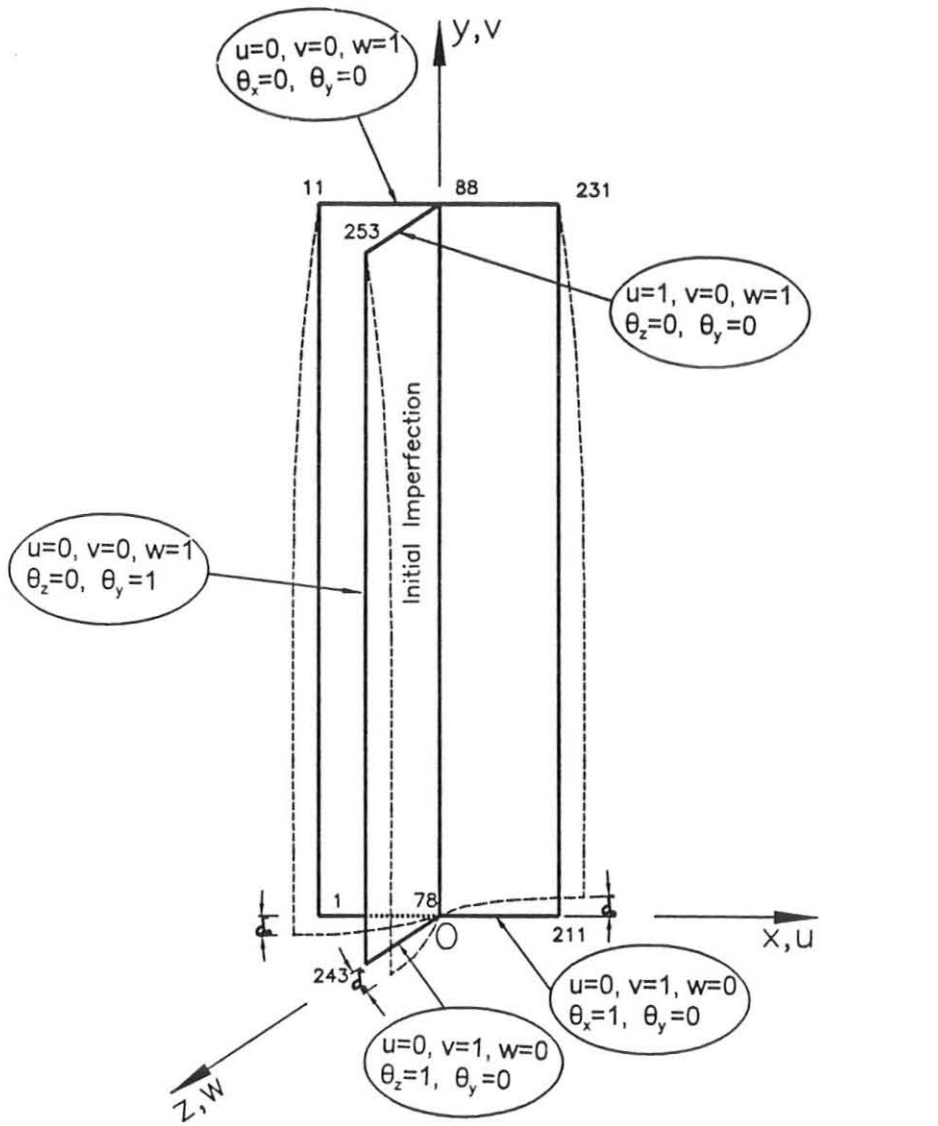

Note: 1 represents fixed boundary condition
0 represents free boundary condition

Figure 5.4 Boundary Conditions and Initial Imperfections of the Finite Element Model

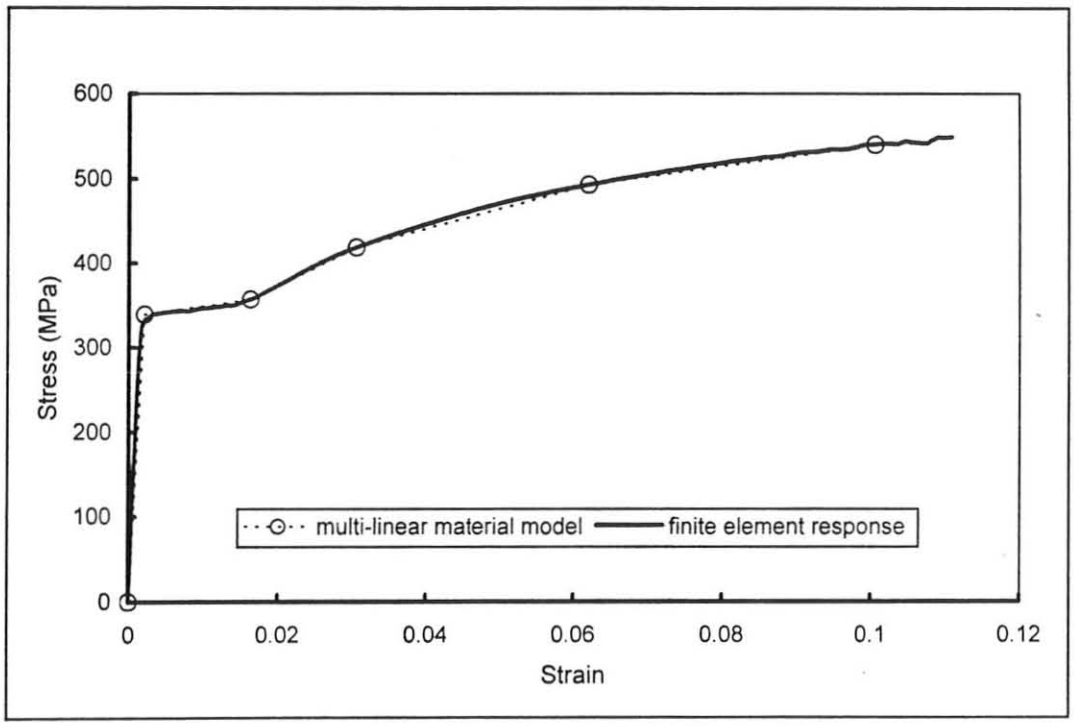

Figure 5.5 Verification of Multi-linear Model with the Finite Element Modeling

(A)

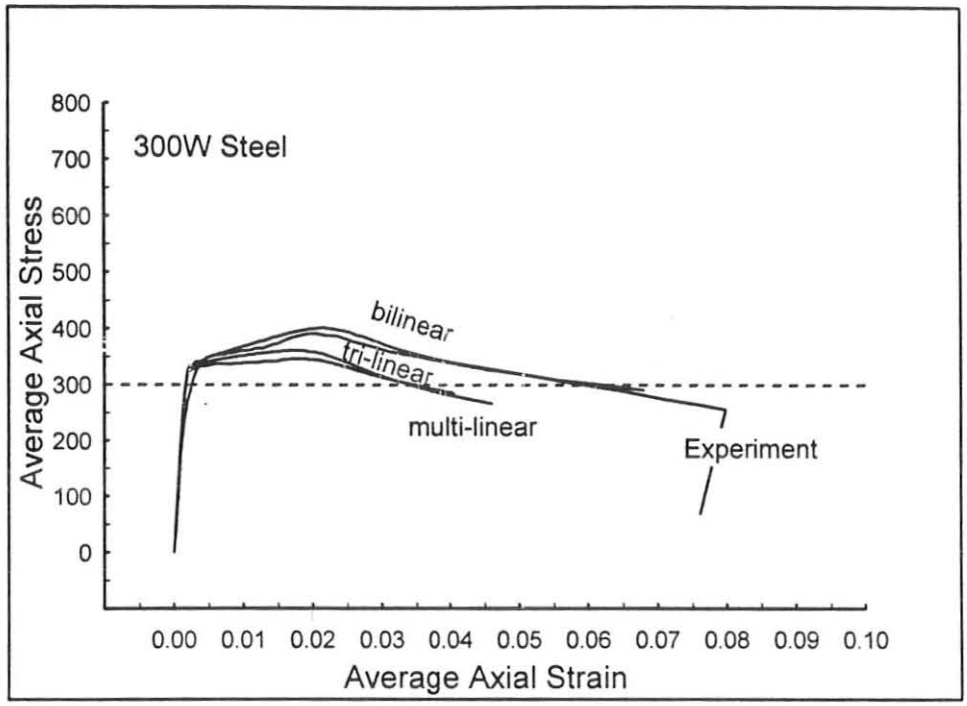

(B)

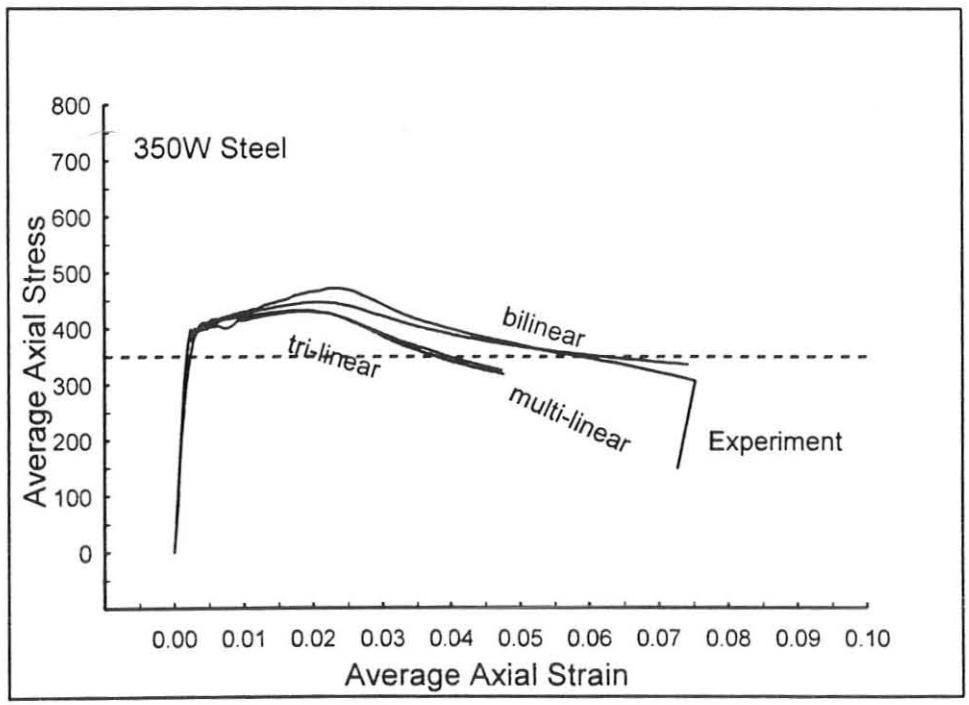

Figure 5.6 (A) - (B) Comparison of the Experimental Results with the Analytical Results from Different Material Models

(C)

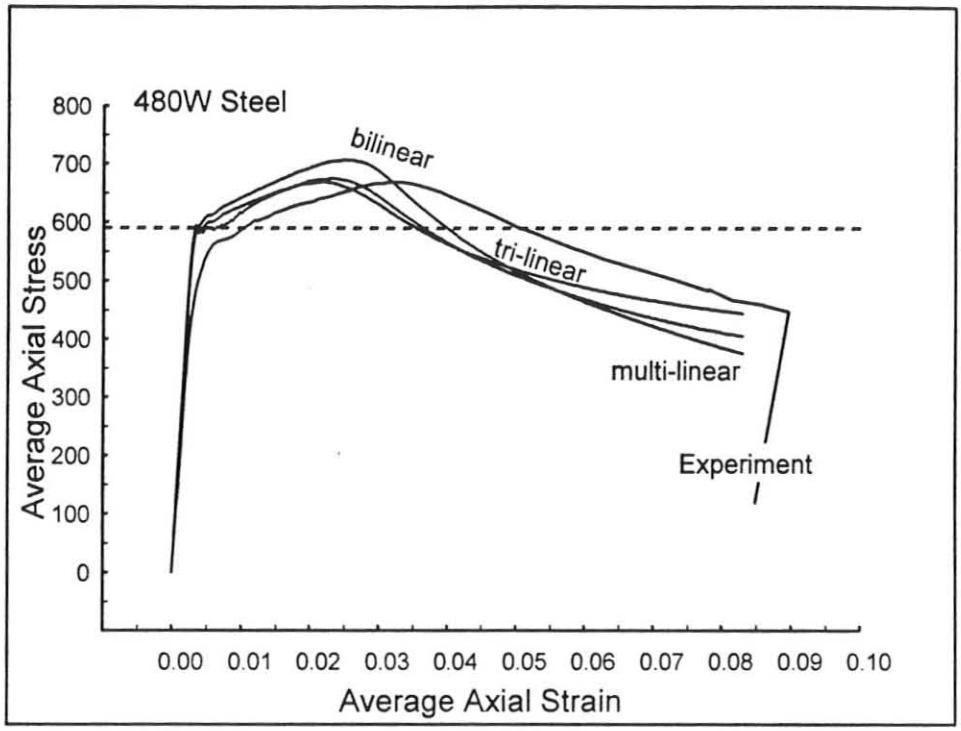

(D)

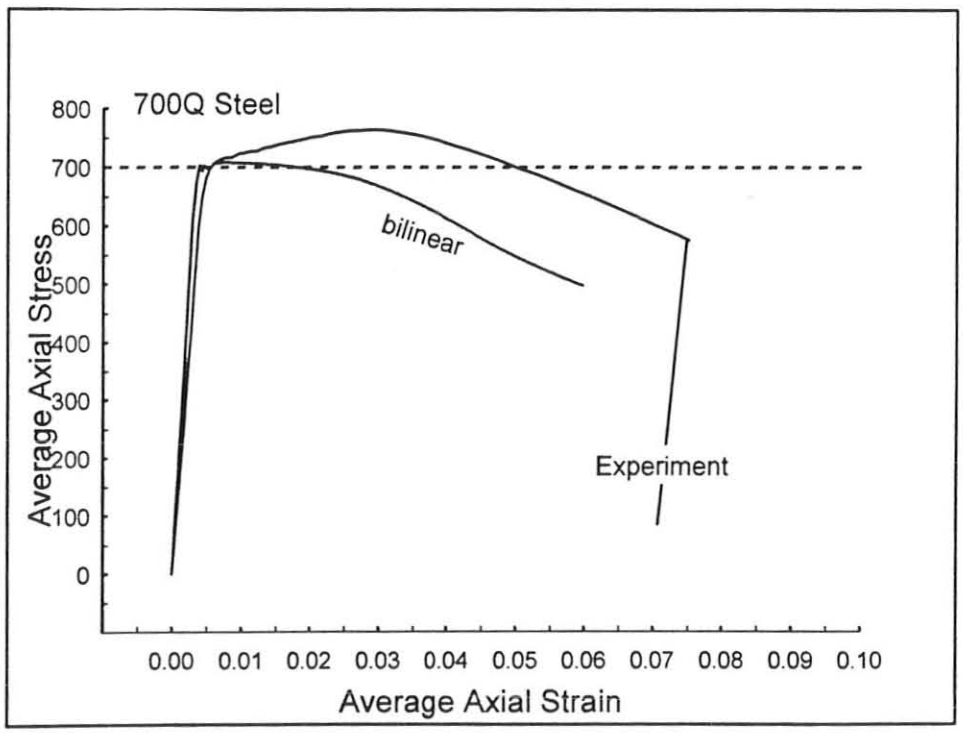

Figure 5.6 (C) - (D) Comparison of the Experimental Results with the Analytical Results from Different Material Models

(I)

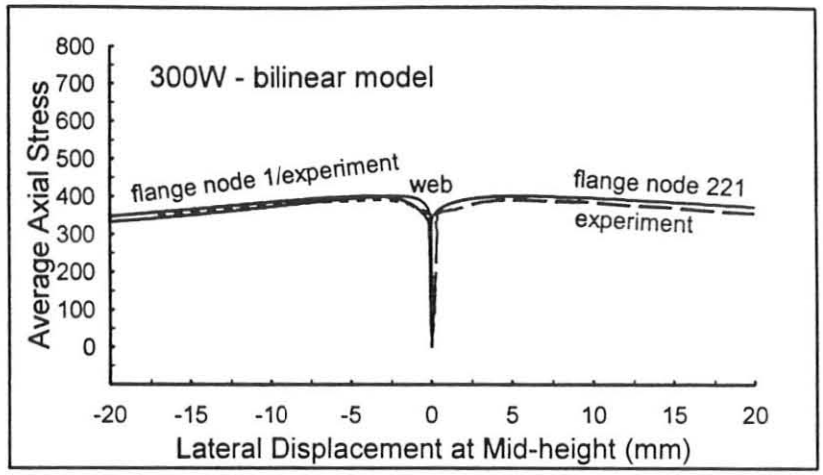

(II)

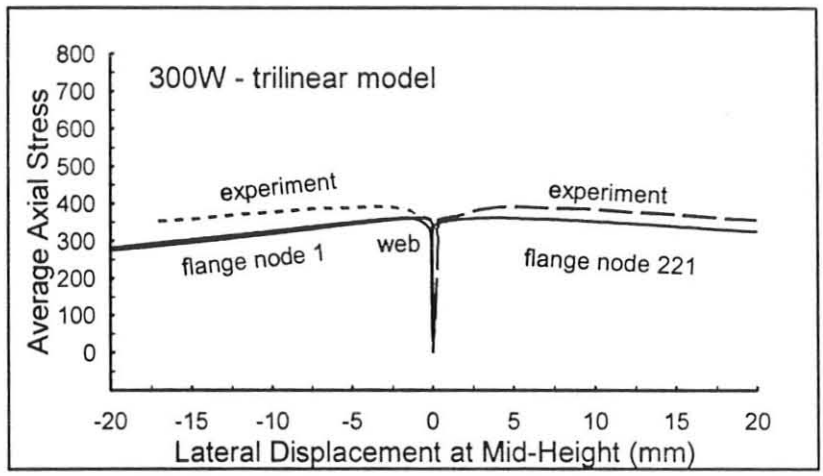

(III)

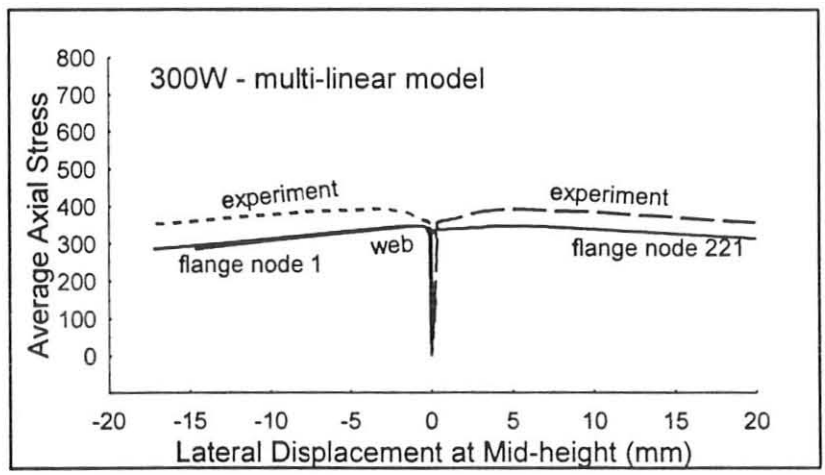

Figure 5.7 (A) Relationships of Average Axial Stress and Lateral Displacements from Different Material Models

(I)

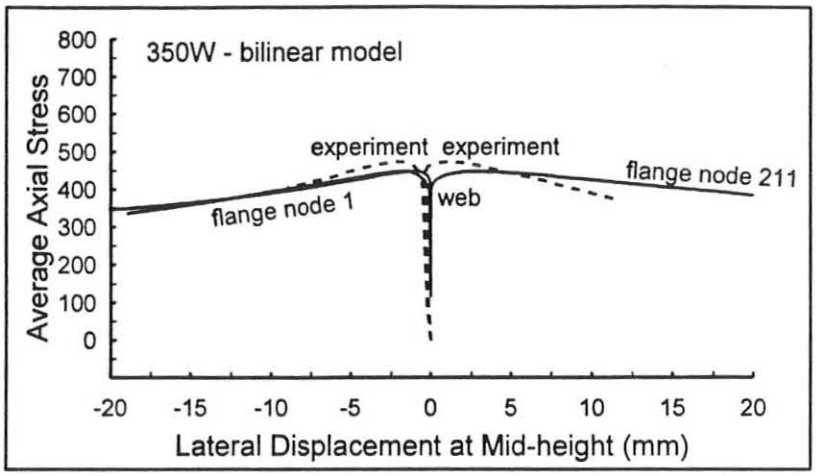

(II)

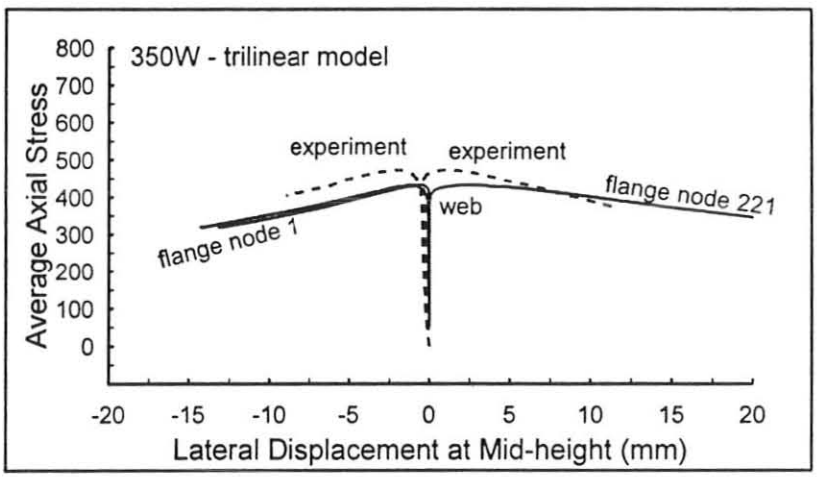

(III)

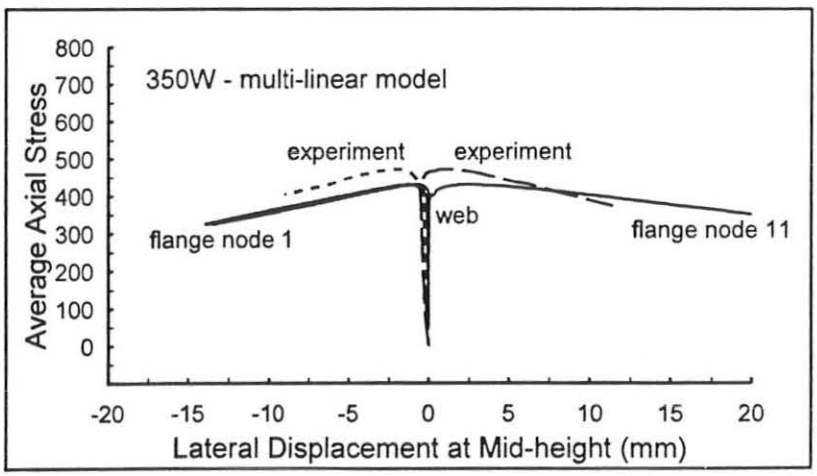

Figure 5.7 (B) Relationships of Average Axial Stress and Lateral Displacements from Different Material Models

(I)

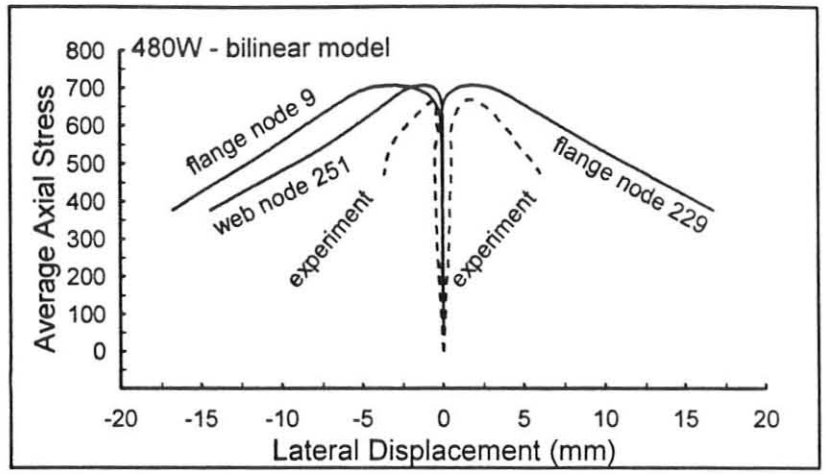

(II)

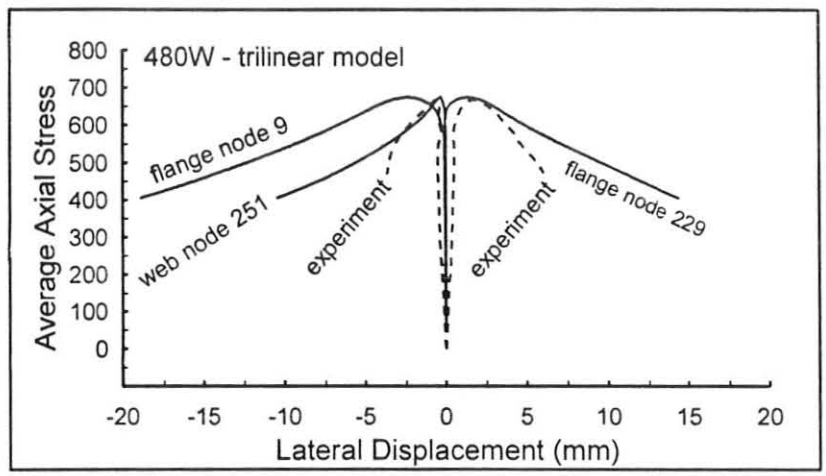

(III)

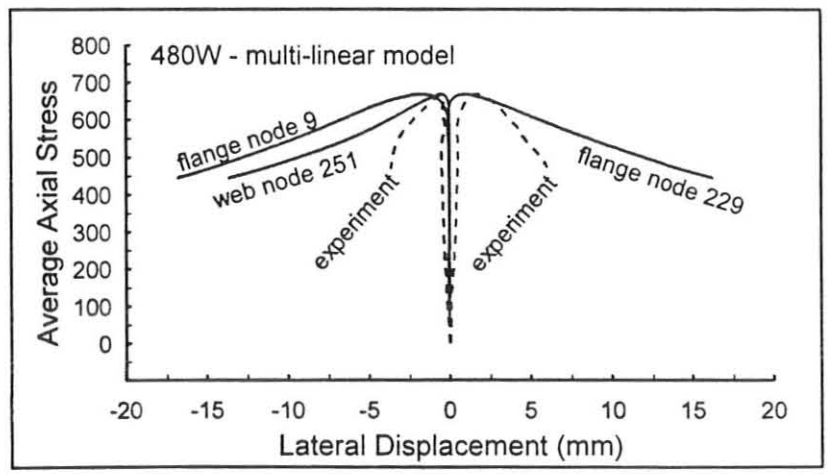

Figure 5.7 (C) Relationships of Average Axial Stress and Lateral Displacements from Different Material Models

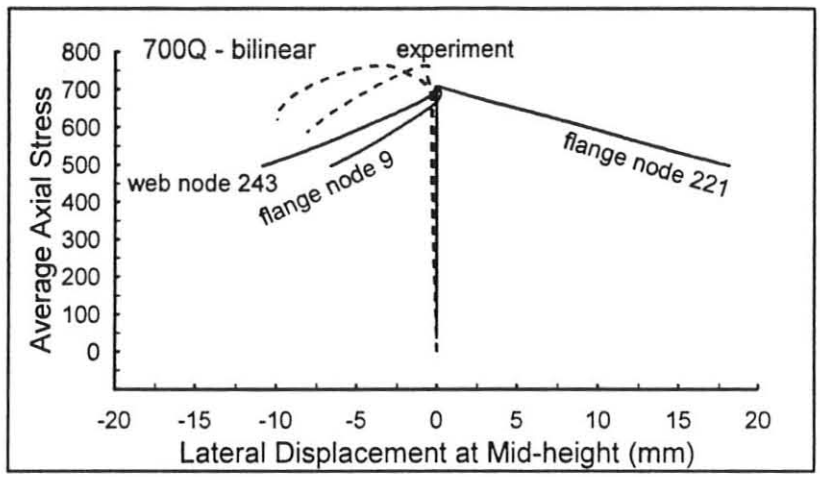

Figure 5.7 (D) **Relationships of Average Axial Stress and Lateral Displacements from Different Material Models**

(I)

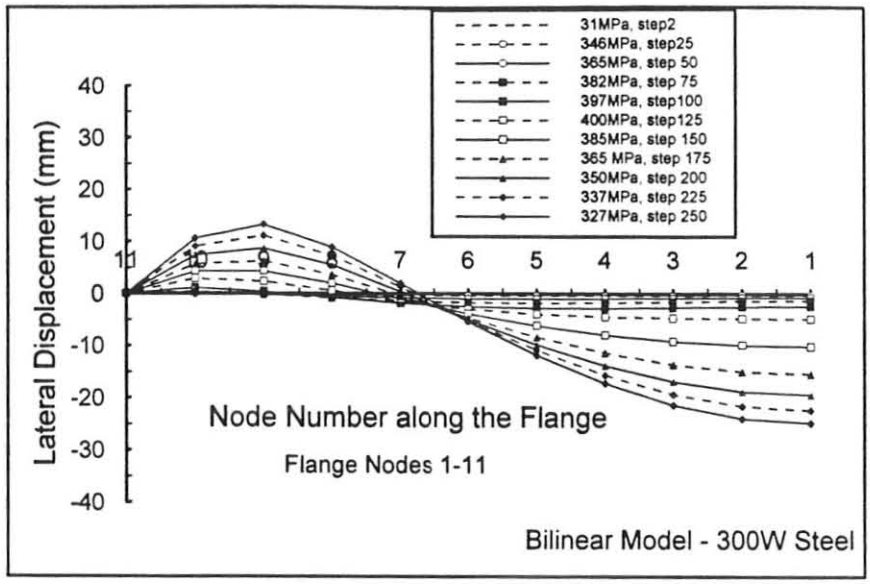

(II)

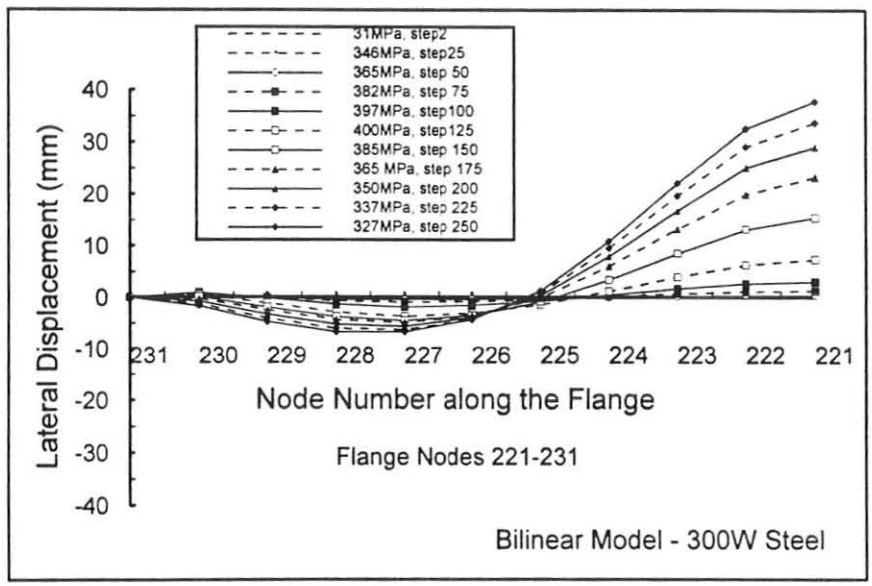

(III)

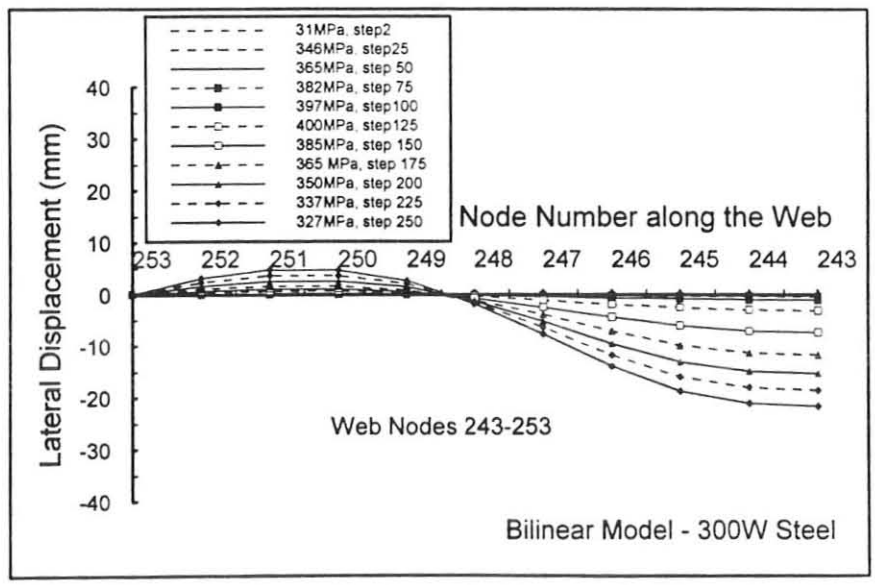

Figure 5.8A Deformed Shapes in the Longitudinal Direction of the Column at Various Stress Levels

(I)

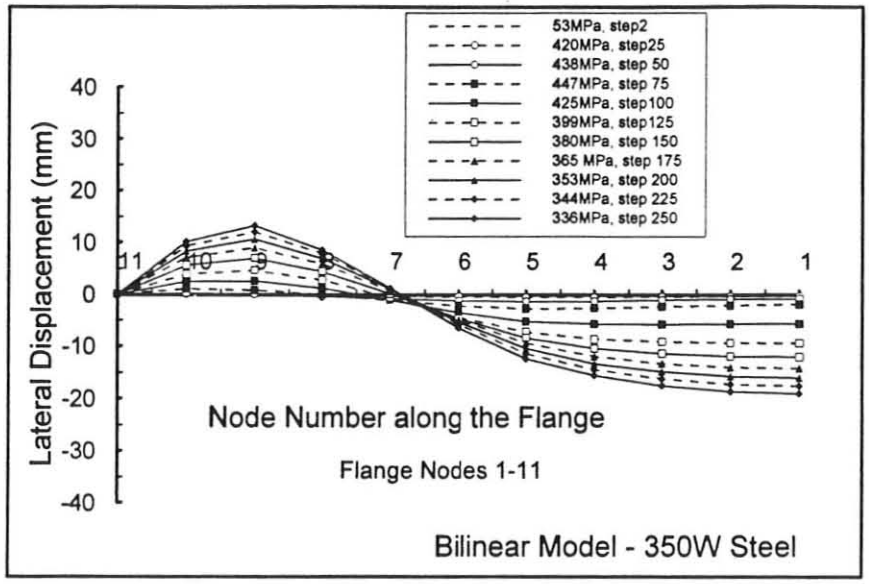

(II)

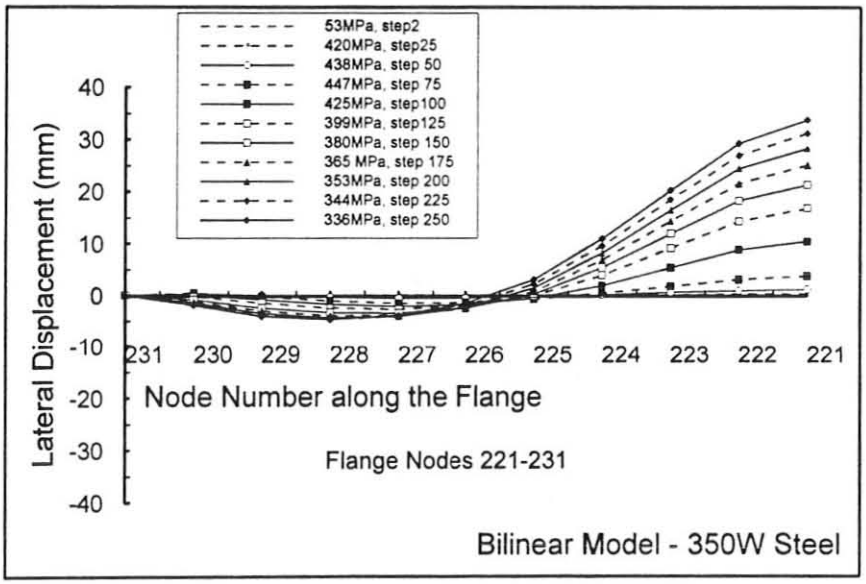

(III)

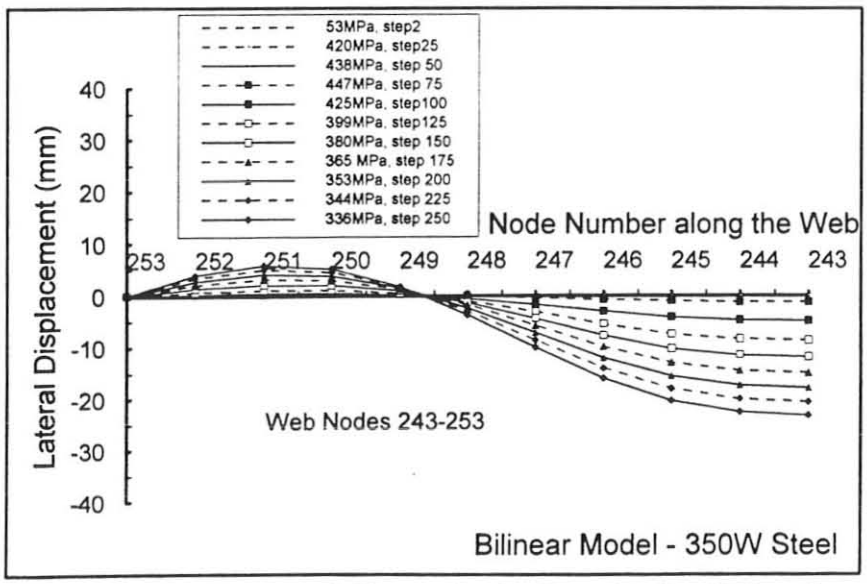

Figure 5.8B Deformed Shapes in the Longitudinal Direction of the Column at Various Stress Levels

(I)

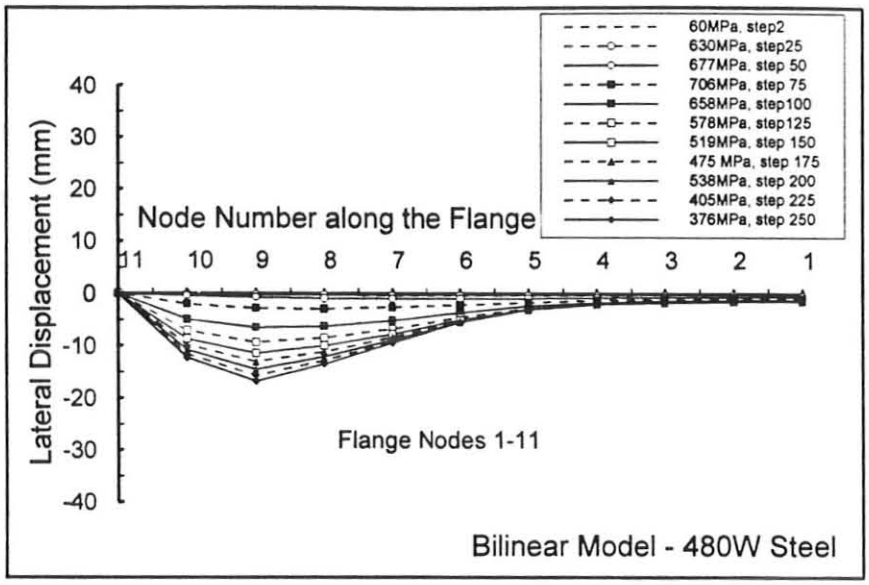

(II)

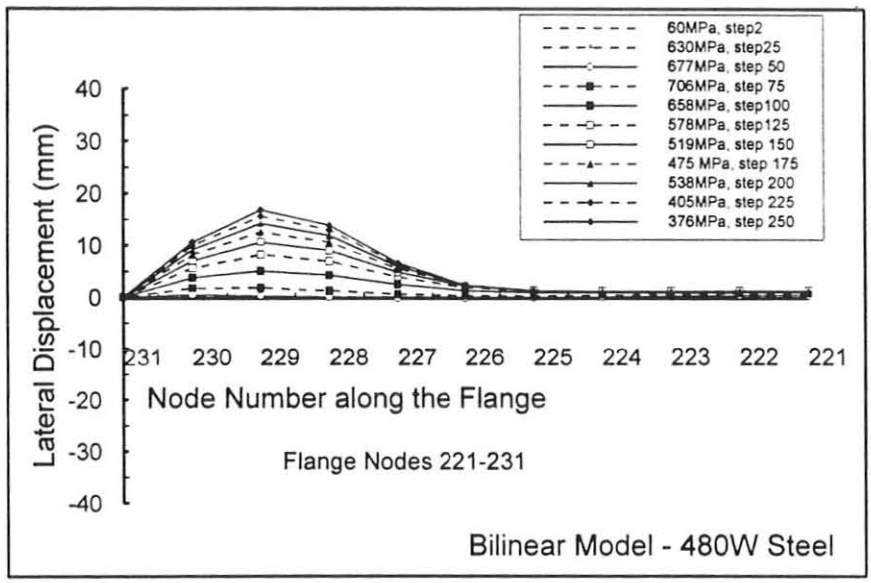

(III)

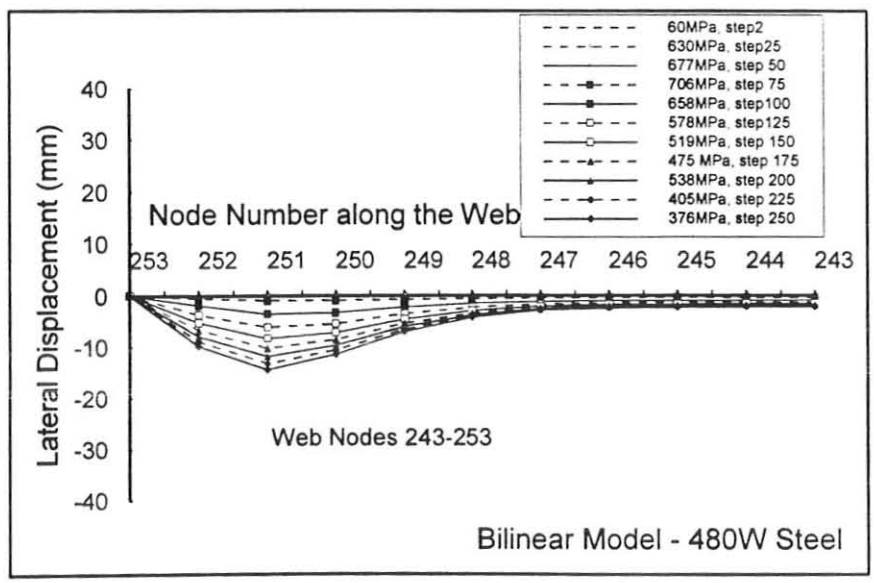

Figure 5.8C Deformed Shapes in the Longitudinal Direction of the Column at Various Stress Levels

(I)

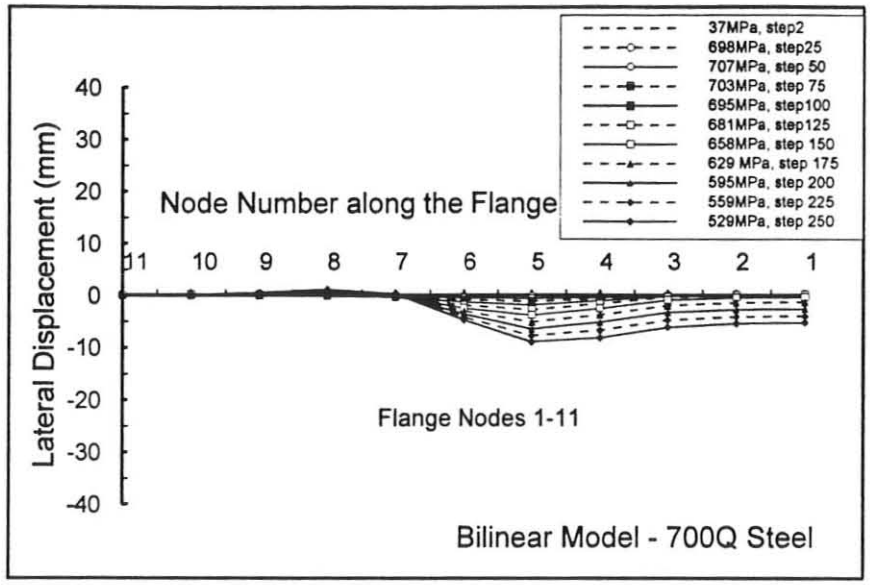

(II)

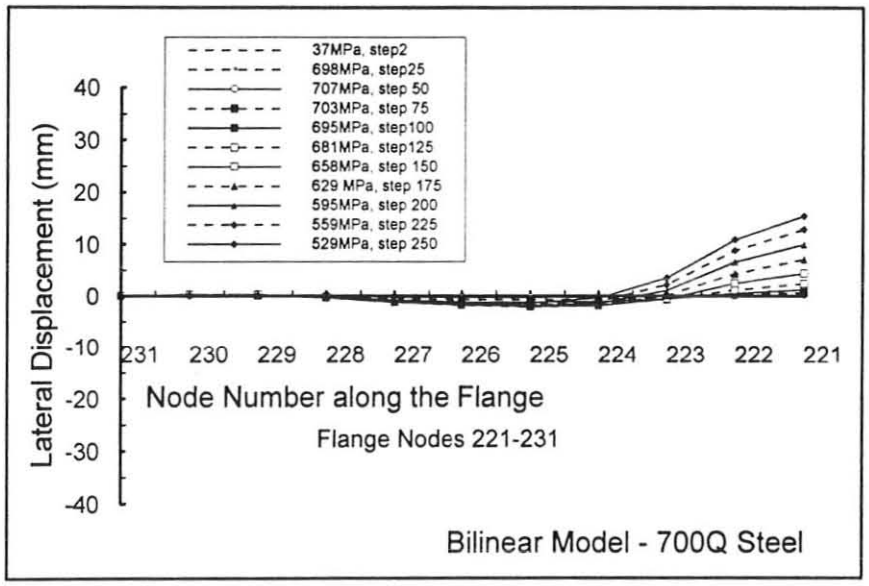

(III)

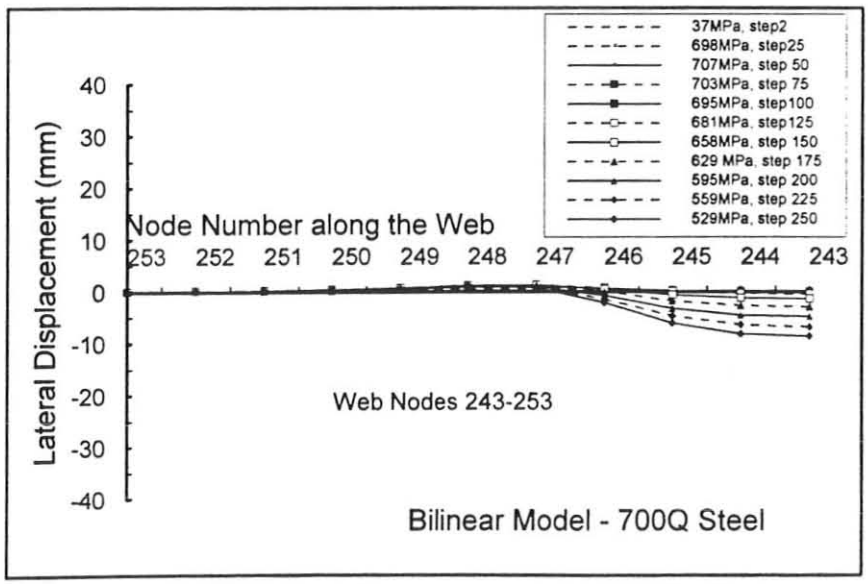

Figure 5.8D Deformed Shapes in the Longitudinal Direction of the Column at Various Stress Levels

(A)

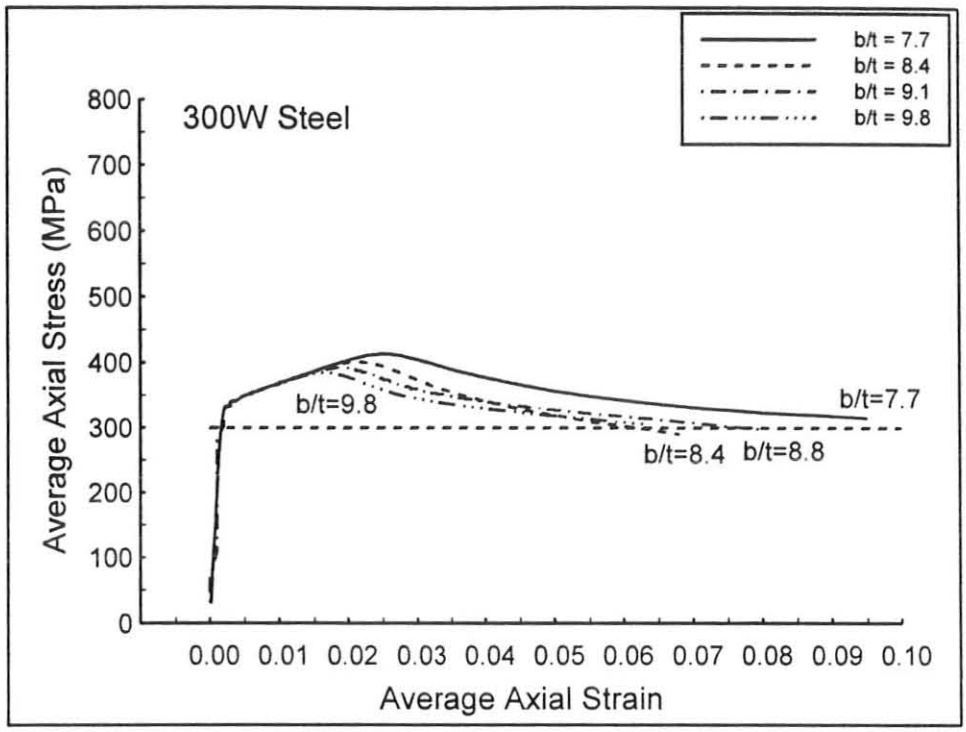

(B)

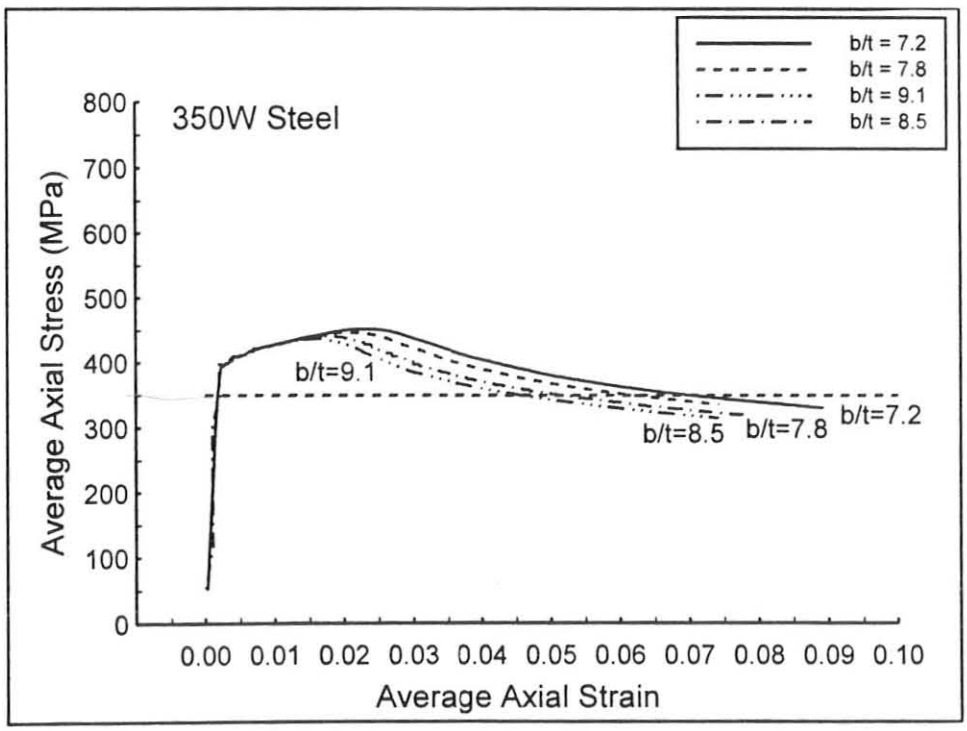

Figure 5.9 (A) - (B) Effects of b/t Ratios on Strength of W-shaped Columns (300W, 350W Steel)

(C)

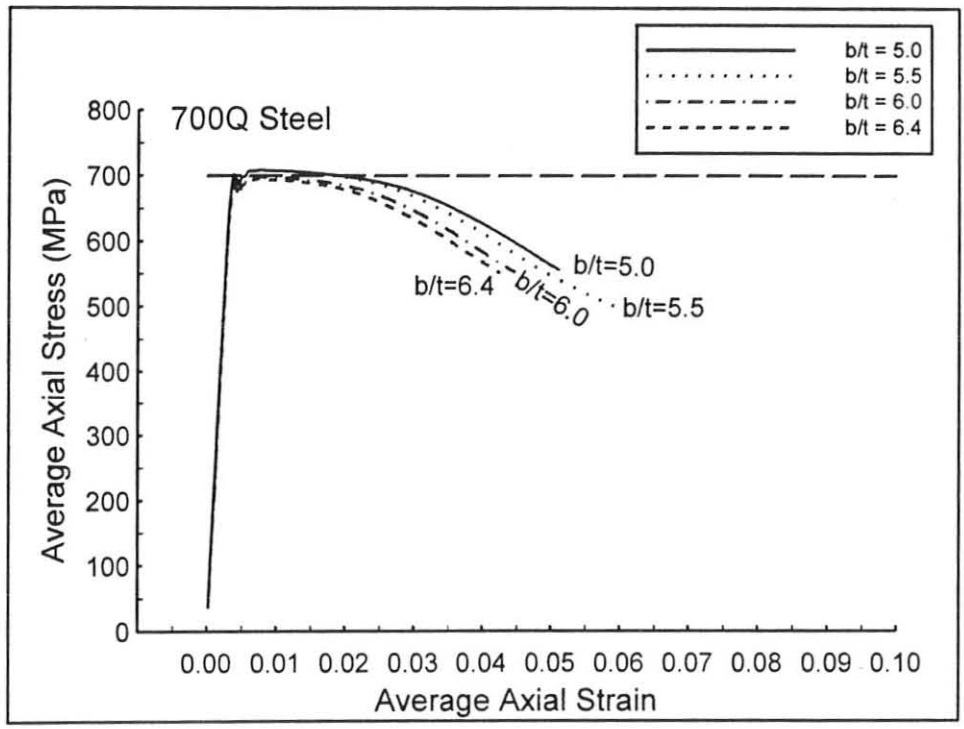

Figure 5.9 (C) Effects of b/t Ratios on Strength of W-shaped Columns (700Q Steel)

Chapter 6

Summary, Conclusions and Recommendations

The W-shaped steel members have been widely used in various contemporary structures such as buildings, bridges, and industrial complexes. These members possess considerable high strength/weight ratio and high ductility, thus they are used as beams, columns, and beam-columns. However, the strength and ductility of these members are limited by local buckling of the plate components of these members. In order to avoid local buckling, the design procedure for W-shaped members usually includes limitations on the acceptable width-to-thickness ratios for web and flanges. By controlling the width-to-thickness ratios of the plate components, local buckling load can be varied until the member has achieved the desired strength and deformation capacity. The current local buckling rules given in the steel design standard (CSA 1995) are primarily based on 300W steel, known as structural mild-carbon steel. The 300W steel has excellent ductility, but lesser strength. Therefore, when a light-weight structure is preferred in a structural design, high strength steels may be considered. High strength steels tend to be used more often in steel construction, and recently the 300W steel has been replaced by 350W steel. Even though these new sections produced with 350W steel have higher strength, they may possess less ductility. Little research has been done on such high strength structural steel sections. Therefore it is necessary to have a better understanding of how the high strength steel behaves and whether the current design specifications are applicable to structural members made of such material.

This investigation is intended to study the effects of material behavior of high strength steel on the local bucking behavior of W-shaped steel members, and to determine whether the current specifications related to local buckling of W-shaped sections are suitable to high strength steel members. In this study, tensile tests on steel coupons made from different steel grades were performed to obtain the stress-strain relations of these steels and to determine appropriate analysis material models for finite element analysis. This investigation also includes tests on stub columns of 300W, 350W, 480W, and 700Q steels, whose flange dimensions were in accordance with Class 1 limits based on the current design standard (CSA 1995). These tests were carried out to establish the strength and ductility of compression flanges of W-shaped sections of these steel grades undergoing local buckling failure. From the results of these stub column tests, the applicability of b/t limits of Class 1 sections defined in the current CSA standard were assessed. The final part of this study was to use the material models derived from the tensile tests to obtain results using finite element modeling. The finite element model uses 9 node shell element, and includes imperfections, such as residual stresses and geometric imperfections. The finite element analysis results are compared with the corresponding experimental results. Depending on the agreement with the experimental results from the stub column tests, an appropriate material model was selected to incorporate into a parametric study using the finite element analysis. Strength and compression flange ductility of W-shaped sections with varying flange width-to-thickness ratio (b/t) and constant web width-to-thickness ratio (w/t) were determined from finite element analysis. Conclusions were made to the applicability of the local buckling rules to high strength steel W-shaped sections.

Tensile tests have been performed on 300W, 350W, 480W and 700Q steel grades. Based on these tensile tests, only 300W steel possess obvious yield plateau on the stress-stain curves. 350W steel has very little yield plateau on the stress-strain curves, and 480W and 700Q steels showed no yield plateau on the stress-strain curves. The material ductility and the amount of strain hardening or reserve capacity of 300W steel and 350W steel were comparable. 480W steel had yield strength abnormally higher than the minimum specified yield strength and it was considered the results from testing on only one tensile coupon of this steel grade may misrepresent the material properties of this steel grade. 700Q steel had the highest yield strength, and the least material ductility and reserve capacity in all steel grades considered in this study. In addition, based on these material properties obtained from tensile tests, a modified bi-linear, a modified tri-linear, and a multi-linear material model corresponding to each steel grade were determined for the purposes of finite element modeling.

Tests on stub columns of these same steel grades, as used in the tensile tests, were performed to obtain strength and compression flange ductility of high strength W-shaped steel sections. The b/t ratios of the specimens corresponding to each steel grade were based on Class 1 limit as defined by the current steel design standard (CSA 1995). All stub columns with relatively lower strength (300W and 350W) tended to have symmetric locally buckled forms on the tips of the flanges, but some stub columns of higher strengths (480W and 700Q) showed unsymmetric and erratic locally buckled shapes on the flanges. In all specimens, the experimental results of the reserved capacity (f_u/f_y) were close to the same, regardless of the steel grade. However, the ductility values of the specimens corresponding to each grade

differed substantially. The compression flanges of 300W and 350W steel displayed much more ductility than the 480W and 700Q steel. From these experimental results, it can be concluded that the b/t limits of a Class 1 section, which was based on studies on 300W steel, can also be applied to 350W steel grade, but may not be suitable to the higher strength steels such as 700Q steel.

Based on the material models obtained from the tensile test results, a finite element model was established to simulate the stub column test of the selected steel grades. Output from this analytical model showed that the modified bi-linear model best represented the experimental results. Results associated with the bi-linear model for the 300W and 350W grades showed very good correlation with experimental findings, especially when compared with the results of the 480W and 700Q steels. The poor correlation associated with the latter two grades was possibly a product of the tangent modulus value chosen at the onset of strain-hardening. It appeared that the analytically obtained average stress-strain curves experience disturbances at the onset of strain hardening when the tangent modulus was near or lower than 1000 MPa.

Using the finite element model incorporating the bi-linear material model, the strength and ductility of W-shaped sections of 300W, 350W and 700Q steels with variable b/t ratios and constant w/t and were studied. The 480W steel was excluded from this part of the study because the material properties obtained from the tensile test were questionable. The 300W steel, which was used to establish the b/t limits in the current design standards, exhibited

considerable ductility and reserve capacity. The 350W steel demonstrated characteristics similar to the 300W steel. However, the 700Q steel possessed very little compression flange ductility and reserve capacity. In all these steel grades, it was found that ductility and reserve capacity decreased as the b/t ratio increased. From both the experimental investigation and the finite element analysis, the b/t limits in the current design standard were found to be applicable to both 300W and 350W steels, but not to the 700Q steel.

It is suggested that future studies of this kind employ a greater variety of high strength steel grades. This would minimize the heavy reliance placed on the results of one or two steel grades, in the event that some data is found to be questionable.

Furthermore, investigations should be carried out to better understand local buckling behavior of the web under compression, and both web and flange local buckling behavior subjected to other loading conditions, such as pure flexure, or flexural compression.

Finally, based on the findings of this study, b/t limits associated with high strength steel should be established and the current design standard should be revised to include local buckling rules that govern such high strength steel.

References

Abdel-Rahman, N.M. (1997). Cold-Formed Steel Compression Members With Perforations, Ph. D. Thesis, McMaster University, Hamilton, Ontario, Canada.

Akay, H.U., Johnson, C.P., & Will, K.M. (1978). Lateral and Local Buckling of Beams and Frames, Journal of the Structural Division, Vol. 103, No. ST9, ASCE, pp. 1821-1832.

ASCE. (1971). Plastic Design in Steel. A Guide and Commentary, Number 41. American Society of Civil Engineers.

ASTM Standards (1994b). Standard Test Methods and Definitions for Mechanical Testing of Steel Products, American Society for Testing and Material, A370-92.

Banwait, A.S. (1987). Axial Load Behaviour of Thin Walled Steel Sections With Openings, M. Eng. Thesis, McMaster University, Hamilton, Ontario, Canada.

Bild, S., & Kulak, G.L. (1991). Local Buckling Rules for Structural Steel Members, Journal of Constructional Steel Research, 20, pp. 1-52

Bradford, M.A., & Azhari, M. (1994). Local Buckling of I-Sections Bent about the Minor Axis, Journal of Constructional Steel Research, 31, pp. 73-89.

Bulson, P.S. (1969). The Stability of Flat Plates, American Elsevier Publishing Company Inc., New York, New York, USA.

Chajes, A. (1974). Principles of Structural Stability Theory, Prentice-Hall Inc., Englewood Cliffs, New Jersey, USA.

Chin, C.K., Al-Bermani, F.G.A., & Kitipornchai, S. (1993). Finite Element Method for Buckling Analysis of Plate Structures, Journal of Structural Engineering, ASCE, Vol. 119, No. 4, pp. 1048-1068.

Daali, M.L., & Korol, R.M. (1995). Adequate Ductility in Steel Beams Under Earthquake-type Loading, Engineering Structures, Vol. 18, No. 2, pp. 179-186.

Daali, M.L., & Korol, R.M. (1995). Prediction of Local Buckling and Rotation Capacity at Maximum Moment, Journal of Constructional Steel Research, 32, pp. 1-13.

Davids, A.J., & Hancock G.J. (1986) Compression Tests of Short Welded I-Sections, Journal of Structural Engineering, ASCE, Vol. 112, No. 5, pp. 960-975.

Dawe, J.L., & Grondin, G.Y. (1985). Inelastic Buckling of Steel Plates, Journal of Structural Engineering, ASCE, Vol. 111, No. 1, pp. 95-107.

Dawe, J.L., & Kulak, G.L. (1986). Local Buckling Behaviour of Beam-Columns, Journal of Structural Engineering, ASCE, Vol. 112, No. 11. pp. 2447-2461.

Dawe, J.L., & Kulak, G.L. (1984). Local Buckling of W Shape Columns and Beams, Journal of Structural Engineering, ASCE, Vol. 110, No. 6, pp. 1292-1304.

Dawe, J.L., & Kulak, G.L. (1984). Plate Instability of W Shapes, Journal of Structural Engineering, ASCE, Vol. 110, No. 6, pp. 1278-1291.

El-Ghazaly, H.A. & A.N. Sherbourne (1985). Plastic Behaviour of Unstiffened Symmetrical Beam-to-Column Flange Connections, Canadian Journal of Civil Engineering, 12, pp. 821-837.

Galambos, T.V., & Lay, M.G. (1965). Studies of the Ductility of Steel Structures, Journal of the Structural Division, ASCE, Vol. 91, No. ST4, pp. 125-151.

Galambos (1988). Guide to Stability Design Criteria for Metal Structures, 4th Edition, John Wiley & Sons Inc., New York, New York, USA.

Haaijer, G, & Thurlimann, B. (1958). Inelastic Buckling in Steel, Transactions, ASCE, Vol. 125, Part 1, pp. 308-345.

Haaijer, G. (1957). Plate Buckling in the Strain-Hardening Range, Transactions, ASCE, Vol. 124, pp. 117-148.

Holtz, N.M. & Kulak, G.L. (1973). Web Slenderness Limits for Compact Beams, Structural Engineering Report No. 43, Department of Civil Engineering, University of Alberta, Edmonton, Alberta, Canada.

Illston, J.M., Dinwoodie, J.M., & Smith, A.A. (1979). Concrete, Timber and Metals, Van Nostrand Reinhold Company Ltd., New York, New York, USA, pp. 140-186, 474-542.

Kato, B. (1991). Deformation Capacity of Steel Structures, Journal of Constructional Steel Research, pp. 33-94

Kato, B. (1990). Tension Testing of Metallic Structural Materials for Determining Stress-Strain Relations Under Monotonic and Uniaxial Tensile Loading, Journal of Materials and Structures, 23, pp. 35-46.

Kato, B. (1989). Rotation Capacity of H-Section Members as Determined by Local Buckling, Journal of Constructional Steel Research, 13, pp. 95-109.

Kemp, A.R. (1996). Interaction of Plastic Local and Lateral Buckling in Design Codes, Journal of Structural Engineering, ASCE, Vol. 122, No. 4, pp. 374-382.

Kemp, A.R. (1985). Interaction of Plastic Local and Lateral Buckling, Journal of Structural Engineering, ASCE, Vol. 111, No. 10, pp. 2181-2196.

Kemp, A.R. (1986). Factors Affecting the Rotation Capacity of Plastically Designed Members, The Structural Engineering, 64B(2), pp. 28-35.

Kuhlmann, U. (1989). Definition of Flange Slenderness Limits on the Basis of Rotation Capacity Values, Journal of Constructional Steel Research, 14, pp. 21-40.

Kulak, G.L., Adams, P.F., & Gilmor, M.I. (1995). Limit States Design in Structural Steel, 5th Edition, Canadian Institute of Steel Construction, Willowdale, Ontario, Canada.

Lay, M.G. (1965). Flange Local Buckling in Wide-Flange Shapes, Journal of the Structural Division, Proceedings of ASCE, Vol. 91, No. ST6, pp. 95-116.

Lukey, A.F., & Adams, P.F. (1969). Rotation Capacity of Beams Under Moment Gradient, Journal of the Structural Division, Proceedings of ASCE, Vol. 95, No. ST6, pp. 1173-1188.

Osman, A. (1991). Extended End-Plate Beam-Column Joints in Seismic Moment Resisting Frames, Ph. D. Thesis, McMaster University, Hamilton, Ontario, Canada.

Rasmussen, K.J.R., & Hancock, G.J. (1995). Tests of High Strength Steel Columns. Journal of Constructional Steel Research, 34, pp. 27-52.

Rasmussen, K.J.R., & Hancock, G.J. (1992). Plate Slenderness Limits for High Strength Steel Sections, Journal of Constructional Steel Research, 23, pp. 73-96.

Rondal, J., & Maquoi, R. (1985). Stub-column Strength of Thin-walled Square and Rectangular Hollow Sections, Thin-Walled Structures, 3, pp. 15-34.

Stewart, J. (1995). Local Buckling Behaviour of W Shape Steel Sections, M. Eng. Thesis, McMaster University, Hamilton, Ontario, Canada.

Timoshenko, S., & Woinowsky-Krieger, S. (1968). Theory of Plates and Shells, 2nd Edition, McGraw-Hill Book Company Inc., New York, New York, USA.

Trahair, N.S. (1977). The Behaviour and Design of Steel Structures, John Wiley & Sons, New York, New York, USA.